

**TRANSPORT AND ADSORPTION PROPERTIES OF
CARBOXYLATED CARBON NANOTUBES FOR ENHANCED SCALE
INHIBITOR SQUEEZE LIFETIME PERFORMANCE**

By

Kevin Adjevi Bahun-Wilson

Submitted in accordance with the requirements for the degree of

Doctor of Philosophy

The University of Leeds

Institute of Functional Surfaces, IFS

School of Mechanical Engineering

October 2018

The candidate confirms that the work submitted is his own, except where work which has formed part of jointly-authored publications has been included. The contribution of the candidate and the other authors to this work has been explicitly indicated below. The candidate confirms that appropriate credit has been given within the thesis where reference has been made to the work of others.

This copy has been supplied on the understanding that it is copyright material and that no quotation from the thesis may be published without proper acknowledgement.

Assertion of moral rights:

The right of Kevin Bahun-Wilson to be identified as Author of this work has been asserted by him in accordance with the Copyright, Designs and Patents Act 1988.

© 2018 The University of Leeds and Kevin Bahun-Wilson

Acknowledgements

First and foremost, I would like to thank my primary academic supervisor, Professor Anne Neville for her continued support, supervision and enthusiasm. Without Anne's supervision and patience, the completion of this work would not have been possible. Also, I would like to extend my appreciation to Dr Thibaut Charpentier, for co-supervising the project, providing knowledgeable insights and for all the support provided throughout this study. I also would like to thank Dr Joseph Lanigan for his supervision during his time at University of Leeds.

I extend my gratitude to Equinor ASA for their financial support and technical contributions towards this project.

I would like to express my gratefulness to Dr Carlos Grattoni and Dr Samuel Allshorn for sharing their knowledge on reservoir engineering, petrophysics and providing support during my time in the Wolfson Laboratory.

I am thankful to the iFS staff for their help throughout the past four years; Jane, Jordan, Michael, Andrew, Paul, Fiona, Farnaz and Judith. I also would like to thank my colleagues and friends in iFS research group at University of Leeds; Leon, Ogbemi, Tiphaine, Josh, Alex, Thawhid, Olujide, Frederick, Doris, Ashley and Ben. Particularly I am thanking Omotayo, for his invaluable day-to-day advice, contribution in hours of discussion and insight towards the completion of this work.

I also would like to thank my close friends Nguru, Sunmade, Anna-Maria, Nadege, Luis, Sheggs, William, Julien, Nicolas and especially Andri, for her constant support and attention.

I would like to express my deepest appreciation to my Father, my Mother and my sisters, Sonia and Sename. I am grateful for their endless encouragements, patience and for always believing in me. I also want to thank my uncles, aunts and cousins, for their relentless affection and support.

Lastly, I would like to dedicate this thesis to my grandparents; Dr Robert Bahun-Wilson, Catherine Bahun-Wilson, Leon and Jeanne Atayi-Guedegbe.

To those unrecognised, I extend to you all my gratitude.

May God bless you all!

“Make it your ambition to lead a quiet life: You should mind your own business and work with your hands, just as we told you, so that your daily life may win the respect of outsiders and so that you will not be dependent on anybody.”

1 Thessalonians 4:11-12 (NIV)

Abstract

Scale formation in oil reservoirs is a primary challenge in the oil and gas industry. If not prevented, the formation of scale can cause the blockage of rock pores or safety valves, leading to reduced well production. One of the best methods to prevent scale formation is by injecting polymeric scale inhibitors into the reservoir; a methodology termed “squeeze treatment”. A significant problem with this current methodology is that a large amount of scale inhibitor does not adsorb effectively on the rock formation and it desorbs from the reservoir rock formation at a high rate. When the inhibitor concentration falls below the Minimum Inhibitor Concentration (MIC) the well will require another squeeze treatment. Consequently, it is highly desirable to enhance the retention of these inhibitors onto the rock formation in order to achieve a longer and more controlled desorption.

In a previous study, Carboxylated Multi Walled Carbon NanoTubes (COOH-MWCNTs) demonstrated the ability to adsorb scale inhibitor (SI) more efficiently than rock. This finding was then conceptualised into a methodology that consists of treating reservoir rocks to bond with CNTs. In this case, the presence of the COOH-MWCNTs on the rock surface will provide more efficient adsorption of scale inhibitors. This novel methodology is called Nanotechnology Assisted Squeeze Treatment (NAST). The current work builds upon this previous research.

The work herein aims to provide a better understanding of the behaviour of COOH-MWCNTs and their interactions with the scale inhibitor Poly Phosphino Carboxylic Acid (PPCA), with the goal to better understand the adsorption and desorption benefits of the NAST methodology in static and dynamic conditions. This research was also conducted for the purpose of understanding the transport and retention of CNTs in porous media and analyse its effects on porous media properties.

The effects of brine and variation in pH values were studied and provided an understanding of the interaction of PPCA with COOH-MWCNTs. The study

showed that the variation in mass-to-volume influenced scale inhibitor adsorption efficiency. Collected data were fitted to Freundlich adsorption isotherm, which provided important information on the adsorption of PPCA onto CNTs. Further characterisation is carried by the use of Phosphorus-NMR.

Data from the transport studies provided a detailed quantitative analysis of the retention of COOH-MWCNTs in a silane-functionalised porous media. Furthermore, information about transport of COOH-MWCNTs across a range of typical rock permeabilities was obtained. It raised questions about permeability impairment issues because the physical properties of the rocks are modified to a point where a realistic application may be unacceptable.

NAST squeeze treatment simulations were explored using coreflood and sand pack experiments; the results demonstrated outstanding performance compared to a conventional methodology.

.

Table of Contents

Acknowledgements.....	ii
Abstract.....	iv
Table of Contents	vi
List of Tables.....	xii
List of Figures	xiii
List of Units and Abbreviations	xx
Chapter 1 Introduction.....	1
1.1. Aims and Objectives	4
1.2. Structure of Thesis	5
Chapter 2 Literature Review and Theory.....	8
2.1. A Review of Scale Formation	8
2.1.1. Scale Formation	8
2.1.2. Supersaturation.....	8
2.1.3. Induction	10
2.1.4. Nucleation	10
2.1.5. Primary Nucleation.....	11
2.1.6. Secondary Nucleation	12
2.1.7. Growth	13
2.1.8. Formation of Calcium Carbonate	14
2.1.9. Calcium Carbonate Reactions	14
2.1.10. Polymorphic Phases of Calcium Carbonate.....	16
2.1.11. Factors Affecting Calcium Carbonate Scale Formation.....	17

2.2. A Review of Scale Inhibition Techniques	20
2.2.1. Scale Inhibition.....	20
2.2.2. Poly Phosphino Carboxylic Acid (PPCA)	20
2.2.3. Inhibitor Mechanisms	21
2.2.4. Field Squeeze Procedure.....	21
2.2.5. Adsorption Squeeze.....	24
2.2.6. Inhibitor Placement	25
2.2.7. Inhibitor Performance.....	27
2.3. A Review of Nanotechnology and its Application in Porous Media	30
2.3.1. Carbon Nanotubes	31
2.3.2. Single Walled Carbon Nanotube (SWCNTs).....	33
2.3.3. Multi Walled Carbon Nanotubes (MWCNTs).....	34
2.3.4. Transport and Retention Properties of MWCNTs in Porous Media	34
2.3.5. Adsorption Properties of CNTs	37
2.3.6. Nanotechnology Assisted Squeeze Treatment (NAST).....	38
2.3.7. Summary and Scope of Study.....	43
Chapter 3 Methodology	45
3.1. Introduction	45
3.2. Materials.....	46
3.2.1. Minerals	46
3.5.3. Ultra-Violet Visible Spectrophotometer	66
3.5.4. Scanning Electron Microscope and Energy Dispersive X-ray Analyzer	66

3.5.5.	Thermogravimetric Analysis	67
3.5.6.	Raman Spectroscopy.....	67
3.5.7.	Turbiscan	68
3.5.8.	Phosphorus 31 Nuclear Magnetic Resonance	69
3.5.9.	Transmission Electron Microscopy.....	69
3.5.10.	Dynamic Light Scattering	69
Chapter 4 Adsorption of Poly Phosphino Carboxylic Acid onto		
Carboxylated Multiwalled Carbon Nanotubes (NAST2)		
71		
4.1.	Introduction	71
4.2.	Adsorption Data	73
4.2.1.	Adsorption of Polyphosphino Carboxylic Acid with Complex Brines onto COOH-MWCNTs in Comparison to Sand.....	73
4.2.2.	The Rate of Adsorption of PPCA on COOH- MWCNTs.....	75
4.2.3.	Adsorption of PPCA on CNTs at Various pH Values 76	
4.2.4.	Static Adsorption - Adsorption of Various PPCA Concentration on Different Masses of COOH-MWCNTS	78
4.2.5.	Freundlich Isotherm Fittings.....	79
4.2.6.	Phosphorus Nuclear Magnetic Resonance	82
4.3.	Conclusion	83
Chapter 5 Transport and Retention of COOH-MWCNTs and their		
Effects in Porous Media (NAST1)		
85		
5.1.	Overview	86
5.2.	Characterisation of COOH-MWCNTs.....	87

5.2.1.	Transmission Electron Microscopy of Carboxylated Carbon Nanotubes	87
5.2.2.	Thermogravimetric Analysis Results of 95% pure Carboxylated Multiwalled Carbon Nanotubes	89
5.2.3.	Dynamic Light Scattering and Size Distribution	90
5.2.4.	Stability Analyser – “Turbiscan Lab”: Assessment of Stability of COOH-MWCNTs solution with time.....	92
5.3.	Step 1/ NAST 1: Injection and Retention of COOH-MWCNTs in porous media.....	94
5.3.1.	Transport and Retention of Dispersed COOH-MWCNTs in Silane-functionalised Sand Pack Porous Media	94
5.3.2.	Optimisation of Transport and Retention of Dispersed COOH-MWCNTs in Silane-Functionalised Sand Pack Porous Media	97
5.4.	Effect of COOH-MWCNTs on the Permeability of the Porous Media	100
5.4.1.	Effect of Nanoparticle Injection on Differential Pressure in Rock Cores.....	101
5.4.2.	Permeability Impairment due to COOH-MWCNT Injection in Various Sandstone Cores	102
5.4.3.	Optical Inspection of Retention of COOH-MWCNTs	103
5.5.	Core flood: Injection and retention of COOH-MWCNTs	108
5.5.1.	Transport and Retention of COOH-MWCNTs in core flooding	109
5.5.2.	Permeability Impairment due to COOH-MWCNT Injection in Coreflood	111
5.5.3.	Petrophysical Nuclear Magnetic Resonance.....	112

5.5.4. Scanning Electron Microscope Results of Bonded COOH-MWCNTs onto the Doddington Rock Porous Media	113
5.6. Conclusion	115
Chapter 6 Inhibitor Dynamic Testing of the NAST methodology	117
6.1. Experimental Details	119
6.2. Results	120
6.2.1. Sand Pack Flood: NAST VS Conventional PPCA flood at 25°C	120
6.2.2. Sand Pack Flood: Conventional, NAST and NAST re-squeeze in sand pack flood at 50°C	124
6.2.3. Coreflood: Conventional Flood vs NAST and NAST Re-squeeze at 25°C	128
6.3. Conclusion	132
Chapter 7 Discussion.....	134
7.1. Studying the Adsorption of Scale Inhibitor on CNTs	136
7.2. Transport and Retention of Nanoparticles in Porous Media	142
7.3. Squeeze Performances of the NAST Methodology	149
7.4. Relevance of the Research.....	155
Chapter 8 Conclusion and Future Work.....	157
8.1. Summary of the Key Results	157
8.2. Breakdown of the Conclusions.....	158
8.2.1. Step 1/NAST 1: Surface Pre-treatment and CNT Attachment onto Rock.....	160
8.2.2. Adsorption of SI onto the CNTs.....	161
8.2.3. Step 2/NAST2: Sand pack and Coreflood Testing of the NAST Methodology	161

8.3. Recommendations for Future Work	162
References.....	165
Appendix A Design of Pressure Cell	176
Appendix B Detection of CNTs on in Postflush effluents.....	178
Appendix C Hyamine method procedure	179

List of Tables

Table 2-1 Details on calcium carbonate polymorphs [12].....	17
Table 3-1 Synthetic Formation Water Composition [49].....	51
Table 3-2 Sand pack parameters	59
Table 3-3 Core flood parameters: Initial comparison of rock cores before experiment	60
Table 5-1 Compositions of individual metal catalysts nanoparticles present in COOH-MWCNTs based on TEM/EDX analysis	88
Table 5-2 COOH-MWCNT zeta potential at 25°C and 50°C	92
Table 5-3 COOH-MWCNTs retained in sand pack porous media	97
Table 5-4 COOH-MWCNTs retained in sand pack porous media: Optimised vs regular system	99
Table 5-5 Permeability post and pre-experiment of Doddington rock sample	102
Table 5-6 Doddington core permeability pre and post CNT injection.	111
Table 6-1 Core flood characterisation	128
Table 7-1 Isotherm parameters of PPCA adsorption on various CNT mass	141
Table 7-2 Summary of formation damage on coreflood after experiments	147
Table 7-3 Average COOH- COOH-MWCNTs attached in sand pack porous media	148

List of Figures

Figure 1-1 Scale deposition in a pipe [1]	1
Figure 1-2 Comparison results between adsorption of PPCA on CNTs and PPCA on standard rock by Ghorbani [6] in distilled water	3
Figure 2-1 Types of nucleation [12]	11
Figure 2-2 Process of scale formation [5]	12
Figure 2-3: Calcium carbonate crystals and their morphology [21]	16
Figure 2-4 . Influence of temperature on the morphology of CaCO ₃ . Temperature : (a) 30°C, (b) 40°C, (c) 50°C, (d) 60°C, (e) 70°C, (f) 80°C [24]	18
Figure 2-5 Effect of pH on calcium carbonate precipitation potential [27]....	19
Figure 2-6 PPCA Molecular structure [29]	20
Figure 2-7: Steps involved in squeeze treatment (adapted from [41])	22
Figure 2-8 Ideal squeeze return curve [6]	24
Figure 2-9 Typical return curve [6]	25
Figure 2-10 Inhibitor efficiency can vary due to sodium chloride concentration [55]	29
Figure 2-11 Conceptual sketches of SWNT and MWNT [61]	33
Figure 2-12 SWCNTs from graphene sheets [61]	33
Figure 2-13 CNTs Structures	34
Figure 2-14 Illustration of different type of retention: adsorption, straining and log jamming (Inspired from [74])	35
Figure 2-15 Breakthrough of MWCNTs in porous media [79]	36
Figure 2-16 Two Main Steps of NAST	39
Figure 2-17 Reaction of organosilane on substrate surface [6]	40

Figure 2-18 Schematic of CNTs attached to surface via organosilane bond [6]	42
Figure 3-1 Overview of the experimental methodology chapter	45
Figure 3-2 SEM picture of silica sand coated with kaolinite.....	47
Figure 3-3 High magnification of SEM/EDX picture showing kaolinite (alumina) in purple	47
Figure 3-4 Illustration of Saint Bees sandstone [94].....	48
Figure 3-5 Illustration of Doddington sandstone [94].....	48
Figure 3-6 Illustration of Darney sandstone [94].....	49
Figure 3-7 Illustration of Stanton Moore sandstone [94].....	49
Figure 3-8 Polyelectrolyte PPCA [1].....	50
Figure 3-9 Polysorbate 80 chemical structure	52
Figure 3-10 Linear regression relating concentrations of PPCA to absorbance values to produce calibration curves to measure PPCA concentrations via C18-hyamine method using UV-Vis spectroscopy at 500 nm	53
Figure 3-11 Linear regression relating concentrations of COOH-MWCNT to absorbance values to produce calibration curves to measure COOH-MWCNT concentrations using UV-Vis spectroscopy at 500 nm.....	54
Figure 3-12 Schematic diagram of the sand pack setup	57
Figure 3-13 Electric engraver is used to settle the sand down in column thanks to vibrations provided by the machine	58
Figure 3-14 The packed sand has to be in contact with the borderline stoppers. If the column is shaken, no movement should be detectable on both ends of the packing. If movement is detected, then the packing is considered unsuccessful.	58

Figure 3-15 Schematic diagram of Hassler type Coreflood used for this study	60
Figure 3-16 The schematic shows the mini pressure cell designed to test rocks of various permeabilities. The core holder is used to tightly seal the top during experiment. The core supporting is to keep the core in place, and in a steady position.	61
Figure 3-17 Hydrogen Nuclei resonating within a pore. The relaxation time T_2 taken by the Hydrogen Nuclei to resonate is related to the size of the pore [98].....	64
Figure 3-18 Types of NMR graphs. Classification of pore size distribution graphs of porous media ranging from microporous to macroporous [98].....	65
Figure 3-19 Linear regression relating concentrations of COOH-MWCNT to the count of Raman intensity of D peak values to produce calibration curves to measure COOH-MWCNT concentrations using Raman Spectroscopy	68
Figure 4-1 Overview of the experimental work carried to investigate the interaction of PPCA on CNTs being studied	72
Figure 4-2 Comparison of results between adsorption of PPCA on COOH-MWCNTs and rock by Farooqui et al. [29]	74
Figure 4-3 PPCA adsorption onto COOH-MWCNTs within 24 hours at 50°C	75
Figure 4-4 Adsorption of PPCA on CNTs over three pH values with 4 mg of CNTs in 10 mL of a 5000 ppm PPCA solution	76
Figure 4-5 Change in PPCA concentration from 100 to 5000 ppm with various CNT masses 4, 6 and 10 mg.....	78
Figure 4-6 Apparent PPCA adsorption onto different CNT masses at 50°C.....	79

Figure 4-7 Freundlich isotherm fit for adsorption data with 4 mg of CNTs as adsorbent	80
Figure 4-8 Freundlich isotherm fit for adsorption data for 6 mg of CNTs as adsorbent	81
Figure 4-9 Freundlich isotherm fit for adsorption data with 10 mg of CNTs as adsorbent	82
Figure 4-10 Phosphorus bonding indicating the presence of PPCA.....	83
Figure 5-1 Overview of the chapter	86
Figure 5-2 TEM images (A) circle indicates residual metal catalyst impurity marked within the nanoparticle. Nanoparticles overlaying one another are also visible, however impurities were no detected. EDX peaks represent elements within the nanoparticle, except for iron from the TEM grid (B) EDX detected impurities within the nanoparticle (cobalt and carbon).....	88
Figure 5-3 TGA of COOH-MWCNTs in air	89
Figure 5-4 COOH-MWCNT hydrodynamic particle size distribution at 25°C	91
Figure 5-5 COOH-MWCNT hydrodynamic particle size distribution at 50°C	91
Figure 5-6 Stability analysis of Tween 80 dispersed COOH-MWCNTS analysed by Turbiscan at room temperature.....	93
Figure 5-7 Stability analysis of Tween 80 dispersed COOH-MWCNTS analysed by Turbiscan at 50°C	93
Figure 5-8 Breakthrough profiles of dispersed COOH-MWCNTs in transport experiments 1 and 2 at 50°C. Data were experimentally obtained.	95
Figure 5-9 Cumulative mass adsorbed obtained from transport experiments 1 and 2 at 50°C in sand pack porous. Data were experimentally obtained.	96

Figure 5-10 Breakthrough profiles of dispersed COOH-MWCNTs in optimised transport experiments at 50°C. Data were experimentally obtained.	98
Figure 5-11 Mass gain of COOH-MWCNTs retained during injection in porous media at 50°C	99
Figure 5-12 Differential pressure graph of CNT injection into all rocks.....	101
Figure 5-13 Doddington profiling A) Inlet before injection B) Outlet after injecting C) Inlet post injection D) Outlet post injection E) Cross section.....	104
Figure 5-14 Darney sandstone profiling A) Inlet before injection B) Outlet after injecting C) Inlet post injection D) Outlet post injection E) Cross section	105
Figure 5-15 Saint Bees sandstone A) Inlet before injection B) Outlet after injecting C) Inlet post injection D) Outlet post injection E) Cross section.....	106
Figure 5-16 A) Inlet before injection B) Outlet after injecting C) Inlet post injection D) Outlet post injection E) Cross section.....	108
Figure 5-17 Breakthrough profiles of dispersed COOH-MWCNTs core flood experiments at 25°C performed to evaluate the impact of silane functionalisation on COOH-MWCNT transport and retention. Data were experimentally obtained.	109
Figure 5-18 Mass gain of COOH-MWCNTs retained during injection	110
Figure 5-19 a) Before CNT injection b) After CNT injection.....	111
Figure 5-20 Pore size distribution of core before and after experiment.....	112
Figure 5-21 Doddington SEM pictures A) Rock Inlet B) Rock inlet within a pore pathway C) Magnification to illustrate deposition of CNTs within pore pathway D) Cross section of core showing an uniform deposition of COOH-MWCNTs E)COOH-MWCNTs deposition in front of a pore pathway	114

Figure 5-22 A and B - Doddington SEM pictures without CNTs attached to the rock surface.....	115
Figure 6-1 Schematic of adsorption and desorption curve of effluent concentration of flooding experiments.....	118
Figure 6-2 Sand pack experiments comparison of conventional method and NAST at 25°C effluents concentration as a function of PV.....	121
Figure 6-3 Mass of SI adsorbed onto sand pack as a function of PV (NAST vs Conventional).....	123
Figure 6-4 Monitoring of calcium with ICP as function of pore volumes injected.....	124
Figure 6-5 Sand pack experiments comparison of conventional method NAST and NAST Re-squeeze at 50°C effluents concentration as a function of PV. The faded area is being magnified to show the adsorption rate of each experiment.....	125
Figure 6-6 Mass of SI adsorbed onto sand pack as a function of PV (NAST vs Conventional vs NAST re-squeeze).....	127
Figure 6-7 Core flooding experiments comparison of conventional method NAST and NAST Re-squeeze at 50°C effluents concentration as a function of PV. The faded area is being magnified to show the adsorption rate of each experiment.	129
Figure 6-8 Mass of SI adsorbed onto core floods as a function of PV (NAST vs Conventional vs NAST re-squeeze).....	131
Figure 7-1 NAST methodology process. Stage 1: Silane functionalisation of rock surface. Stage 2: Delivering CNTs to bond to rock. Stage 3: Pumping SIs to adsorb on the CNTs. Stage 4: Resume production. Stage 5: Re-injection of SIs when SI desorption is below MIC.....	135
Figure 7-2 COOH-MWCNTs in acidic and alkaline environment [104]	139

Figure 7-3 Illustration of CNT adsorption on porous media. A) A high permeability (rock) have pores still opened after CNT adsorption. B) Lower permeability will have most pores blocked because of CNT adsorption	144
Figure 7-4 Pore size distribution of core before and after experiment. A) Conventional core. B) NAST core	145
Figure 7-5 A) SEM image of the Doddington core at the end of NAST experiment showing particle deposition onto the pore wall. B) An adsorption schematic is also shown to prove that adsorption theory is matched by experiment.	146
Figure 7-6 Highlight on enhanced adsorption rate with NAST with the coreflood experiment.....	150
Figure 7-7 PPCA inhibitor adsorbed on NAST core and sand pack porous media at shut in at 25°C.....	151
Figure 7-8 Scale inhibitor retained in core flood experiments.....	152
Figure 7-9 Proposed adsorption mechanism with calcium ions, CNTs and PPCA.	153
Figure 7-10 A comparison of static and dynamic experiments for adsorption of PPCA on CNTs.....	154
Figure 8-1 Design details of pressure cell lid used for pressure profiling tests	176
Figure 8-2 Design details of pressure cell body used for pressure profiling tests.....	177
Figure 9-1 At 15 PV, during PPCA post flush period of the sand pack experiment done at 50°C. Result shows little desorption of CNTs in a sample by the presence of a G peak. It was not detectable in other PVs inspected.....	178

List of Units and Abbreviations

Units

Units	Definition
Å	Angstrom
cm	centimetre
g	grams
mL	MilliLitre
mL/hour	MilliLitre per hour
mm	Millimetre
mg/L	Milligram per Litre
nm	nanometre
ppm	Parts per million
PSI	Pounders per square inch
µm	micron
wt. %	Weight percent

Abbreviations

Abbreviation	Definition
ζ	Zeta potential
$BaSO_4$	Barium sulphate
Ca^{2+}	Calcium ion
$CaCO_3$	Calcium Carbonate
CNTs	Carbon nanotubes
C_o	Initial concentration (mg/L)
C_f	Final Concentration (mg/L)
COOH	Carboxylated
DMF	Dimethylformamide
EDL	Electric Double Layer
EDX	Energy dispersive X – ray spectroscopy

EOR	Enhance Oil Recovery
Hr	Hour
H_2CO_3	Carbonic acid
H_2O	Water
ICP - MS	Inductively Coupled plasma – mass spectroscopy
K^+	Potassium
K_{sp}	Solubility product
MIC	Minimum inhibitor concentration
m/V	Mass Volume ratio
Mg^{2+}	Magnesium ion
MWCNTs	Multi Walled Carbon nanotubes
NaCl	Sodium Chloride
Na^+	Sodium cation
NAST	Nanotechnology-assisted Squeeze Treatment
PPCA	Poly Phosphino Carboxylic Acid
ppm	Parts per million
ρ	Surface relaxivity
ppt	Parts per trillion
PZC	Point of Zero Charge
SBDS	Sodium DodecylBenzeneSulfonate
SEM	Scatter electron microscopy
TGA	ThermoGravimetric Analysis
SI	Scale inhibitor
Sr^{+2}	Strontium cation
SR	Saturation Ratio
SWCNTs	Single Walled Carbon nanotubes
Γ_{app}	Apparent Adsorption
TEM	Transmission electron microscopy
T_2	Relaxation time
Wt%	Weight percentage

Chapter 1 Introduction

Scale formation is a significant challenge to meeting flow assurance standards in the oil and gas industry. It reduces production rates and results in severe economic losses. Mineral scale formation, also known as mineral fouling, refers to the build-up of inorganic mineral salt on a surface. It also forms and deposits in down-hole completion equipment, such as subsurface safety valves, or deposition in an oil pipe (see Figure 1-1). This is a great concern, as it can cause dramatic and unacceptable safety risks associated with production losses and operational problems.



Figure 1-1 Scale deposition in a pipe [1]

Various types of scales are found in the oil industry; some of the most common include calcium carbonate (calcite, aragonite and vaterite), barium sulphate (barite), strontium and calcium sulphate [2].

Calcium Bicarbonate $Ca(HCO_3)_2$ is water soluble but calcium carbonate ($CaCO_3$) is not. Formation water normally contains bicarbonate as well as calcium ions [3]. Typically, reservoir wells which contain scale originate from the formation of sulphate or carbonate scales of calcium and barium because of their hardness and low solubility ($K_{sp}=2.8 \times 10^{-9}$ and $K_{sp}=1.1 \times 10^{-10}$ for calcium carbonate and barium sulphate respectively)[2]. The mechanisms of calcium carbonate ($CaCO_3$) scale formation, specifically the

several factors which affect inhibition, thermodynamics and kinetics of ($CaCO_3$) will be described in the literature review (Section 2.1.).

Approaches to chemical scale control can be divided into three categories: acidization, dissolvers, and the use of scale inhibitors such as Poly Phosphino Carboxylic Acid (PPCA) applied by, for example, a squeeze treatment [3]. Acidization removes scale and improves flow by clearing, and enlarging pores to allow the flowing of oil [4]. Dissolvers are able to turn insoluble scale into a solution that clears pore blockage [5]. These two control methods have their own advantages and limitations. The third approach is squeeze treatment; it is considered one of the most efficient methods to deploy scale inhibitors because “squeeze lifetime” can last up to several years if properly designed. However this method is limited by the high costs of implementation and loss of oil production [6, 7].

Squeeze treatments aim to prevent scale deposition and formation damage in the well downhole [3] and protect the pipeline from scaling. In a squeeze treatment, the scale inhibitor is injected into the well and pushed through the well formation rocks [3]. After this step, the well is generally shut-in for a period of several hours, in which the inhibitor will be retained by adsorbing/precipitating on the rock [3]. When the production resumes again, the produced water injected will pass through the pores where the inhibitors have retained, and some of them will flow back (post-flush) [3]. As a result, the produced water must contain enough scale inhibitor to prevent scale formation. When the inhibitor concentration drops below the Minimum Inhibitor Concentration (MIC) the well should undertake another squeeze treatment [3].

Ghorbani [6] conducted research aimed at improving current squeeze treatment methodologies. This work showed that Carbon NanoTubes (CNTs) are capable of adsorbing scale inhibitor more efficiently than rock; this helped conceptualising a new method to attach the CNTs onto the rock to increase the adsorption of the scale inhibitors. This methodology, which has shown to be promising, is now called Nanotechnology Assisted Squeeze Treatment (NAST). It is separated in two steps:

NAST 1/Step 1: Bonding CNTs to a rock surface

- Treatment of the internal rock surface of the reservoir to be reactive with CNTs.
- Injection of CNTs to bond with the rock surface.

NAST 2/Step 2: Adsorption/desorption of SI on/from CNTs

- Injection of scale inhibitors to be adsorbed onto the reservoir by CNTs by using a regular squeeze treatment method.
- Re-start production [6].

In dynamic experiments, a significant amount of scale inhibitor remained after post-flush, and it was discovered that desorption was slower leading to a longer squeeze lifetime.

Work by Ghorbani [6] showed promising results:

- From static adsorption results, the retention of scale inhibitors was 70 times higher with CNTs when compared to silica rock, see Figure 1-2.

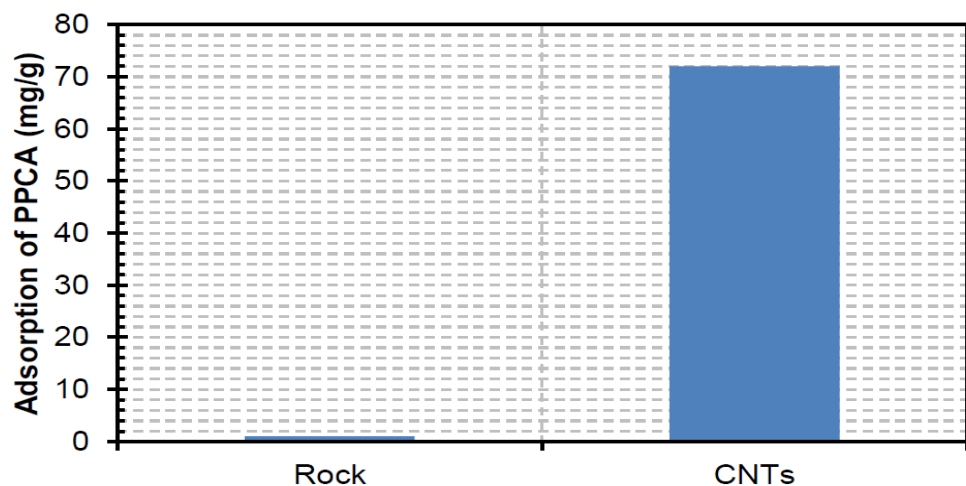


Figure 1-2 Comparison results between adsorption of PPCA on CNTs and PPCA on standard rock by Ghorbani [6] in distilled water

With this context in mind, the present study builds upon Dr Ghorbani's work by developing an experimental methodology to understand the transport and retention of CNTs in such porous media (i.e. transport and retention). The goal is to optimise the process and define its limitations (i.e. permeability impairment). Static adsorption tests are performed to better understand the PPCA and CNT interactions. Sand packs are used as a reservoir analogue to evaluate NAST under various conditions. Once the concept is proven and optimised, a core flood test is done in which the methodology is tested under a range of reservoir characteristics (i.e. chemistry, porosity, permeability).

1.1. Aims and Objectives

This research project seeks to accomplish the following three aims. First, to provide a comprehensive definition of the adsorption of PPCA onto Carboxylated Multiwalled Carbon Nanotubes (COOH-MWCNTs). Second, to assess the transport and retention of COOH-MWCNTs, and explore the effects on the porous media characteristics (i.e., porosity, permeability). Third, to evaluate the enhancement in SI squeeze performance through sand pack and coreflood experiments by using the NAST methodology. The outcomes of this research will be to produce new insights into this novel methodology, specifically in more realistic conditions compared to previous work. In order to achieve these aims, the following objectives are outlined and organised into three main streams of investigation:

Stream 1: Study the adsorption of PPCA onto COOH-MWCNTs

- To study the adsorption of PPCA onto COOH-MWCNTs in a realistic brine and at a moderately high temperature (50°C).
- To identify the effect of variation in environmental factors, such as pH values.
- To develop knowledge of the adsorption of PPCA onto COOH-MWCNTs through the use of adsorption isotherm fittings.

- To provide additional data on the interaction between PPCA and COOH-MWCNTs with the use of Phosphorus-NMR analysis.

Stream 2: Transport, retention and effects of dispersed COOH-MWCNTs in silane-functionalised porous media

- To study the retention and transport of COOH-MWCNTs in a silane-functionalised porous media.
- To identify and understand the release rate mechanism of COOH-MWCNTs from the porous media.
- To assess and understand the negative effects of retention of COOH-MWCNTs in porous media (permeability impairment).
- To gather data on the amount of COOH-MWCNTs adsorbed onto the silane-functionalised porous media.

Stream 3: Squeeze treatment simulations: NAST vs conventional method

- To study adsorption kinetics of PPCA in porous media using the NAST methodology.
- To evaluate the mechanism of desorption of PPCA from the porous media using the NAST methodology.
- To study and identify why the adsorption of PPCA on porous media using the NAST methodology is more effective than the conventional method.

1.2. Structure of Thesis

This work advances the science associated with the proposed NAST methodology by further defining the interaction between COOH-MWCNTs and PPCA and by determining the transport and retention effect of CNTs on porous media properties. There are 8 chapters in this thesis, including the current one.

Chapter 2 provides a review of mineral scale formation and its mechanisms. It explores advances and challenges in current squeeze treatment applications. Lastly, it reviews nanoparticle transportation and adsorbing properties in porous media.

Chapter 3 outlines the experimental techniques used in the work during the static adsorption experiments, transport and retention studies of COOH-MWCNTs in porous media and squeeze treatment simulations in sand packs and core flood experiments.

Chapter 4 concentrates on studying the adsorption of PPCA on COOH-MWCNTs and determines the various factors affecting the sorption of PPCA. The results are presented and discussed.

Chapter 5 presents dynamic experiments to study transport and retention of COOH-MWCNTs in sand pack and core flooding experiments. It also assesses its effects on the porous media characteristics.

Chapter 6 establishes a sand pack and coreflood study in order to assess the NAST methodology in squeeze treatment. The aim of this research is to understand the adsorption and desorption processes of the methodology.

Chapter 7 contains a detailed discussion of all experimental research presented in this thesis. The main contribution is that it combines data from all chapters to discuss the physical and chemical modifications NAST methodology induces to a porous media to enhance the adsorption of scale inhibitor.

Chapter 8 presents the main conclusions of this work and explores relevant areas of future work to support the deployment of the NAST methodology in the oilfield.

Chapter 2 Literature Review and Theory

2.1. A Review of Scale Formation

2.1.1. Scale Formation

In all hydrocarbon reservoirs, before any drilling or recovery processes, the waters in the rock formation porous media are often saturated with dissolved salt from the reservoir rock and in equilibrium with the surrounding environment. Drilling operations lead to a thermodynamic and chemical disturbance, resulting in the initiation of the scale formation [8]. When waters within the porous media are disturbed from their natural state, ions are capable of forming compounds of limited solubility related to the excess of dissolved ions in the solution [9].

Scale formation, also known as the crystallization of sparingly soluble substances or crystallization by precipitation, is the result of nucleation and growth processes that happen during the whole or part of the crystallization [10].

Scale formation results from precipitation in bulk and/or deposition on a surface. Supersaturation occurs when a solution has excess ions beyond what it can dissolve and precipitation is initiated. Thus, scale precipitation or deposition can be described as the formation of a material that forms when its solubility exceeds the saturation threshold [9, 11].

2.1.2. Supersaturation

Supersaturation denotes a solution that contains more ions than the solution can maintain in a dissolved state [12].

The saturation ratio quantifies the supersaturation of a given solution and describes the excess of dissolved ions in solution over the solubility product K_{SP} [12, 13].

$$SR = \frac{IAP}{K_{SP}} \quad (2.1)$$

Where IAP is the product of ion activity and K_{sp} the solubility product.

K_{sp} represents the equilibrium constant for the dissolution of the salt. It measures the number of moles of ions per volume can be in the system before a salt precipitate. Solubility can be described as the amount of a chemical substance being dissolved in a known weight or volume of fluid. It can also be defined as a measurement of its capability to remain liquid without precipitating under specific conditions. The values of K_{SP} have been found to be 4.55×10^9 at 25°C and 1.06×10^9 at 80°C in terms of calcium carbonate [12].

The scaling nature of the water is defined according to the value of the saturation ratio (SR) [14], where:

- $SR < 1$ indicates that: the solution is undersaturated. Scale formation is not possible and the solution is likely to dissolve further deposit.
- $SR = 1$ indicates that: the solution is in equilibrium, as both the scale formation and dissolution rate are equal.
- $SR > 1$ indicates that: the solution is supersaturated; scale formation is very likely to occur. It means that scaling is thermodynamically possible.
- $SR > 40$ indicates that scale formation of calcium carbonate automatically occurs, meaning that the scaling will automatically occur.

Equation (2.2) is an example of the saturation ratio used on calcium carbonate ions which consist of Ca^{2+} and CO_3^{2-}

$$SR = \frac{[Ca^{2+}][CO_3^{2-}]}{K_{sp}} \quad (2.2)$$

When supersaturation is reached, the process of scale formation is followed by induction and nucleation.

2.1.3. Induction

Induction time refers to the duration in which the solution is in metastable equilibrium where nucleation is impossible and the solution has to attain a non-stable state for nucleation to occur. The notion of induction implies an elapsed time between the start of supersaturation and the initial changes in the physical properties of a system [10]. The period between the metastable saturation state and the appearance of the first nuclei is known as “induction time”: [12, 15, 16]. Induction time is representative of the appearance of visible crystals, a rise in turbidity, and a concentration alteration in solution conductivity [12].

Other factors affect the induction such as temperature; interfacial tension or the activation energy for nucleation. The correlation between the induction period of the nucleation can be summed up as: the greater the supersaturation, the shorter the induction time [17].

2.1.4. Nucleation

Nucleation time is a phase that follows the induction period. It corresponds to the growth of particles and it manifests in the metastable zone. The amount of crystals in the solutions increase at the early stage of the nucleation period and the growth of these occur at the end of the nucleation. The nucleation time will not start immediately; the process only becomes possible when at least one crystal nucleus is formed at the early stage of the nucleation.

Nucleation involves two stages: primary and secondary nucleation. Primary nucleation corresponds to heterogeneous nucleation, occurring in an active site (for example: metal surface, sand grains) in order to grow, and homogenous nucleation, occurring in bulk solution in the absence of surfaces. A classification is shown in Figure 2-1.

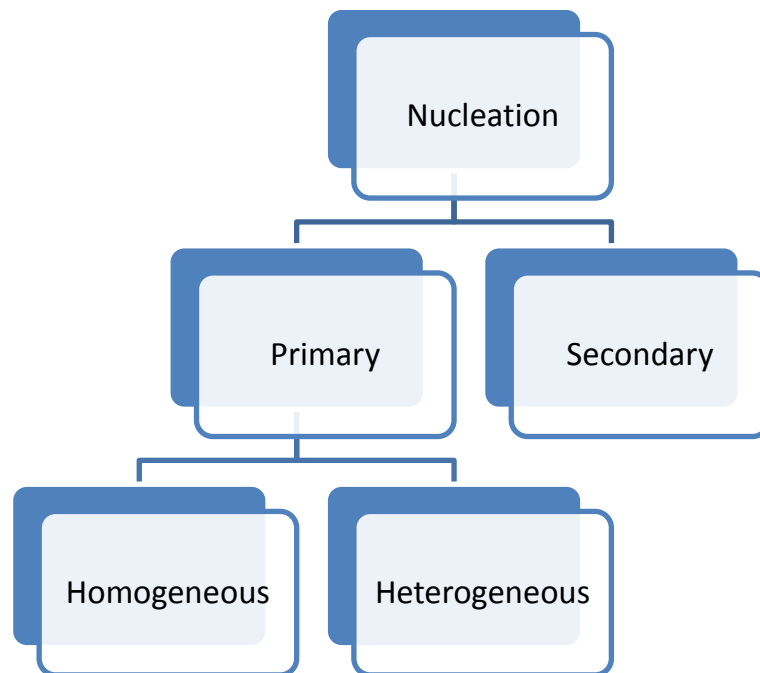


Figure 2-1 Types of nucleation [12]

2.1.5. Primary Nucleation

In a dissolved solution, there are electrostatic interactions between anions and cations. This represents the kinetic interaction to grow mineral scale formation; a process called “ion pairing”. After this step, aggregation creates bigger particles, which remain in equilibrium in the solution (see Figure 2-2).

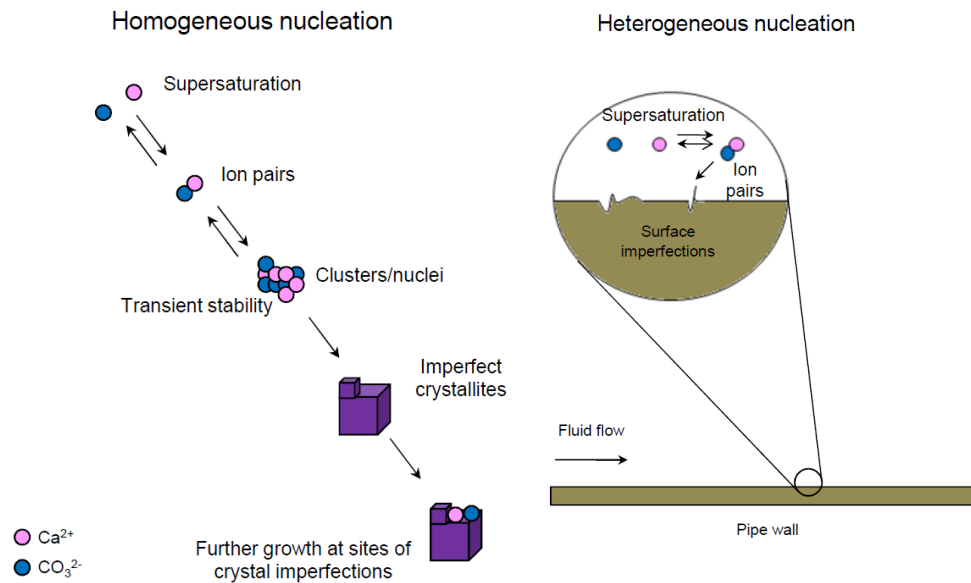


Figure 2-2 Process of scale formation [5]

Typically, at extremely high supersaturation degrees, homogeneous nucleation dominates whereas heterogeneous nucleation has a major role at low supersaturation. This occurs due to impurities or foreign particles lowering the critical saturation value for heterogeneous nucleation [8].

2.1.6. Secondary Nucleation

A certain amount of crystallizing material is necessary for secondary nucleation to manifest. The mechanisms of secondary nucleation are categorised into three distinctive types:

- Apparent secondary nucleation in which the nuclei are brought into the system along with inoculating crystals
- Real secondary nucleation: Involving nuclei formation due to crystal solution interactions
- Contact nucleation where crystals are formed by collisions between crystals.

Secondary nucleation involves a three-part mechanism: abrasion, attrition, and fracture. Abrasion is the process by which all tiny parts are removed, it is followed by a disintegration of the crystal into dissimilar size; this step is called attrition. The last stage consists of fracture, where the crystal is fragmented into two or more parts of similar size [12].

In precipitation of sparingly soluble substances, primary nucleation mechanisms dominate because the particles formed are too small for secondary nucleation mechanisms to play an important role. Subsequent to the formation of nuclei in supersaturated solutions and on solid surfaces, the growth process is initiated.

2.1.7. Growth

In crystallisation, single crystals enlarge in a process called the growth mechanism [12]. This is the aspect of scale formation that involves an increase in size of nucleated crystals to form larger crystals. Both the supersaturation ratio and temperature play important roles in this process. The mechanisms of crystal growth are linked to the smoothness or roughness of its surface and thus is also related to its surface area and the surface energy. Low surface energy and surface area have been shown to promote stability, whereas surface irregularities result in higher surface energy site and favour crystal growth [12].

The rate of growth quantified by Nonyes and Whitney [18] is as follows :

$$\frac{dm}{dt} = k_m A (c - c^*) \quad (2.3)$$

Here m denotes mass of solid deposited as a function of time A denotes the surface area of the crystal, c denotes the solute concentration in the supersaturated concentration, c^* is the equilibrium saturation concentration and k_m is the mass transfer coefficient.

After scale deposition and nuclei growth, the next step is the adhesion of the crystals to create a scale layer [19]. The scale deposition will attach at different strengths according to the surface nature, type of scale and also according to the forces involved in the crystal structure itself.

2.1.8. Formation of Calcium Carbonate

Calcium carbonate is among the most common scales found in an oilfield. $CaCO_3$ scale formation is the result of Ca^{2+} with CO_3^{2-} or HCO_3^- ions (depending on the pH) which are present in the formation water.

Calcium carbonate scale is a consequence of the pressure drop associated with oil production. It occurs when the pressure is less than the carbon dioxide bubble point, CO_2 is released from solution into the gas phase and therefore $CaCO_3$ precipitates.

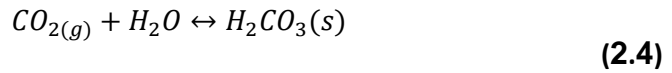
The pressure drop leads to the release of dissolved CO_2 with an increase of the pH value of produced water, the water becomes supersaturated with $CaCO_3$ leading to its precipitation [9].

When the pressure drop is high enough, the concentration of CO_2 is at its saturation limit and is close to being exceeded. The CO_2 cannot mix with solution anymore, thus CO_2 reacts with water and forms carbonic acid leading to a change in water pH.

2.1.9. Calcium Carbonate Reactions

Calcium carbonate equilibrium can be predicted from Chatelier's principle. This principle states that if equilibrium is disturbed by changing the conditions, the position of equilibrium moves to counteract the change and a new equilibrium is established [12]. This principle is used to manipulate results of reversible concentrations, the subject is due to change of pressure, concentration and pH [12].

Dissolution of carbonate and carbon dioxide minerals into water is caused by a drop in pressure. This can be described as follow:

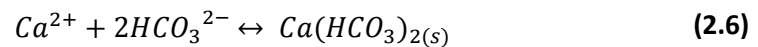


Later on, carbonic acid is dissociated to bicarbonate ($H_2CO_3^-$) and carbonate (CO_3^{2-}) due to increase in pH.

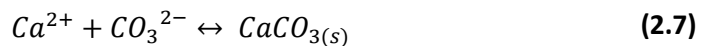


The bicarbonate and carbonate ions then react with calcium ions, thus creating calcium carbonate

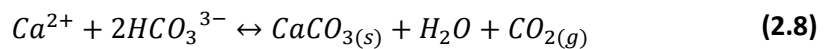
From bicarbonate



From carbonate



The whole process is summarised in the following equation:



The chemical equilibrium constant for calcium carbonate assumed at 20°C and $K_{sp} = 2.8 \times 10^{-9}$ is given by:

$$K_{eq} = \frac{[CaCO_3][CO_2]}{[Ca^{2+}][HCO_3^-]^2} \quad (2.9)$$

A pressure drop will liberate CO_2 from the solution and there the CO_2 concentration will reduce. More calcium carbonate (so more scale) will be formed to keep the chemical equilibrium K_{eq} .

2.1.10. Polymorphic Phases of Calcium Carbonate

Calcium carbonate can exist in various polymorphic phases, including vaterite, aragonite, and calcite. These forms of scale have various solubilities, morphological and crystallographic characteristics. The formation at different conditions (i.e., high pH, high calcium, high carbonate concentrate) results in the formation of a precursor phase containing amorphous calcium carbonate, which then evolves anhydrate phases; calcite (most stable), aragonite (stable), and vaterite (metastable) [20, 21]. See Figure 2-3.

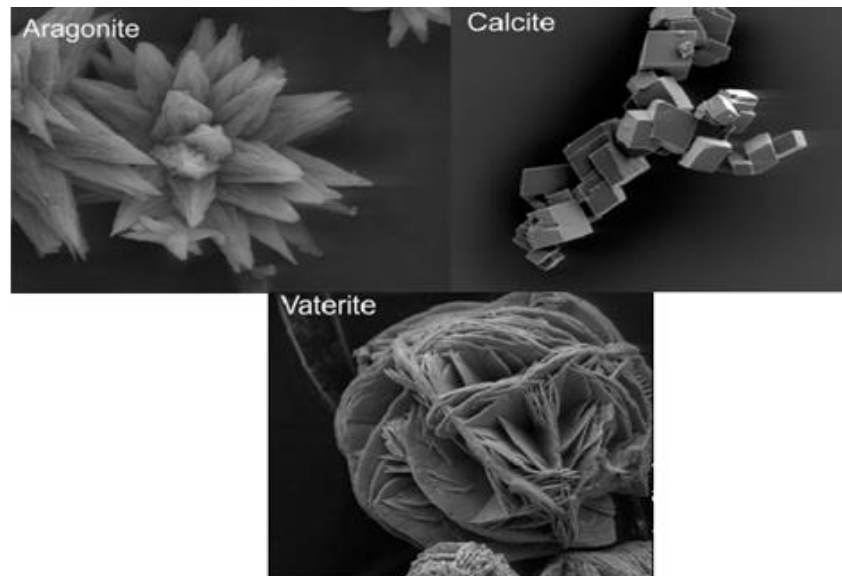


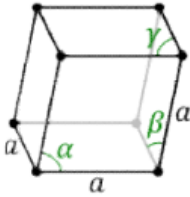
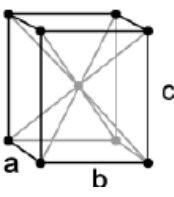
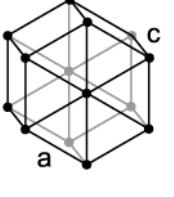
Figure 2-3: Calcium carbonate crystals and their morphology [21]

The crystal morphology can affect the ease of attachment and removal of calcium carbonate. Some of them aggregate really easily e.g. calcite, whereas vaterite is very easy to remove from the surface and can be flushed away. Among them all, calcite is the easiest to remove compared to vaterite and carbonate [12].

Depending on the fluid conditions (composition, temperature, pH, fluid dynamics and substrate), the less stable calcium carbonate crystals will be stabilized, the more likely it will be converted thermodynamically into calcite. It is normally formed at lower temperatures. Aragonite phase precipitation

occurs above ambient temperature, whereas vaterite appears at moderate temperatures. Some of the characteristics of the calcium carbonate polymorphs are shown in Table 2-1.

Table 2-1 Details on calcium carbonate polymorphs [12]

Crystal	Calcite	Aragonite	Vaterite
Crystal System	$\alpha, \beta, \gamma \neq 90^\circ$ 	$a \neq b \neq c$ 	$a \neq c$ 
Morphology	Cubic to Rhombohedral	Needle shaped	Hexagonal Hemispherical
Favourable Condition	<ul style="list-style-type: none"> ➤ Initiated by foreign ions. 	<ul style="list-style-type: none"> ➤ High pH value ➤ Temperature above 50 °C 	<ul style="list-style-type: none"> ➤ High saturation ratio
State	<ul style="list-style-type: none"> ➤ Most stable ➤ Single crystal. 	<ul style="list-style-type: none"> ➤ Stable ➤ Single crystal. 	<ul style="list-style-type: none"> ➤ Metastable. ➤ Microcrystalline. ➤ Porous.
Density in (g/cm³)	2.66	2.93	2.71

2.1.11. Factors Affecting Calcium Carbonate Scale Formation

2.1.11.1. Effects of Temperature

Previous studies have demonstrated how temperature can influence particle size [22]. It has also been shown that homogeneous nucleation is more frequent at high temperatures, whereas heterogeneous nucleation occurs at

low temperatures. Other studies have also shown that temperature increases can promote faster crystallisation [23].

Temperature also has a direct influence on the process of formation and morphology of calcium carbonate [24] (see Figure 2-4).

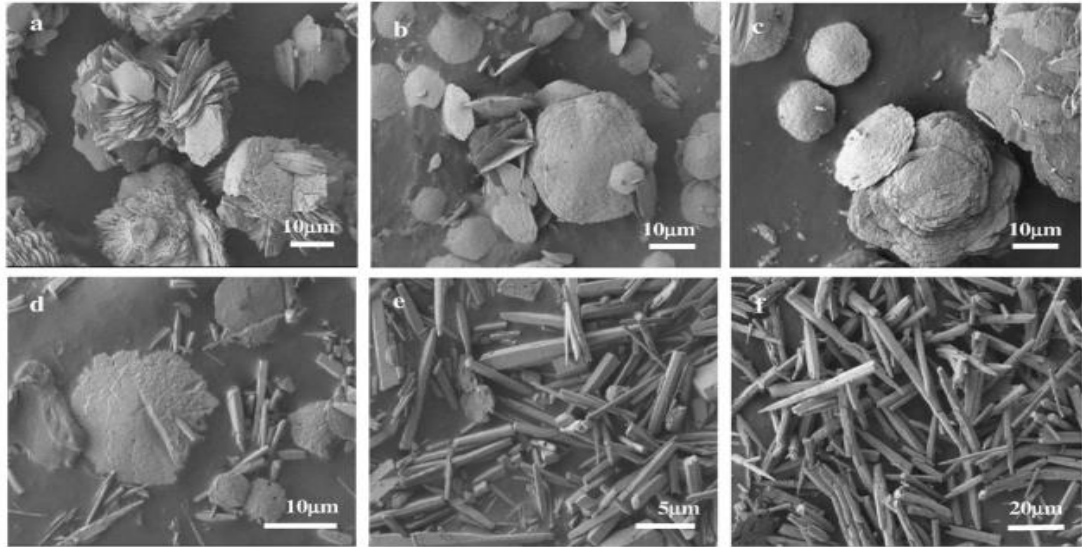


Figure 2-4 . Influence of temperature on the morphology of CaCO_3 . Temperature : (a) 30°C, (b) 40°C, (c) 50°C, (d) 60°C, (e) 70°C, (f) 80°C [24]

In Figure 2-4, vaterite is apparent between 30 to 50°C, vaterite and aragonite were both present between 60°C, and aragonite only manifested above 70°C.

2.1.1.1. Effects of pressure

The saturation threshold diminishes because of a pressure drop, and as a consequence the scale formation/precipitation of calcium carbonate rises up. Equilibrium forces attempt to compensate by increasing the pressure and causes an excess of production of CO_2 . As a result, a pressure drop will then lead to more precipitation. High pressure would lead to a high solubility, and low pressure lead to low solubility [13].

The pressure drop will cause pH to increase and will contribute to scale precipitation. The lack of CO_2 due to the pressure drop provokes the carbonate precipitation.

2.1.1.2. Effects of pH

High pH permits high saturation in a solution to occur, and therefore leads to greater scale formation rates [25].

Cheng *et al.* [22] reported that the primary particle size lowers with an increase of pH because of the increase in nucleation rate. Greater ionic strength results in decreased probability of carbonate formation, however, if the pH drops, formation of $CaCO_3$ is less likely to happen [26].

Andritsos and Karabelas[27] demonstrated how increasing the pH from 8.8 to 10, influenced the deposition of calcium carbonate, as can be seen in Figure 2-5.

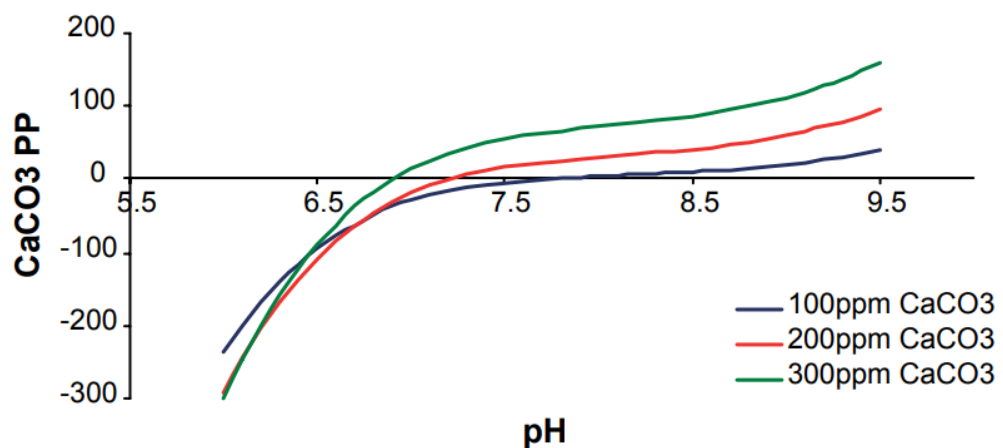


Figure 2-5 Effect of pH on calcium carbonate precipitation potential [27]

2.2. A Review of Scale Inhibition Techniques

2.2.1. Scale Inhibition

Scale inhibition is often achieved by chemical treatments that allow the prevention and control of scale formation. Scale inhibitors can be continuously injected and be deployed in periodic squeeze treatments.

Efficiency of scale inhibition relies on the dosage, the inhibitor's physical properties, the number of functional groups in the molecule, the molecular weight, and the composition of the polymer [28].

2.2.2. Poly Phosphino Carboxylic Acid (PPCA)

PPCA is a commonly used polymeric inhibitor in the oilfield. It is an affordable and high quality inhibitor. The presence of phosphorus atoms can ease the analysis of PPCA attachment [29]. PPCA is also known for its thermal stability properties and dispersion properties [30, 31]. See Figure 2-6.

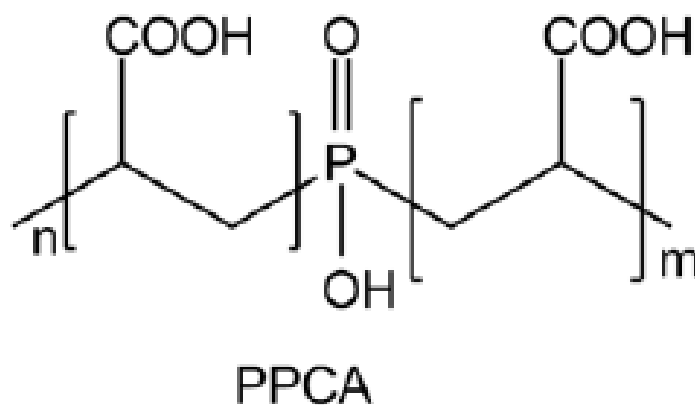


Figure 2-6 PPCA Molecular structure [29]

PPCA can react with aragonite and calcite crystals to promote a more soluble scale : vaterite [32]. PPCA is soluble with water which allows high

inhibition because of its active sites (also metal surfaces). However, PPCA is not resistant to high pH [33].

2.2.3. Inhibitor Mechanisms

Scale inhibitors can slow and act on nucleation, growth steps and crystallisation. It disturbs the thermodynamics of the nuclei growth [34, 35]. In order to disrupt nucleation and prevent growth of crystals scale inhibitors must attach to the surface of nuclei and growing crystal [36]. There are several mechanisms for scale inhibition including “threshold or stabilization effect”, dispersion and crystals distortion.

- Threshold effect: An organic chemical capable of preventing or delaying scale formation is qualified as “threshold effect”. This occurs because it acts on the nucleation sites causing nucleation inhibition or limitation of growth and crystal retardation [5]. Inhibitors can also adsorb on surfaces to inhibit formation or growth.
- Dispersion: This process allows the inhibitors to prevent and reduce agglomeration of scale deposits. It works by repulsion: the chemicals are negatively charged, during adsorption by the surface leading to repulsion. These inhibitors are able to react with calcium ions and therefore are capable of delaying scale formation [37].
- Crystals distortion: The other inhibition mechanism is based on acting and modifying the morphology of grown crystal. Adhesion of scale is lowered because scale inhibitors adsorb on the surface.

2.2.4. Field Squeeze Procedure

Squeeze treatment is one of the most common and efficient methods to prevent scale formation in oil reservoirs [38], although it is considered as a

secondary oil recovery method [39]. It is widely use in order to prevent scale formation in oil reservoirs, near oil wellbores, production tubings, and to protect safety valves from scaling [40]. The steps of squeeze treatment are shown and explained below in Figure 2-7.

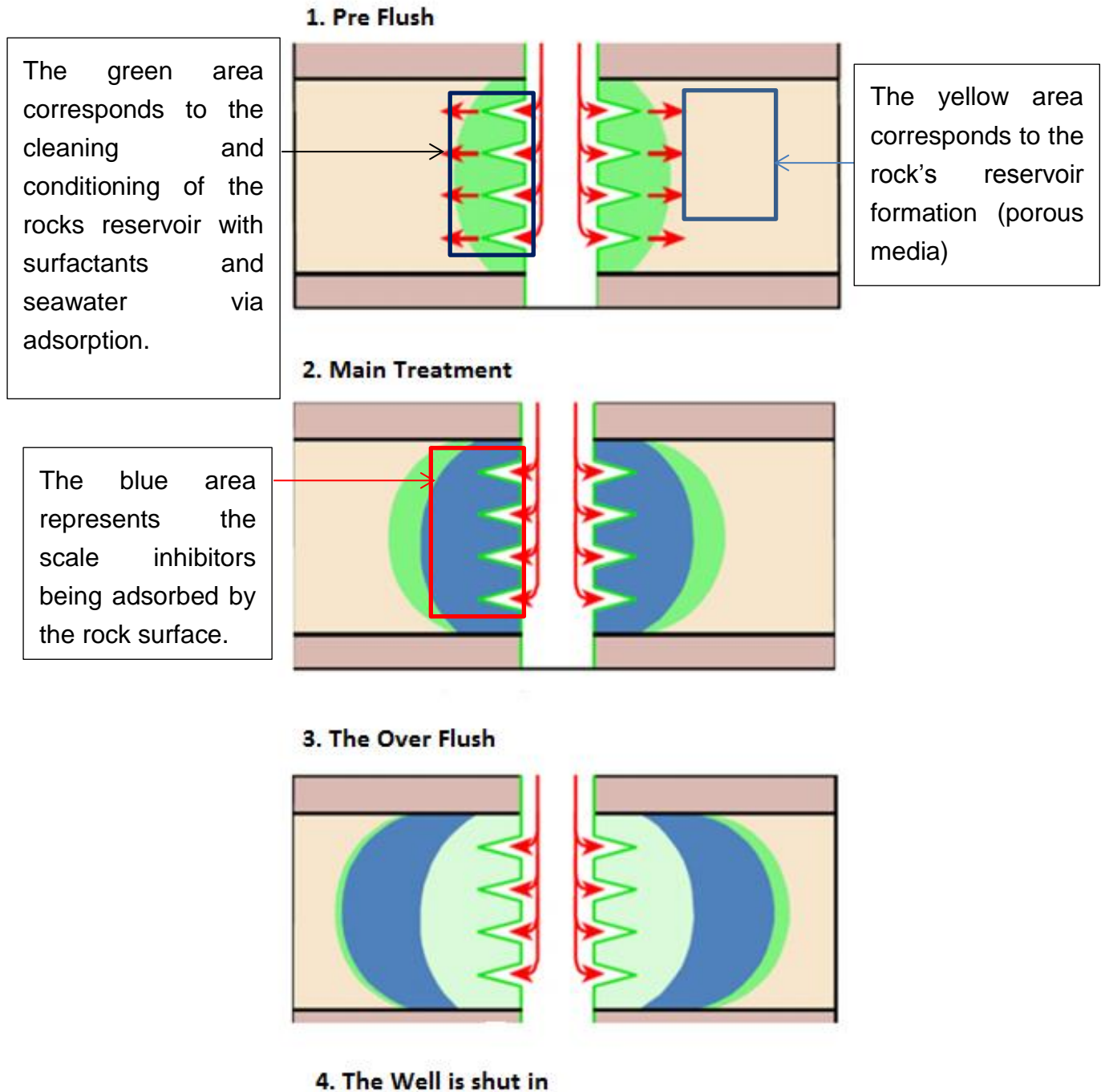


Figure 2-7: Steps involved in squeeze treatment (adapted from [41])

1. Pre-flush consists of cleaning and conditioning the near well bore for the scale inhibitor, in order to maximize contact with rock and avoid well bore damage.
2. The main treatment consists of injecting about 2.5% to 20% of scale inhibitors with brine within rock formation,
3. Over flush consists of flushing/pushing the chemicals deeper in the formation.
4. The shut in period lasts for generally about 12-24 hours, so the chemicals can adsorb on the rock surfaces.
5. Oil production can then resume, while the scale inhibitors desorb slowly into the produced water in order to prevent scale formation. When the inhibitor concentration falls below the Minimum Inhibitor Concentration (MIC), a new treatment must be initiated. A squeeze lifetime can last from 12 to 18 months [6].

When the production starts again, a high concentration of scale inhibitor flows back immediately for a period of 1 to 15 days [42]. The better the adsorption rate, the slower the rate of desorption would be and the longer the squeeze lifetime will be. More concepts about adsorption and squeeze treatments are explained in the inhibitor performance (section 2.2.7) literature.

One of the main advantages of scale inhibitors is that it reduces costs and prolongs squeeze lifetime. One of the challenges facing the industry, as well as the challenge of the NAST project, is to maximise squeeze lifetime through development and deployment of new technology.

Many techniques have been used to increase scale inhibitor retention and enhance the squeeze lifetime [43]:

1. Precipitation squeeze treatment
2. Raising the pH in the reservoir
3. Change of wettability
4. Use of kaolinite or clay to enhance inhibitor adsorption
5. Cross-linked inhibitors

6. Use of micro particles
7. Use of surfactant

2.2.5. Adsorption Squeeze

Scale inhibitor return profile determines the squeeze process when the oil production resumes after the shut in period. The adsorption-desorption of an inhibitor on or off the formation is dependent on the strength of the inhibitor-formation rock associations and can be predictable with an adsorption isotherm [39, 44].

Ideally, in a squeeze treatment, the scale inhibitor concentration return curve would have a high adsorption rate and a slow desorption rate [6, 38]. The ideal curve would mimic the one presented (Figure 2-8). The initially steep isotherm clearly indicates very strong rapid adsorption for scale inhibitor reaching a saturated high plateau [28].

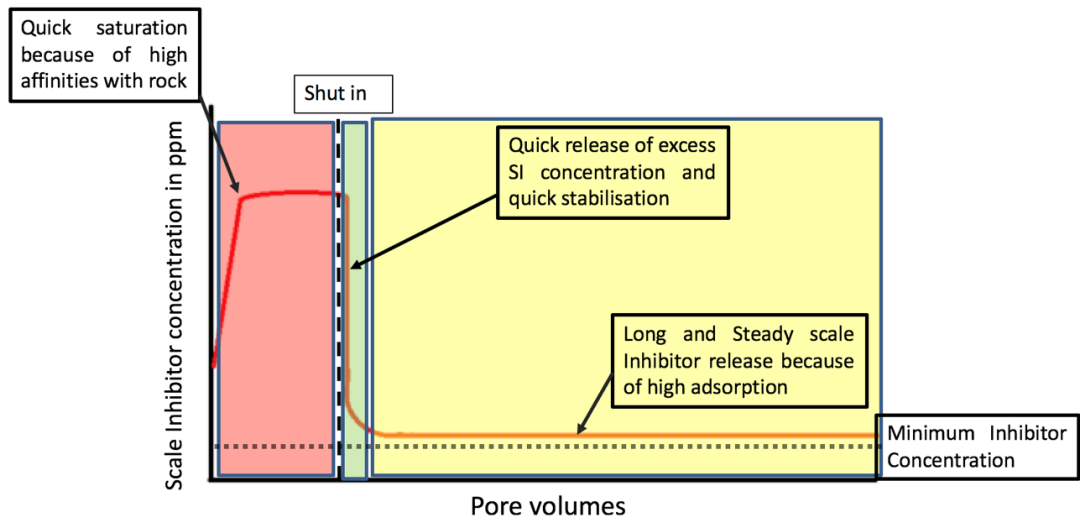


Figure 2-8 Ideal squeeze return curve [6]

In contrast of Figure 2-8, Squeeze treatments rarely have such a perfect profile as represented in Figure 2-9. Researchers are attempting to develop better squeeze methodologies that would either help enhance the adsorption and/or help control the desorption rate of the inhibitor.

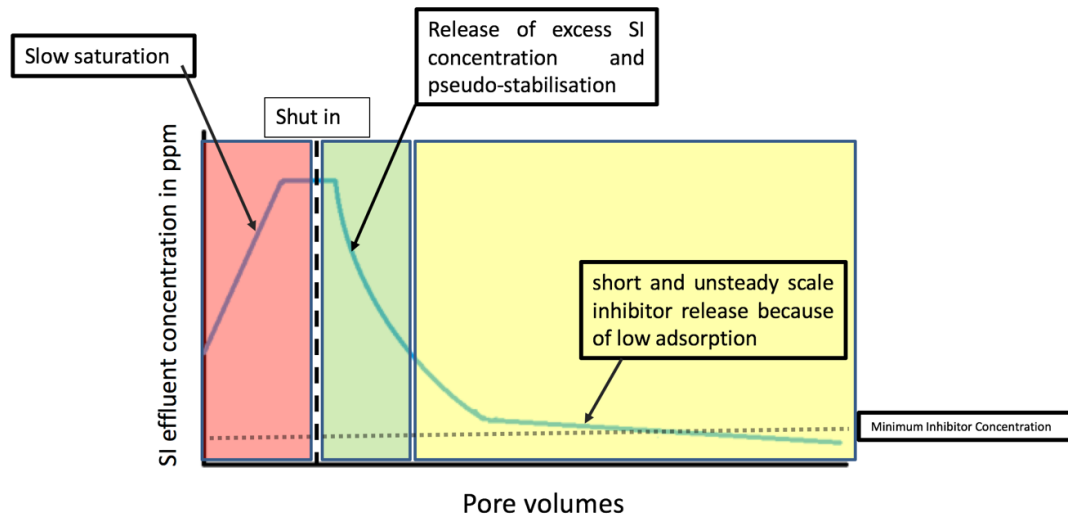


Figure 2-9 Typical return curve [6]

One of the purposes of this research is to focus on squeeze treatment with the use of nanoparticles to enhance scale inhibitors adsorption on rocks and have a slower desorption when flushed with realistic brine solutions.

2.2.6. Inhibitor Placement

Successful placement of the inhibitor into the near wellbore zone at the location of scaling is fundamental for an effective inhibitor treatment of a well [28, 45, 46]. Successful squeeze treatments rely strongly on field data and can be improved either from analysis of real field return data or from study of field core flood return data [38, 46]. This includes the use of radial flow computer modelling software that is capable of incorporating inhibitor interactions with the near wellbore formation [47]. The SQUEEZE VI software, established at Heriot-Watt University can be consistently used for such

functions [7, 47, 48].

Inhibitor propagation in adsorption/desorption squeeze treatments is related to the shape of the inhibitor adsorption isotherm [7]. This describes the relationship between the level of inhibitor adsorption at the rock surface, $\Gamma(C)$ (in mg/g or mg/m²) and the inhibitor concentration in solution, C . When inhibitor adsorption/desorption reaches equilibrium, the propagation velocity of a given concentration C is given by the equation:

$$V_c = V_{fluid} / (1 + (\rho/\phi) / (\delta\Gamma/\delta C)) \quad (2.10)$$

Where:

V_c = Velocity of a given concentration of inhibitor

V_{fluid} = Fluid (Water) velocity

ρ = Rock density

Evidently, the return velocity to the wellbore will be lowest when the factor $(\rho/\phi) / (\delta\Gamma / \delta C) \gg 1$. Whether the adsorption is an equilibrium or non-equilibrium state, the underlying adsorption isotherm, $\Gamma(C)$, govern the form of the inhibitor return curve.

For inhibitor adsorption, the Freundlich and Langmuir isotherms are generally used to describe the process.

Freundlich isotherm	$\Gamma = kC^n$	(2.11)
------------------------	-----------------	---------------

Where Γ is the amount adsorbed, n is the isotherm index obtained from slope of the log portion of the adsorption curve. k is a Freundlich constant, C is the solution concentration.

Langmuir Isotherm	$\Gamma = \frac{abC}{1 + bC}$	(2.12)
----------------------	-------------------------------	---------------

Where Γ is the amount adsorbed, a is maximum absorption concentration, C is the solution concentration, b is obtained from the gradient slope of the linear regression of the graph $1/\Gamma$ as a function of $1/C$.

These constants, k, n, a and b can be altered in the mathematical model until values are obtained, which allow the particular return profile to be simulated. In this way inhibitor return data from core flood experiments can be used to design and optimize a field squeeze strategy [47]. Adsorption/desorption characteristics are obtained from sand pack or coreflood experiments and these data are input to the SQUEEZE VI emulator. Optimised squeeze treatments can then be modelled. Alternatively, inhibitor return data after a squeeze treatment are used as input to SQUEEZE VI and simulations can be developed for further optimisation of the treatment.

2.2.7. Inhibitor Performance

As previously mentioned, considerable research has been done with the goal to improve scale inhibitor retention, and therefore enhance the squeeze lifetime of a squeeze treatment.

As a reminder adsorption/retention can be defined as a process in which a gas or a liquid accumulates on the rock surface of the rock reservoir. Adsorption can be further defined based on the strength of interaction between the substrate and the adsorbed molecules. Desorption can be defined as the release of one substrate from the surface.

In previous studies, the adsorption and desorption are evaluated in order to simulate squeeze treatment by flooding porous media. In reviewing this area of research, the mechanism of inhibitor adsorption or coupled precipitation in squeeze treatment is explained by examining the main mechanisms of the

scale inhibitor squeeze process. Past experiments of scale inhibitors are reviewed.

Static adsorption tests are performed using minerals like sand, clays as well as a volume of scale inhibitor in a beaker. In general, the main factors, which influence the inhibitor adsorption, are pH, inhibitor type, mineral substrate type, brine composition, time and temperature [49].

In dynamic tests, in most cases, the method involves the injection of an inhibitor slug into a sand pack followed by a post flush slug and then monitoring the effluent composition as a function of time or cumulative pore volume of fluid [49]. Against the aforementioned, literature on inhibitor performance is detailed.

Vetter's goal [50] was to first determine adsorption, desorption and inhibitor feedback. The adsorption isotherms were done at various concentrations, temperatures and pH values. All tests were executed with sand, dolomite or limestones. Vetter [50] found that temperature had an effect on isotherm; specifically, adsorption decreased with increasing temperature [12].

Durham [51] reported that squeeze lifetime depended on the production rates, desorption, temperature, and formation type; findings that largely confirmed those of Vetter [51]. His work also determined that adsorption was probably related to electrical attraction between reservoir formation and the scale inhibitor [49, 51]. Payne [52] analysed that the squeeze lifetime of a well was longer after its first injection.

Breen et al. [53] investigated the use of scale inhibitors in an acidic environment, and concluded that polymeric phosphonates inhibitors showed greater performance at higher pH due to electrostatic effects on the scale surface and that are dependent on the ionization [49, 53]. These arguments reinforce the ideas of King and Warden [54] who also found that the amount of adsorption depends on the quantity of active surface area in contact and the thickness to which the inhibitor molecules adsorb [49, 54].

Vetter [55] demonstrated that adsorption/desorption is time dependent and desorption is associated with the velocity. He also stated that dynamic tests were more accurate than static adsorption because they are more field achievable than static adsorption tests.

Vetter et al [55] determined variation in NaCl and rare earth metal can either increase or decrease inhibitors efficiency. These effects are due to the ionic strength of the brine (See Figure 2-10).

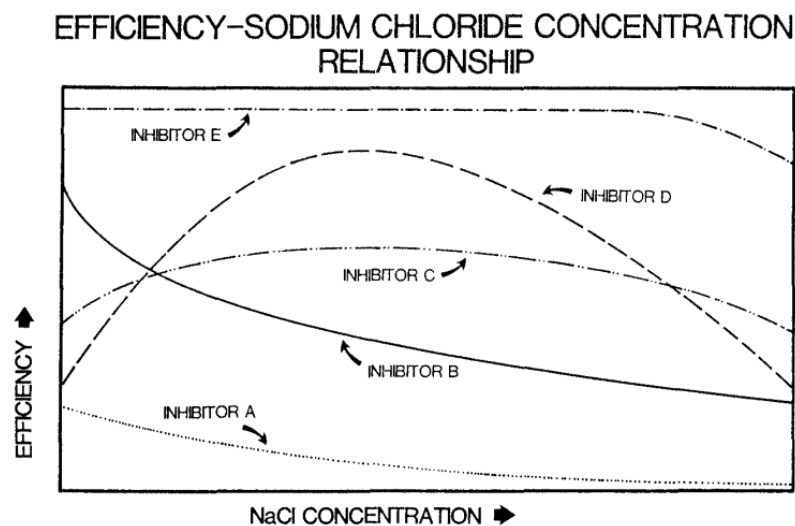


Figure 2-10 Inhibitor efficiency can vary due to sodium chloride concentration [55]

Przybilinski's [56] results agree with many researchers on the importance of the kinetics of inhibitor adsorption/desorption process. His work concluded that phosphonate adsorbs better on silica, and rates of adsorption increase with increasing temperatures. This study also showed that adsorption/desorption depends on the partitioning of the SI between the solution and the solid surface; an interaction that is strongly influenced by the mineral types (kaolinite, sand, siderite, etc) [49, 56].

Sorbie [7] found that SI adsorption increases at higher temperatures under all conditions, and the adsorption of phosphonates decreases predictably as pH

increases in the absence of calcium ions because of the lack of hydrogen bonding. However, with the presence of calcium ions the adsorption is enhanced [49].

Kan *et al.* [57], later presented evidence that the presence of calcium ions can enhance the retention of scale inhibitor into rocks formation, and therefore enhance the squeeze lifetime [49, 57].

Funkhouser [44] reported that static adsorption results can be correlated to sand pack results. Their research showed that static adsorption data has a direct bearing on scale inhibitor adsorption/desorption in dynamic sand pack [44]. They also found that a wide range of adsorption data can be fitted by using the Langmuir equation. Among the rock types, inhibitor returned profiles can be classed in 3 groups: strongly adsorbing (siderite $FeCO_3$), moderately adsorbing (silica SiO_2 and kaolinite $Al_2Si_2O_5(OH)_4$), and weakly adsorbing (alumina Al_2O_3 and smectite $(AlSi)_3O_4$) [49].

The recent findings to better understand adsorption of inhibitors led to create innovative methods for enhancing the squeeze lifetime. For example, Nalco Champion [58] designed additives that appear promising to enhance squeeze lifetime. Zhang *et al.* [30] at Rice University synthesised nanoinhibitors that showed the ability to travel deep in rock formations and to also enhance squeeze lifetime. Farooqui and Ibrahim [49, 59], from Heriot University studied precipitation in order to be able to create more realistic squeeze design models. NAST is an innovative methodology that has shown great potential, thus the leading point of this research is to improve the NAST methodology to be able to deploy it for a realistic application.

2.3. A Review of Nanotechnology and its Application in Porous Media

Nanotechnology has challenges, their new properties and special phenomena occurring in the nano scale range are currently being discovered [60]. These

properties are of high interest from an engineering point of view: nanoparticles may be a way of controlling oil recovery with processes that can be unrivalled by the current and past technologies [60]. This project, nanoparticles, especially carbon nanotubes, are used to adsorb scale inhibitors and desorb them at a slower rate [60].

2.3.1. Carbon Nanotubes

Carbon atoms in carbon nanotubes are sp^2 bonded. The sp^2 bond is the mixing of one 2s and two 2p atomic orbital, which involves the promotion of one electron in the s orbital to one of the 2p atomic orbital [61]. They are part of the fullerene structural family [61].

Carbon nanotubes (CNTs) are composed of cylindrical sheets of graphene. CNTs are divided into two main groups: single-walled carbon nanotubes (SWCNTs) containing only a single graphene layer, and multi-walled carbon nanotubes (MWCNTs) containing two or more (mostly between 7-10) concentric layers of graphene sheets with an intrinsic distance of $\sim 3.4 \text{ \AA}$ [62, 63]. CNTs range from 2 to 30 nm in diameter and up to 1 μm or more in length, based on direct observation with TEM [64]. CNTs have note-worthy properties such as large surface area to volume ratios, low densities, low flexural strength, high mechanical and tensile strengths, inferior stress transfer, high aspect ratios, high electric and thermal conductivity, high hydrogen storage potential, and high adsorbency properties, when compared to other materials [62] [65].

The physicochemical properties of CNTs results from their unique structure and chemical composition. This has led to numerous industrial and commercial applications for CNTs and their derivatives in various commercial areas. For instance, CNTs are used as probe tips of atomic force microscopy (AFM) or scanning tunnelling microscope (STM) due to their small size, high electrical conductivity, and high modulus [66-68]. Moreover, polymer matrices

strength and modulus have been enhanced thanks to the addition of CNTs [69, 70]. CNTs have also been used in water purification systems due to their antimicrobial property [71]. CNTs are also possible candidates for the storage of H₂. A significant amount of H₂ storage in CNTs has been reported in experimental literature [65, 71]. Although theoretical explanations for such phenomena are still incomplete [65], this phenomenon is believed to be an intermediate between physisorption and chemisorption [72].

CNTs are also slowly being incorporated in high semiconductor devices, energy-conversion devices, sensors, drug delivery systems, field emission displays and radiation sources [61]. Most of these innovations are still prototypes for now. One main problem with nanotubes comes with the high pricing and low availability of high quality products, this is limiting the development of carbon nanotubes technology [61].

In the NAST methodology, one of the main obstacles is to effectively disperse carbon nanotubes as they are inert and insoluble in water or any solvent. Dimethylformamide (DMF), N-methylpyrrolidone (NMP) and hexamethylphosphoramide (HMPA) or Tween 80 have shown ability to disperse CNTs in aqueous solution [61].

Dispersion of MWCNTs in solution can be achieved either by steric or electrostatic interactions. Steric effects are caused by a surfactant adsorption on the nanoparticle, and this will cause a steric repulsive force. Electrostatic interaction is created by 2 main mechanisms: isomorphic substitution of ions or physical adsorption of charged matrix onto the surface.

CNTs are classified into two main types: Single walled Carbon Nanotube (SWCNT) and Multi Walled Nanotube (MWCNT) [61, 73].

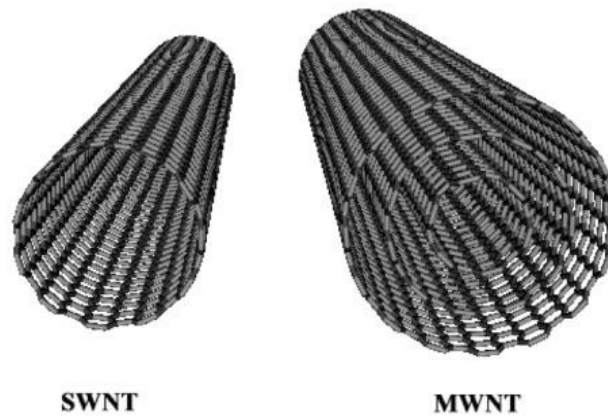


Figure 2-11 Conceptual sketches of SWNT and MWNT [61]

2.3.2. Single Walled Carbon Nanotube (SWCNTs)

SWCNTs are rolled up sheets of graphene [61]. They have a chiral, zigzag or armchair structure [61]. SWCNTs can have diameters ranging 1nm to 2nm and have length of several microns (depending on the manufacturer) [61].

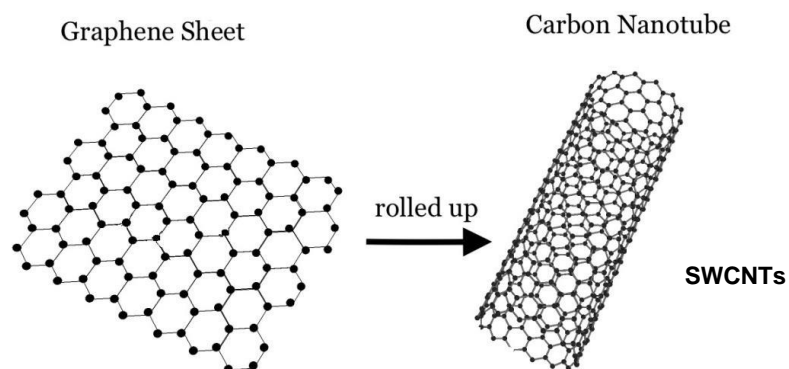


Figure 2-12 SWCNTs from graphene sheets [61]

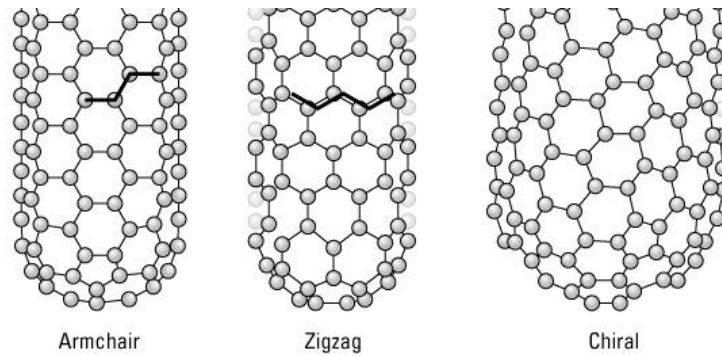


Figure 2-13 CNTs Structures

2.3.3. Multi Walled Carbon Nanotubes (MWCNTs)

MWCNTs are made of two or more concentric cylindrical layers of graphene, they have diameters ranging from 2 to 25nm and length of several microns. The graphene layers interact due to van der waal forces and $\pi - \pi$ stacking [61].

2.3.4. Transport and Retention Properties of MWCNTs in Porous Media

In this context, retention refers to the process of colloidal attachment onto surfaces of a large material. Transport, on the other hand, refers to a more general and complex set of processes that affect the movement of colloidal particles in the solid environment.

There are three main mechanisms of retention/mechanical entrapment in porous media.

- Adsorption of particles onto rock surface caused by Brownian motion, and the electrostatic interaction between the migration particles and the solid surface of the pores [74].
- Straining (also known as mechanical entrapment or deep-bed filtration) in small pores is recognized as another element of retention. Straining,

leads to blocking of narrow pore throats by larger particles [74]. Evidence for mechanical entrapment is inferred by the fact that the particle concentration in the effluent does not reach the injected concentration, or that it would do so only after injecting a large volume of particles [74].

- Log-jamming is a form of straining but particles can block pores larger than the particle size [74]. Due to density differences between moving particles and carrying fluid, sedimentation or gravity settling will occur. Water molecules will then accelerate faster than heavier particles, and agglomeration will occur. Due to gravity settling or adsorption, the pore throat will gradually be reduced and eventually blocked [74]. The main factors governing the log-jamming effect are particle concentration and effective hydrodynamic size, pore size distribution, and flow rate [74].

A schematic is shown in Figure 2-14 to illustrate various types of retention in porous media.

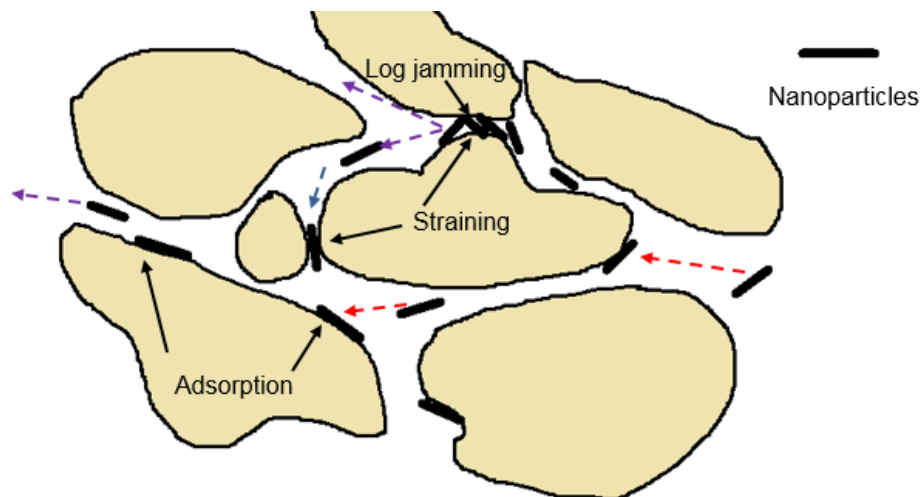


Figure 2-14 Illustration of different type of retention: adsorption, straining and log jamming (Inspired from [74])

Sand packed columns are commonly used to investigate CNT transport and retention abilities in porous media [75]; as it is in this study. This methodology reflects many characteristics of the actual reservoir and is therefore able to

provide information that is directly relevant to real-world conditions [71, 76]. Studying the implications of CNTs presence on the porous media and its environment is important. Indeed, the injection of nanoparticles can modify the permeability and porosity of the porous media. Yuan et al. [77] concluded that straining is the dominant effect in permeability impairment, thus minimising straining and optimising adsorption will improve the permeability of the porous media.

Hendraningrat et al. [78] investigated the possibility of using nanofluids for oil and gas applications in low and medium permeability reservoir rocks and investigated acceptable nanofluid concentrations. One of the key conclusions from this was that retention of nanoparticles inside core plugs induced porosity and permeability impairment.

The transport of MWCNTs in laboratory porous media experiments is known for breaking through in the 1st pore volumes injected. Figure 2-15 illustrates a quick breakthrough of the carbon nanotubes over a small pore volume within a sand packed column. The experiment consisted of passing 4.5 PVs of MWCNTs, followed with 4.5 PV of brine [79]. COOH-MWCNTs concentration ratio of the concentration coming in over the concentration coming out (C/C_0) as a function of pore volumes (time). It is evident that a small quantity of CNTs is being retained in the porous media as C/C_0 ($C/C_0 = 0.75$) does not reach 1.

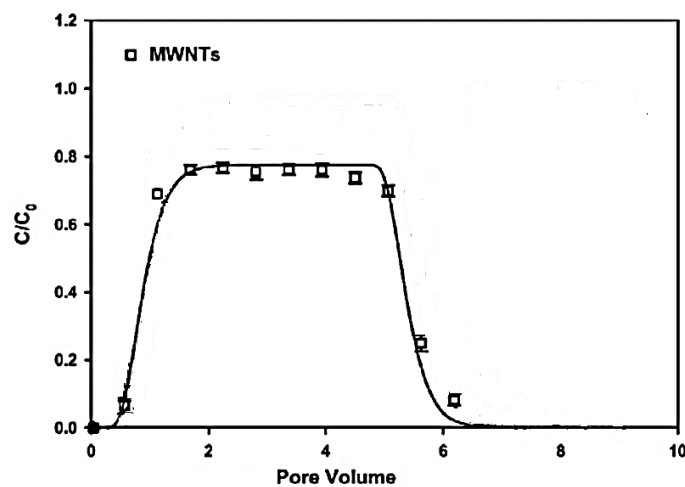


Figure 2-15 Breakthrough of MWCNTs in porous media [79].

The sorbing capabilities of an untreated porous media are naturally low. Hence, a catalyst such as silane is used in this study to cause the adsorption of MWCNTs onto the porous media, as this is an important step of NAST.

2.3.5. Adsorption Properties of CNTs

The adsorption of heavy metals as well as polymeric and organic compounds onto CNTs has been investigated thoroughly in last decade [71]. It is a great adsorbent because of it is has great physical properties (large surface), and chemical properties (great attraction properties to ions). One of the main motivations is to assess if CNTs could be utilised as strong adsorbents to adsorb polymers, organics and heavy metals from water or wastewater. CNTs as adsorbents may be applicable to be incorporated in fixed beds, and systems of treatment facilities[71].

For example, Rouhi [80] reported CNTs with larger diameter had the ability to better adsorb polymer chains on CNTs than their smaller counterparts. A large diameter typically implies that there more graphene layers, which improve the mechanical and electronical properties of tubes and create a stronger interaction with the polymer.

Lu [81] showed that the specific adsorption capacity of MWCNTs (used as received) and functionalised CNTs for Zn^{2+} was significantly greater than that of powdered activated carbon, char and lower than activated carbon.

Likewise, Cho et al. [82] as well as Li et al.[83] demonstrated that the surface functionalisation and presence of defects on CNTs had note-worthy effects on their ability to adsorb metallic contaminants, the more defects and functional groups the higher the adsorption capacity. Carboxyl groups have shown to have a particularly strong adsorption ability for divalent metallic cations. This is of great interest for NAST because Ca^{2+} is known for enhancing the adsorption of scale inhibitors [59].

2.3.6. Nanotechnology Assisted Squeeze Treatment (NAST)

Oil reservoirs have pores in the order of micrometres to nanometres, so nanoparticles are able to enter a certain range of oil reservoirs and also according to thermal conditions and the dynamic energies changes in the reservoir, nanoparticles may or may not stay stable [60]. Against the aforementioned, a background and a detailed methodology of the NAST methodology will be explained.

The goal of NAST is to develop steps that can be applicable to a diverse array of oil wells [6]. Adsorption squeeze treatment is the most desired method for squeeze treatment. There are 3 main determinants of adsorption:

- Characteristics of adsorbate (Scale Inhibitor)
- Solution properties (temperature, composition, pH)
- Adsorbent characteristics (CNTs and porous media)

Scale inhibitor properties were revealed well before first being used in the oil field. The appropriate scale inhibitor is selected based on the reservoir conditions and the purpose [29].

The concept behind NAST is to improve the adsorption of scale inhibitor in order to increase squeeze lifetime [6]. This is achievable by altering the rock surface by retaining CNTs onto it. The retention of the carbon nanotubes is achievable due to a prior treatment that makes the rock surface able to adsorb CNTs. The real benefit and potential of this system is that it theoretically is versatile to function in various reservoirs of various physicochemical compositions. NAST is broken down in 2 main steps described in Figure 2-16.

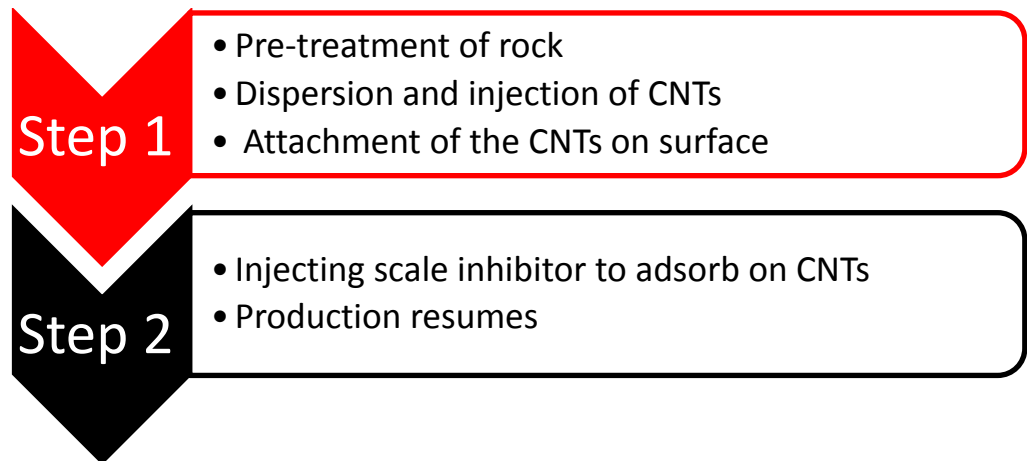


Figure 2-16 Two Main Steps of NAST

Step 1/NAST1: Pre-treatment of the rock to adsorb CNTs.

The 3 components in the first step are described in Figure 2-16 :

- Pre-treatment of rock with 3-aminopropyltriethoxysilane
- Injection and dispersion of CNTs
- Attachment of the CNTs on surface

Stage 1: Pre-treatment of rock surface with 3-aminopropyltriethoxysilane

In order to functionalise the quartz surfaces, 3-aminopropyltriethoxysilane (organosilanes) is used to create a “sticky-like” surface so that COOH-MWCNTs can adsorb on the surface. The reaction of organosilanes with substrates can be divided into 4 components [6]:

1. Hydrolysis of alkoxy groups to silanol
2. Condensation of oligomers,
3. Hydrogen bonding between oligomers and hydroxyl (OH) groups on the surface.
4. Creation of covalent bonds when water flushes out.

Also, one of the hydrolysed alkoxys normally reacts with OH, and the other two remain in condensed form (Figure 2-17).

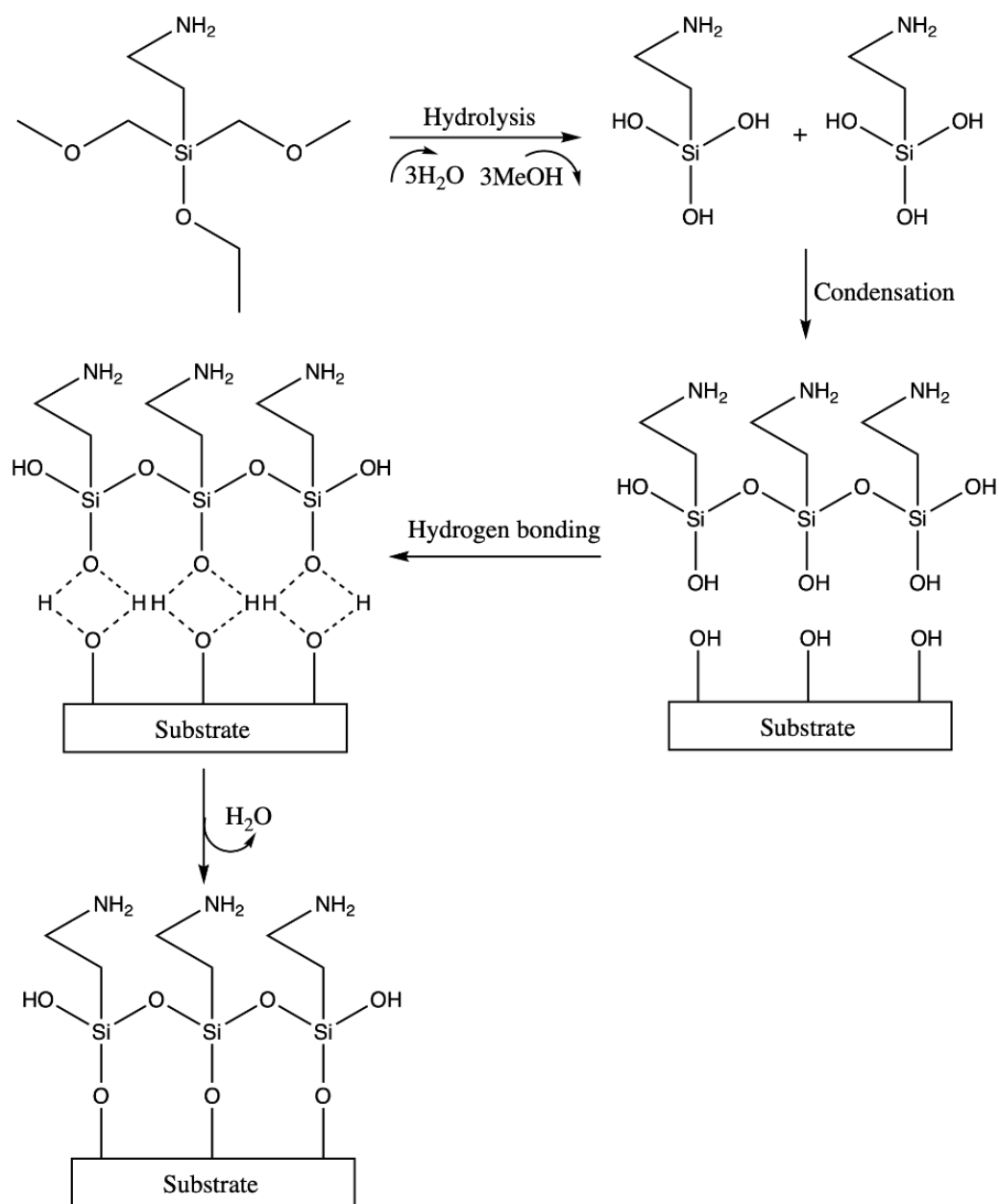


Figure 2-17 Reaction of organosilane on substrate surface [6]

Stage 2: Injection and dispersion of CNTs

CNTs are often placed in surfactants or solvents. CNTs are sonicated for a desired time, during which they are disaggregated from each other using a sonicator which helps overcoming van der Waals interactions between COOH-MWCNTs [84]. Dispersants interact with the CNTs to detangle them by

electrostatic and/or steric repulsion between [61, 84, 85]. Although the concentration and the type of dispersants are the main factors for dispersion of CNTs, the purity of CNTs can play an important role [84]. CNTs can be dispersed in both ionic and non-ionic solutions such as DMF, sodium ndodecylbenzene or Tween 80. Among the many available dispersants, Tween 80 is commonly reported for dispersion of CNTs [86-88]. Indeed, Tween 80 is one of the most efficient surfactants available to keep a stable dispersion of COOH-MWCNTs. DMF was a dispersant used for the previous methodology [6], however, the study herein replaces DMF with Tween 80 as it has proven to be a dispersant that is environmentally friendly in comparison to DMF.

Tween 80 or polysorbate 80 is a non-ionic and organic surfactant. The surfactant molecules attached to the MWCNTs are merely charged; this explains the reason for a low zeta potential [86, 87] (See later in 5.2.3). Furthermore, when dispersed, the double layer electrostatic force from one nanotube to another becomes much lower. When the hydrophobic tails (hydrocarbon chain) of the surfactant molecules from the coated graphene sheets of the MWCNTs interact, the steric repulsion force play an important role for keeping a steady dispersion [86].

Stage 3: Attachment of the dispersed CNTs on the pre-treated surface

Attachment of CNTs onto 3-aminopropyltriethoxysilane functionalised surfaces has been demonstrated repeatedly in previous research [89-92]. The method used in NAST is innovative and requires the purchase of functionalised carboxylated carbon nanotubes. Theoretically, carboxylic groups on CNTs interact with the -NH₂ groups (possibly because of prior 3-aminopropyltriethoxysilane functionalisation) via hydrogen bonds and this causes the attachment of the COOH-MWCNTs onto the surfaces (Figure 2-18) [6]

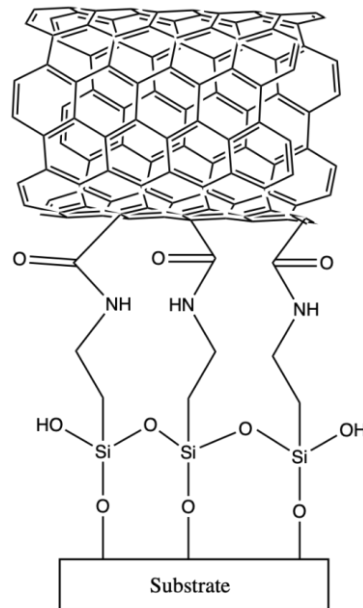


Figure 2-18 Schematic of CNTs attached to surface via organosilane bond [6]

Step2/NAST2: Investigation of adsorption and desorption of PPCA

This step consists of investigating the adsorption and desorption of scale inhibitors (PolyPhosphino Carboxylic Acid). Together, this demonstrates the potentiality of CNTs to be employed for enhanced oil recovery with a regular squeeze treatment. The investigation is done through of analysis of effluents coming off the sand pack column.

The previous study of NAST showed promising results [6]:

- The adsorption of PPCA on CNTs can possibly reduce the 24-hour shut-in period, and consequently reduce production loss.
- Adsorption of PPCA on CNTs is sensitive to the mass of CNTs.
- PPCA adsorption percentage increases as the mass of CNTs increases; studies showed that adsorption reach a plateau at 60% of PPCA adsorbed.
- Desorption was shown as slow, enhancing squeeze lifetime since only 1-20 ppm is necessary to inhibit scale formation.

- Calcium ions have shown to increase adsorption of PPCA (mg/g) on CNTs.

2.3.7. Summary and Scope of Study

The formation of calcium carbonate scale has been described earlier. Calcium carbonate build up is known to cause major flow assurance problems for the oil and gas industry. One major method to ensure a good flow assurance is squeeze treatment. This method requires injecting scale inhibitors downhole, through a porous media, the scale inhibitor then retains/attaches on the rock formation and it slowly desorbs into water to prevent scale formation. In order to assess and track the scale inhibition performance of a squeeze treatment, the use of “return profile”, a measurement of the scale inhibitor concentration decreasing from the rock formation surface, is required. This provides information regarding the minimum inhibitor concentration level and squeeze lifetime. The inhibitor performance and adsorption are mainly dependent on the experimental or field parameters (e.g., pH, temperature, salinity, ions) and the surface chemistry and absorbing minerals (e.g., silica sand, kaolinite, carbonate stones).

The NAST methodology described in section (2.3.6) has shown to be a potential application for the oil and gas industry. Where:

- In distilled water, it can be seen to improve retention of inhibitor at the surface of a rock in a squeeze treatment.
- Calcium ions enhance the adsorption of SI on CNT treated sand.
- The transport of CNTs through porous media proved to be unsuccessful in a few cases; however, the reasons of failure were not investigated, though effective dispersion of Multi Walled Carbon Nanotubes seemed to be an issue.

Therefore, this study aims to provide experimental data for inhibitor/brine/temperature/CNT interactions. These will be performed in static adsorption tests alongside the sand pack and coreflood experiments.

Initially this work will focus on static adsorption tests to further understand the adsorption process onto the CNTs. This will be followed by an investigation into the transportation of CNTs in porous media, specifically in terms of their ability to retain and their effect on permeability. Finally, dynamic tests will be performed with sand packs and corefloods, these results will provide further details regarding the feasibility of NAST in the field.

Chapter 3 Methodology

3.1. Introduction

A schematic displaying the experimental procedure used in this thesis is shown in Figure 3-1.

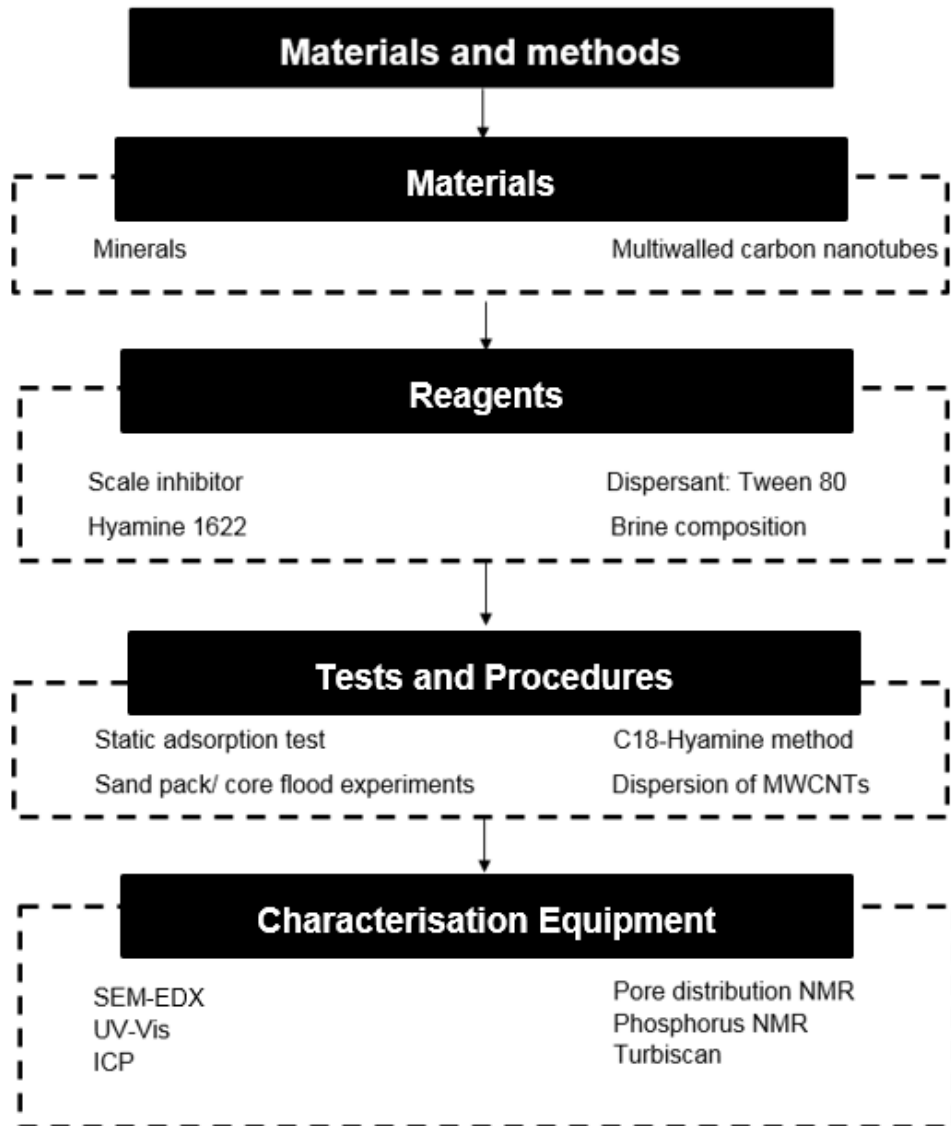


Figure 3-1 Overview of the experimental methodology chapter

The overarching objective of this thesis is to develop a study of the adsorption of PPCA on COOH-MWCNTs by deploying methodologies such as static adsorption tests or the use of Phosphorus Nuclear Magnetic Resonance (P-NMR). An additional goal is to obtain an initial understanding of the effects of transport and retention of COOH-MWCNTs on a silane-functionalised porous media. This was assessed by using the permeability impairment characterisations via pressure gauges, petrophysical Nuclear Magnetic Resonance NMR, Scanning Electron Microscope (SEM), and mass balance calculations obtained from the effluents concentrations measurements. Lastly, squeeze treatment simulations were performed to understand the behaviour of adsorption and desorption of polymeric scale inhibitor in dynamic conditions by the use of sand pack, core flooding experiments and concentration measurements according to the C18-hyamine method.

3.2. Materials

3.2.1. Minerals

3.2.1.1. Silica sand and kaolinite

Silica sand was chosen as an adsorbent for sand pack experiments because it is representative of sandstone rock composed of quartz (SiO_2). It has an average diameter of 0.2 mm (200 μm). Silica is considered a moderately adsorbent rock type for inhibitor adsorption (See Section 2.2.7). It was mixed with kaolinite, a clay mineral of hydrous aluminum silicates, which has an average diameter of 10 to 30 μm . Silica and kaolinite were mixed in the laboratory to mimic a more realistic representation of sandstones. Figure 3-2 and Figure 3-3 illustrate SEM pictures of the sand that was used in the experiments.

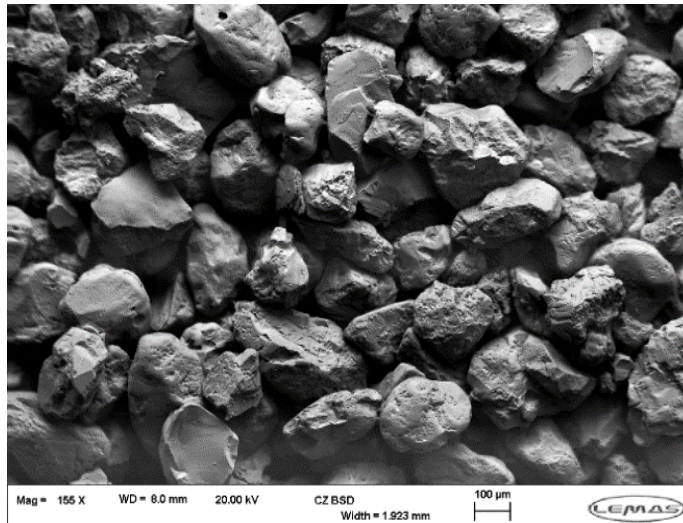


Figure 3-2 SEM picture of silica sand coated with kaolinite

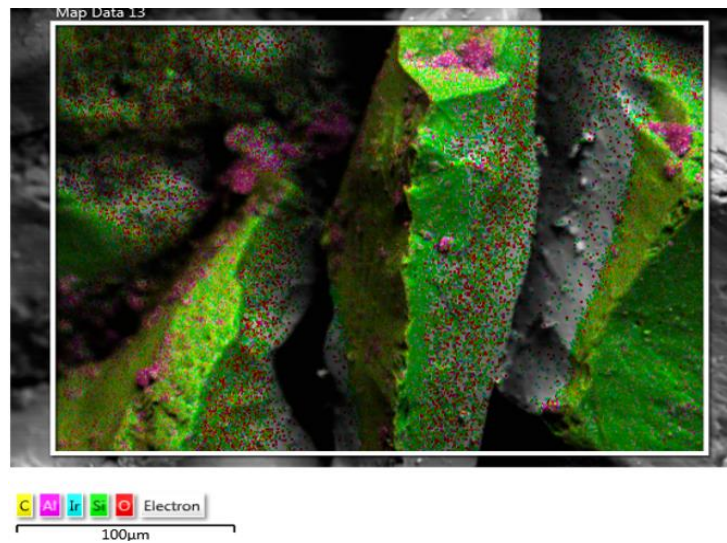


Figure 3-3 High magnification of SEM/EDX picture showing kaolinite (alumina) in purple

3.2.1.2. Saint Bees

Saint Bees rock is a red coloured sandstone which has an average of 69% quartz, 2% feldspar, 5% iron oxide, 5% clay and 19% porosity [93]. This rock was used for mini core flood tests, results are presented in Chapter 5. The rock was obtained from Marshall [94].



Figure 3-4 Illustration of Saint Bees sandstone [94]

3.2.1.3. Doddington

Doddington is a pink, medium grained sandstone. It has an average composition of 69% quartz, 5% feldspar, 2% iron oxide; 5% clay and exhibit a porosity of 19% [93]. This rock was used for mini core flood tests and core flood tests, results are presented in Chapter 5 and 6. The rock was obtained from Marshall [94].



Figure 3-5 Illustration of Doddington sandstone [94]

3.2.1.4. Darney

Darney is a yellow-buffed coloured, medium grained sandstone. It has an average of 73.5 % quartz composition, 1.5% feldspar, 1 % iron oxide,6% clay and average porosity of 18% [93]. This rock was used for mini core flood tests, results are presented in Chapter 5. The rock was obtained from Marshall [94].



Figure 3-6 Illustration of Darney sandstone [94]

3.2.1.5. Stanton Moore

Stanton Moore is a fine grain sandstone, it has an average porosity of 14%. It is a sandstone that is composed of 73.5% quartz, 3.5% feldspar, 2% iron oxide and 7% clay [93]. This rock was used for mini core flood tests, results are presented in Chapter 5. The rock was obtained from Marshall [94]



Figure 3-7 Illustration of Stanton Moore sandstone [94]

3.2.2. Carbon Nanotubes

According to the manufacturer, the purity of the MWCNTs exceed 95% by weight. The multi-walled carbon nanotubes (MWCNTs) have a length ranging from 0.5–2.0 μm . The outer diameter of the MWCNTs is below 8.0 nm. They were purchased from Cheap Tubes Inc. This classifies the particles within the

range of short MWCNTs. These MWCNTs are sold as carboxylated functionalised.

3.3. Reagent

3.3.1. Scale inhibitor: Polyphosphino carboxylic acid

PPCA is a polymeric SI. It is a commercial product commonly used in oilfield applications; the product used was delivered by BWA Water Additives. PPCA is ranked as a polyelectrolyte monomer. It has an active concentration of 42% and molecular weight of 3600 g/mol. The structure of the chemical inhibitor is represented in Figure 3-8.

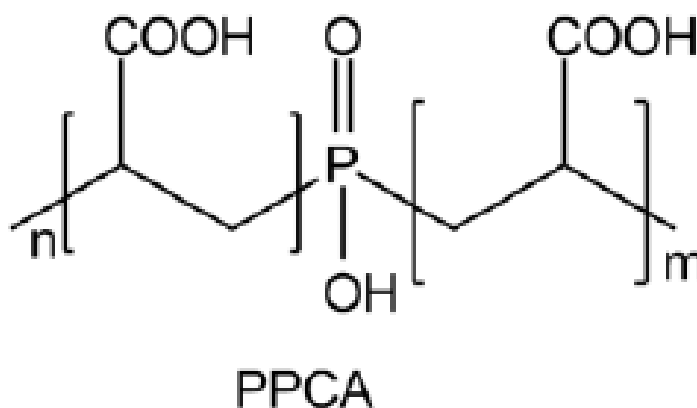


Figure 3-8 Polyelectrolyte PPCA [1]

3.1.1. Brine : Nelson Forties Formation Water

The brine composition used in this study is the Nelson Forties formation water commonly used for SI adsorption test and dynamic tests [49]. The brine was created within University of Leeds laboratory.

Table 3-1 Synthetic Formation Water Composition [49]

Ion	Chemical Formula	Mass (mg/L)
Na^+	$NaCl$	31275
Ca^{2+}	$CaCl_2 \cdot 6H_2O$	2000
Mg^{2+}	$MgCl_2 \cdot H_2O$	739
K^+	KCl	654
Ba^{2+}	$BaCl_2 \cdot 2H_2O$	269
Sr^{+2}	$SrCl_2$	771
Cl^-		50000

3.1.2. Dispersant Tween 80

Polysorbate 80 also known as Tween80, $C_{64}H_{124}O_{26}$, is a viscous, water-soluble non-ionic and non-toxic surfactant, containing hydrophilic polyoxyethylene sorbitan head groups and its tail is composed by monooleate or commonly known as oleic acid, a hydrophobic alkyl group. Its molecular weight is 1310 g mol^{-1} [95]. A structure of the chemical surfactant is represented in Figure 3-9. The dispersant has been bought from Sigma-Alrich.

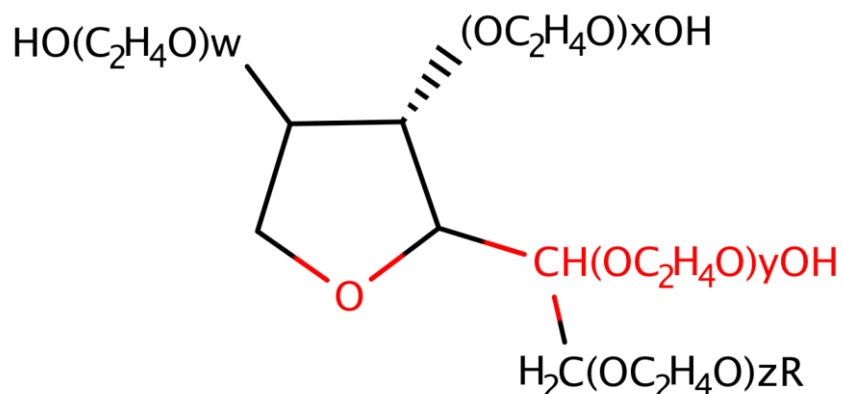


Figure 3-9 Polysorbate 80 chemical structure

3.1.3. Hyamine 1622

Hyamine 1622 is a cationic detergent composed of benzethonium chloride. It is used to measure the concentrations of inhibitor within the solutions produced from dynamic and static experiments. This is explained with more details in section 3.4.1.

3.4. Test Method and Procedures

Test method and procedures are categorized in relation to the three main streams described in the introduction. Literature relevant to each experimental method is discussed.

3.4.1. C18-Hyamine Method

Sep-Pak C18 are a single use disposable cartridge containing an octadecylsilane ($\text{Si}(\text{CH}_3)_2\text{C}_{18}\text{H}_{37}$) bonded phase packing material. When using these cartridges with aqueous solutions, it is necessary to pre-wet the cartridge with a water miscible solvent such as methanol, then flush with water before use [29, 59, 96]. The C18 cartridge adsorbs neutral/hydrogen bonding

species strongly, but does not adsorb charged species. Thus, in order to adsorb, the inhibitor must be in an un-charged state. To achieve this, the pH of the PPCA inhibitor solution is reduced to a level of 1.5–2.0. At these low pH levels the inhibitor is effectively in the uncharged acid form. On passing through the C18 cartridge under such conditions, the inhibitor is adsorbed and effectively separated from the interfering salts, which are charged and thus do not adsorb. The inhibitor can then be eluted from the cartridge free from the interfering salts prior to colorimetric analysis [59, 96]. A step by step guide is described in Appendix C. A calibration curve showing the correlation with absorbance and PPCA concentrations calculated via C18-hyamine method is shown in Figure 3-10.

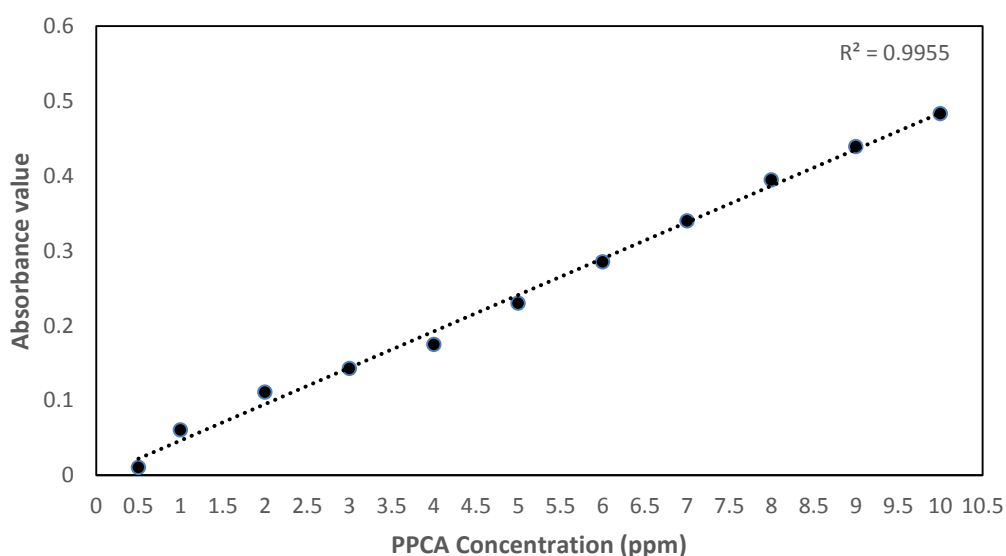


Figure 3-10 Linear regression relating concentrations of PPCA to absorbance values to produce calibration curves to measure PPCA concentrations via C18-hyamine method using UV-Vis spectroscopy at 500 nm

3.4.2. Procedure for Dispersing COOH-MWCNTs in a solution

As previously mentioned, Tween 80 was used in this research as a dispersant. The experimental method to disperse the COOH-MWCNTs followed others found in literature [86, 87].

COOH-MWCNTs were added to 1.5% polysorbate 80 mixed with distilled water, then placed in an ultrasonic bath for 2 hours. After this step, the solution is normally well dispersed. The dispersion was also evaluated by the use of DLS and Turbiscan analysis. Results are shown in sections 5.2.3 and 5.2.4.

3.4.3. Measurement of COOH-MWCNTs concentration

The COOH-MWCNT concentration in a given suspension was determined by measuring its UV-Vis absorbance at 500 nm. Control studies showed good linear relationships ($R^2 > 0.9957$) between absorbance at 500 nm and mass concentrations for the COOH-MWCNTs using this method – see Figure 3-11.

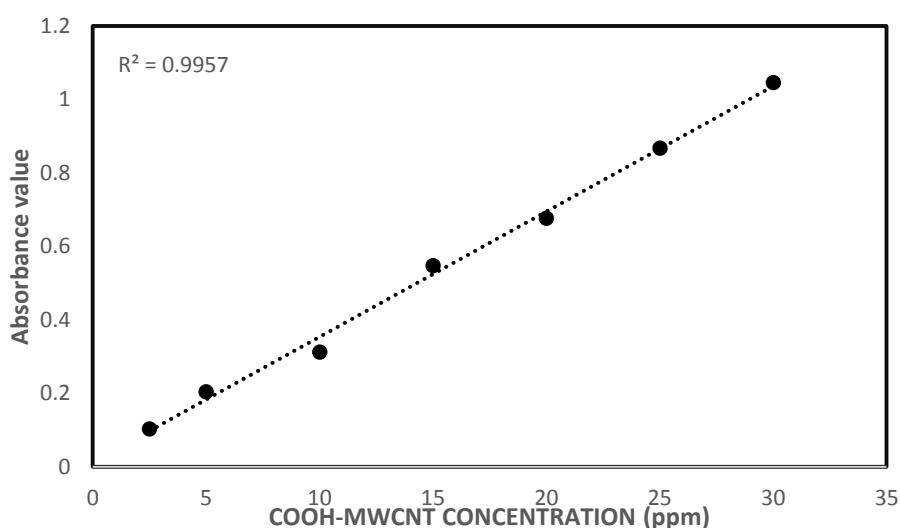


Figure 3-11 Linear regression relating concentrations of COOH-MWCNT to absorbance values to produce calibration curves to measure COOH-MWCNT concentrations using UV-Vis spectroscopy at 500 nm

3.4.4. Static Adsorption Tests

Static adsorption tests consist of immersing a sample in a specific solution. In this case, COOH-MWCNTs were used as adsorbent, and the powder was weighed with an analytical balance (Mettler Toledo XPR). Scale inhibitor solution was the adsorbate. COOH-MWCNTs powder mass was selected based on dynamic experiment results (presented in Chapter 5) show that the average amount of COOH-MWCNTs retained onto the rock matrix is between 4 to 10 mg and the pore volume of the sand pack is approximately 10 mL. The static adsorption experiments were designed using various masses of carbon nanotubes ($m = 4, 6$ and 10mg) at a fixed volume ($V=10$ mL) of scale inhibitor solution. The experiments were carried at the following range of PPCA concentrations: 100, 500, 1000, 2500 and 5000 ppm. The experiments were designed this way to develop a study of adsorption of PPCA onto COOH-MWCNTs.

For the pH value test and the adsorption rate test, a ratio of 4 mg of COOH-MWCNTs for 10 mL of 5000 ppm of PPCA solution and 40 mg of COOH-MWCNTs for 100 mL of 5000 ppm of PPCA solution were chosen, respectively.

All experiments were carefully timed from the moment the adsorbent and adsorbate were in contact for a timed period of 6 hours unless stated otherwise. During the experiment period, the solution was ultrasonicated. The final solution was analysed by the C18-hyamime method before and after experiment in order to quantify the concentration of SI adsorbed after 6 hours onto COOH-MWCNTs.

The amount of SI attached to CNTs can be calculated using the expression:

$$\Gamma_{\text{app}} = \frac{v(c_0 - c_f)}{m} \quad (3.1)$$

Where: I_{app} is in mg/g, c_0 is the concentration in ppm or mg/L, c_f is the concentration in ppm or mg/L, m is the mass of mineral in grams (g), v is volume of the solution in L.

3.4.5. Experimental Methodology: Sand pack

Dynamic flood sand packs are created in order to simulate transport in porous media. In contrast to coreflood, which is designed to handle high pressure or high temperature experiments, sand packs are used for low pressure experiments and moderate temperatures environments. Sand packs are a first step toward a heightened study of the transport and reaction of a chemical specie with certain rock chemistries. For this study, sand packs were created to understand the transport and retention properties of COOH-MWCNTs in a silane-functionalised porous media and study the adsorption of PPCA SI onto the porous media using the NAST methodology. Determining the PPCA concentrations from the effluents will provide information on adsorption of SI onto porous media and desorption off the porous media. Ion interaction was also investigated once with ICP. These data will complement previous NAST data [6].

3.4.5.1. Brief description of experiment

The sand pack is designed to carry low pressure flooding experiments. The main components are a sand column, a pump to flush the brine through the porous media and a sample collector (see Figure 3-12). The sand pack is made from polycarbonate that enables a clear view of the packing. The column is made has an inner diameter of 20mm and outer diameter of 24mm and has a packing length of 10 cm. An unconsolidated packing method is selected because it allows a straight forward way to squeeze the sand uniformly across the sand pack. The fluids injected are flushed through the porous pack using a peristaltic pump (Ismatec ISM596), and the fluids that exit are collected in a fraction collector that rotates by regular time intervals.

The concentration of SI at the outlet is analysed by hyamine method in order to be able to create a return curve.

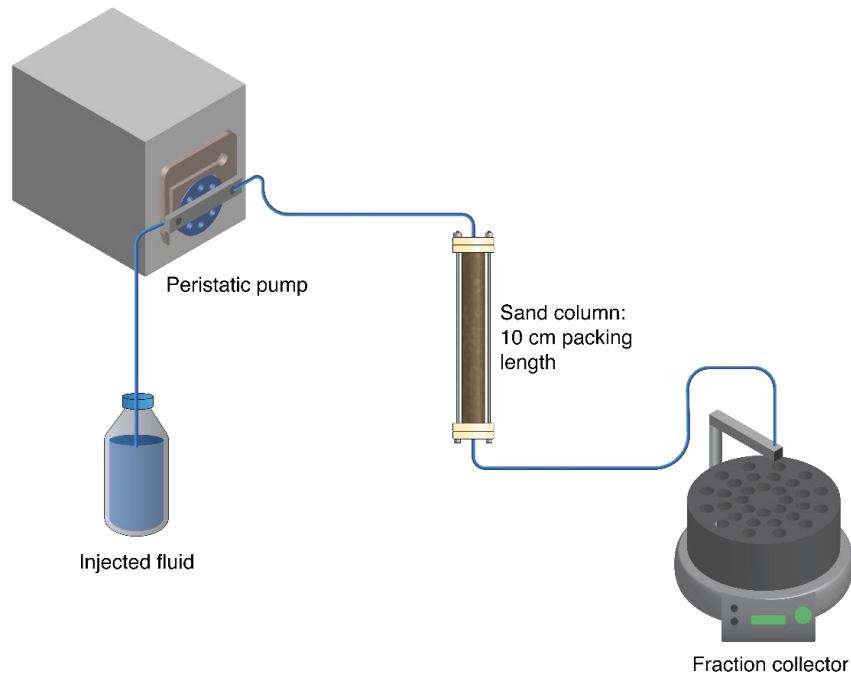


Figure 3-12 Schematic diagram of the sand pack setup

3.4.5.2. Sand Packing

Final column packing and preparation of the columns were done by using a dry pack method. This sand packing technique was selected so that each sand pack made have repeatable properties such as porosity and permeability.

A mesh (Spectrum, stainless steel, 51 microns) is placed on top of the bottom end cap, so the sand only remains in the sand pack and does not fill empty spaces in caps (i.e. the flow channel connecting to wires of pump). The sand is poured in the sand pack column through a funnel. An electric engraver (Burgess model 74) (Figure 3-13) adapted for the sand packing, is used to create vibrations on the sand pack to help pack the sand.



Figure 3-13 Electric engraver is used to settle the sand down in column thanks to vibrations provided by the machine

Once the columns has been filled with the sand at the top, and settled down optically, the top cap is then screwed in. A piece of mesh is also used at the top to ensure that sand remains in the main column and does not fill space in the caps. When the sand is packed, sand movement should not be detectable (by sight) if the column is shaken as shown in Figure 3-14.

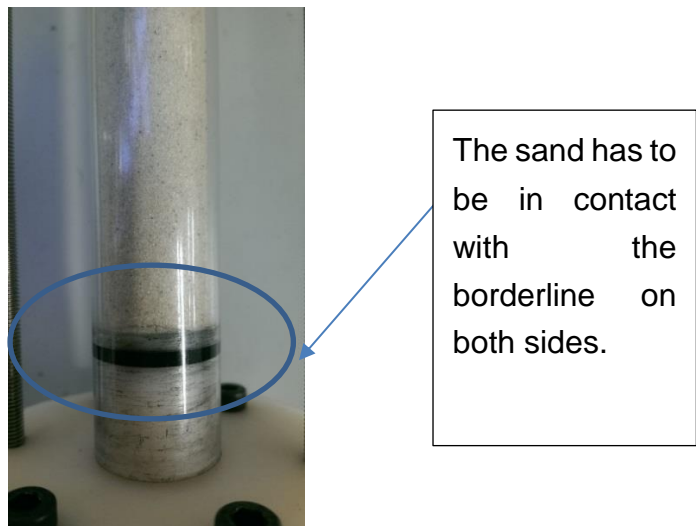


Figure 3-14 The packed sand has to be in contact with the borderline stoppers. If the column is shaken, no movement should be detectable on both ends of the packing. If movement is detected, then the packing is considered unsuccessful.

3.4.5.3. Sand Pack Characterisation of Permeability and Porosity

An average of four sand pack characterisations are shown in Table 3-2 below to prove repeatability and validate the robustness of the methodology.

Table 3-2 Sand pack parameters

Sand Pack ID	Sand Pack ID
Length (cm)	10.00 ± 0.00
Diameter (cm)	2.00 ± 0.00
Dead volume (mL)	1.40 ± 0.00
Pore volume (mL)	11.23 ± 0.03
Pore volume - Dead volume (mL)	9.83 ± 0.03
Bulk Volume (mL)	31.40 ± 0.00
Porosity (%)	31.29 ± 0.08

3.4.6. Experimental Methodology: Coreflood

A schematic of the core flood is shown in Figure 3-15. The core block section consists of Hassler type of core holder and data acquisition units for pressure. The core was held with a confining pressure of approximately 1000 PSI (6894.76 KN/m²) Differential pressure was taken using OMEGA PX409, ranging from 0-150 PSI (0-1034.21 KN/m²). The downstream section is responsible for collecting the effluent and maintain back pressure for the whole set up. The fluids injected are flushed through the porous pack using a peristaltic pump (Ismatec ISM596), and the fluids that exit are collected in a fraction collector which is capable of rotating by regular time intervals.

Doddington rock was selected for the main core flood experiment. This rock is comprised of 69% quartz, 2% feldspar, 5% iron oxide, and 5% clay, and was obtained from the Wolfson Laboratory, University of Leeds.

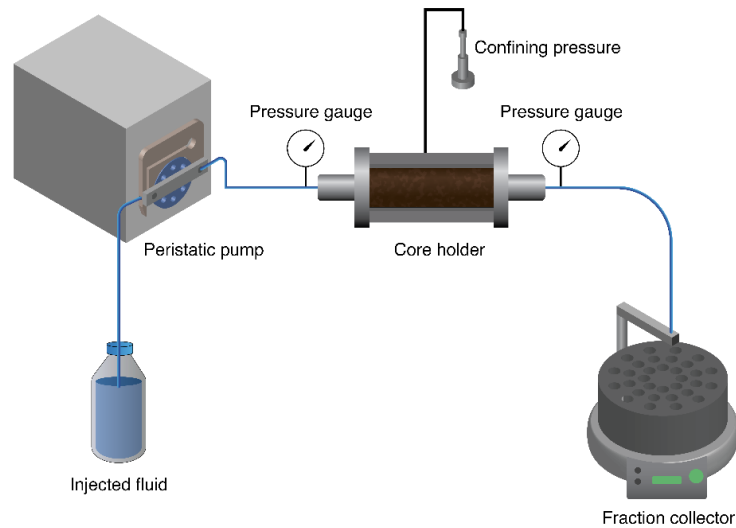


Figure 3-15 Schematic diagram of Hassler type Coreflood used for this study

Porosity (amount of available space within rock) and permeability (ability to fluid through a porous media) characterisation are two critical aspects to consider when performing a coreflood. Two cores were used for this study. These cores demonstrate moderately high permeabilities as shown in Table 3-3, Doddington rock was selected based on pressure profiling tests with in house designed and manufactured pressure cells, see section 3.4.7.

Table 3-3 Core flood parameters: Initial comparison of rock cores before experiment

Core ID	Pore volume	Porosity (%)	Permeability (mD)
A (Conventional)	5.16	17.46	185
B (NAST)	5.65	18.68	193

3.4.7. Experimental Methodology: Mini Core Pressure Cells

One of the aim of the NAST methodology is to create a method that can be widely applied, in as many reservoirs as possible. Better understanding the limitations of transportation of the dispersed COOH-MWCNTs in rocks of various permeability will help narrowing the types of reservoir where NAST could currently be deployed. For this issue, a pressure cell was designed to carry out tests. The core plugs dimensions were averagely of 13.23 mm length, 14.01 mm width and 15.04 mm height. Pressure profiles were taken using OMEGA PX409 pressure gauges, ranging from 0-150 PSI (0- KN/m²).

These tests were designed to select an adequate rock for the coreflood. The pressure drop across the core was recorded during the injection process. All cores were silane functionalised, to better characterise adsorption under the use of the NAST methodology. Cores were injected with a dispersed COOH-MWCNTs solution for a period of 5 hours. Permeability were calculated before and after experiments to obtain permeability impairment data.

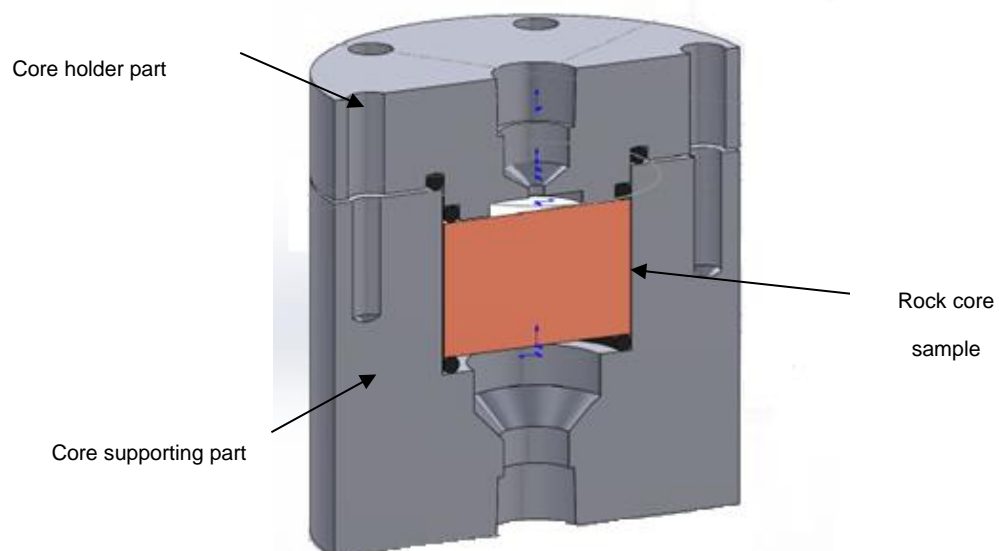


Figure 3-16 The schematic shows the mini pressure cell designed to test rocks of various permeabilities. The core holder is used to tightly seal the top during experiment. The core supporting is to keep the core in place, and in a steady position.

3.4.8. Experiment Parameters

Conventional squeeze and NAST methodologies were adapted for laboratory simulations. Experiments were performed either at room temperature (25°C) or 50°C in sand packs or coreflood set ups. All tests were done at a flow rate of 20 mL/hour.

3.4.8.1. Conventional Flood: Coreflood and sand pack methodology

The following procedure that was used for the conventional method followed the following procedure:

10 pore volume (PV) of brine is injected into the core to pre-condition the core. This step allows to prepare the porous media to retain SI more efficiently. Then, 10 PV of PPCA in brine was injected into the core and samples were taken from the effluent (produced brine) to be measured via the C18-hyamime method. This step gives data about the adsorption process. The core was shut in for 12 hours to allow the scale inhibitor be adsorbed onto the porous media more efficiently. The brine is then injected into the core and samples are collected and samples are taken to be analysed by the C18-hyamime method. This step gives detail about the desorption process of the inhibitor.

3.4.8.2. NAST flood methodology : Sand Pack and Coreflood

NAST methodology was used in sand pack and core floods. The NAST coreflood methodology was separated in two main parts:

- NAST1/Step 1: This step is about making the rock reactive so it can adsorb COOH-MWCNTs. The injection and retention of COOH-MWCNTs in the porous media is the key focus.
- NAST2/ Step 2: This following step is about the adsorption and desorption of scale inhibitor off the core material.

The NAST flood followed the subsequent the steps:

NAST 1/ Step 1: This step is about the injection and retention of COOH-MWCNTs in the porous media.

An injection of 10 pore volume (PV) of brine was flushed into the core to pre-condition the core. Then 5 pore volumes of ethanol was flushed to prevent silane to become immiscible with the brine in the media. 20 pore volumes of 3% (3-aminopropyl) triethoxysilane mixed with 90% ethanol and 10% distilled water was injected in the porous media. The core is then shut in for 2 hours. This step allowed to let the silane react with the porous media. The core was then flushed with ethanol for 10 PV to remove the unreacted silane. 10 ppm for core flood and 20 ppm for sand pack floods of dispersed COOH-MWCNTs were injected until the core was saturated. At this point, the core is shut in, so the COOH-MWCNTs can be adsorbed. The core was subsequently rinsed with 10 PV of distilled water to remove the unretained COOH-MWCNTs.

NAST 2/Step 2: This step is about the adsorption and desorption of scale inhibitor off the porous media.

The scale inhibitor solution was injected for 10 pore volumes to ensure saturation of the core. The core was shut in for a further 12 hours. The injection of the brine was done until the concentration of PPCA effluent coming out is less than 1 ppm. When the concentration of PPCA fell below 1 ppm, then on a few experiments, the PPCA was reinjected.

3.5. Equipment for Analysis

Equipments are required to analyse the results of this research project. Inductively Coupled Plasma-Mass spectroscopy (ICP-MS), Ultraviolet-Visible spectroscopy (UV-Vis), Scanning Electron Microscope (SEM), Thermogravimetric Analysis (TGA), Raman Spectroscopy, Nuclear Magnetic Resonance (NMR) and Phosphorus Nuclear Magnetic Resonance (P-NMR)

were used in this work. Brief description of these devices are briefly provided below:

3.5.1. Nuclear Magnetic Resonance

Petrophysical Nuclear Magnetic Resonance (NMR), or T_2 spin-lattice relaxation measurements, are used to investigate pore structures and fluid distributions within porous media [97].

In this process, Hydrogen Nuclei (protons) magnetic moment are excited and while relaxing they emit a signal at a radio frequency, which can be detected by NMR spectrometer. The protons diffuse to the pore wall where their spin has a high probability to be relaxed (Figure 3-17) [97]. The NMR relaxation times are closely linked to the volume and geometry of the water-saturated pore space [97].

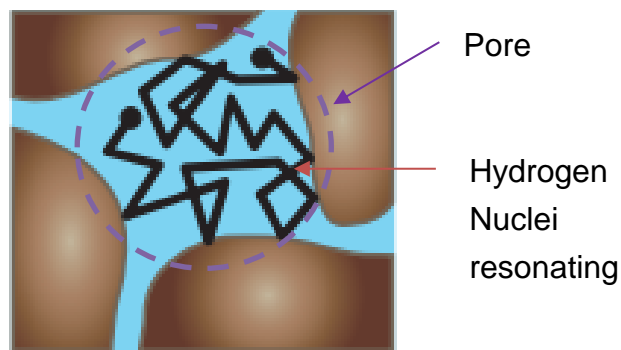


Figure 3-17 Hydrogen Nuclei resonating within a pore. The relaxation time T_2 taken by the Hydrogen Nuclei to resonate is related to the size of the pore [98]

The value of T_2 increases with the mobility of the molecules and the time required for the molecule to relax. Therefore, larger pores will relax more slowly compared to smaller pores, as shown schematically in Figure 3-18 [97].

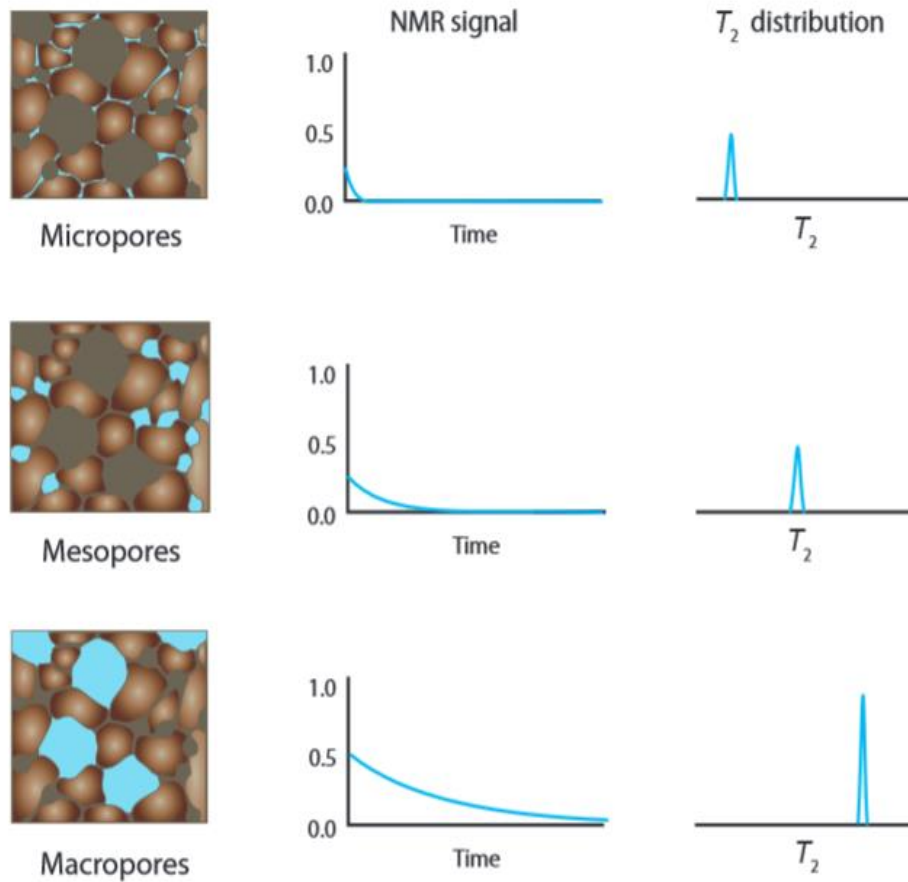


Figure 3-18 Types of NMR graphs. Classification of pore size distribution graphs of porous media ranging from microporous to macroporous [98]

The surface relaxation time is controlled by the surface-to-volume ratio as given by the equation below :

$$\frac{1}{T_2} = \rho \quad (3.2)$$

Where ρ the surface relaxivity is measured in microns per second, S is the pore surface area in squared meter, and V is the pore volume in L (S/V is the pore size), and T_2 is the surface relaxivity measured in milliseconds. The surface relaxivity value is required to convert relaxation time distributions to pore-size distributions or fluid distributions at partial saturations.

3.5.2. Inductively Coupled Plasma Mass Spectroscopy (ICP-MS)

ICP-MS is an effective tool to measure several metal and non-metal ion in water originating from natural processes, experiments or industry. In the oil and gas industry, many laboratories use this technique to determine the composition of ion in oilfield brines [49]. In this work, ICP will be used for the analysis of cation brine analysis.

3.5.3. Ultra-Violet Visible Spectrophotometer

Ultraviolet-visible spectroscopy (UV-Vis) refers to absorption spectroscopy or reflectance spectroscopy in the ultraviolet-visible spectral region. UV-Vis can be used to determine the concentration of a solution. A Hach DR6000 was used as the Ultraviolet Visible spectrophotometer. It was used to measure concentrations of inhibitors via the hyamine method and dispersed CNTs at a spectrum of 500 nm.

3.5.4. Scanning Electron Microscope and Energy Dispersive X-ray Analyzer

In a Scanning Electron Microscope (SEM), an electron beam impacts the sample to interact with the atoms of the surface in order to produce signals. These signals contain information about the topography and composition of the substrate. The Energy Dispersive X-ray analyzer provides elemental and quantitative information about the composition of the substrate being analysed.

There were 2 SEMs used within this study. A low resolution SEM Carl Zeiss EVO MA15, with an 80mm² XMax SDD EDX detector running Aztec software. It is normally run at 20 kV, for both imaging and EDX. A high resolution Hitachi SU8230 SEM was also used. It normally runs at 2kV and EDX at 15 kV.

3.5.5. Thermogravimetric Analysis

The main purpose of thermogravimetric analyses (TGA) is to observe the thermal stability of the samples with regard to the temperature. The process is performed by two pans inside the TGA, a sample pan and a reference pan with thermocouples at the bottom of each pan to measure the temperatures. TGA can quantify the mass of metal impurity and the functional group on CNTs. A Mettler Toledo TGA-DSC1 was utilized in this work. CNTs are stable up to $\sim 600^{\circ}\text{C}$ depending on types of CNTs and gas environment. CNTs are heated in air up to 1000°C and the weight loss is measured in order to understand how pure the CNT is. The experiment carried was performed at temperatures ranging from 25 to 1000°C and a heating rate of $40^{\circ}\text{C}/\text{min}$.

3.5.6. Raman Spectroscopy

Vibrational and rotational frequency of the carbon-atom based materials can be investigated by Raman spectroscopy. The phonon and electronic properties along with defects of CNTs are featured by Raman spectroscopy, which relies on inelastic scattering of monochromatic light. The laser light interacts with molecules to excite an electron from the valence band to the conduction band energy. Afterwards, phonons will be absorbed or released once the excited electrons are scattered. A photon will then be emitted in order to relax the electron in the valence band, which results in changing the energy of the photon [6].

Different features of CNTs are defined by Raman spectroscopy. In the case of this thesis it was used to quantify the concentrations of CNTs in solution. The calibration curve can be seen in Figure 3-19. The analysis of dispersed CNTs with Raman was done by Omotayo Ikwue (Reseracher at University of Leeds). An important advantage of Raman is that CNTs are quantifiable below 2.5 ppm and detectable up to 0.5 ppm, a property not offered by UV-Vis.

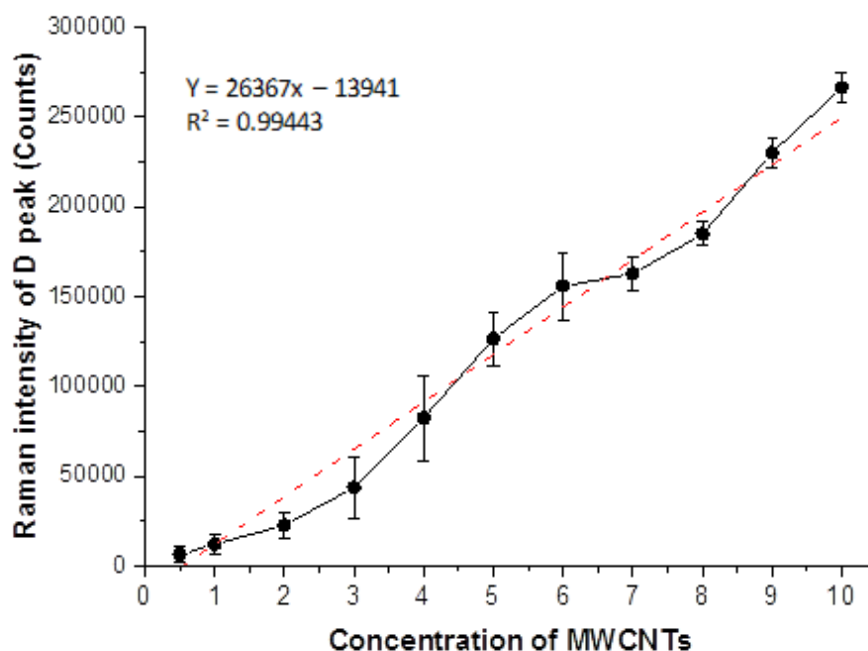


Figure 3-19 Linear regression relating concentrations of COOH-MWCNT to the count of Raman intensity of D peak values to produce calibration curves to measure COOH-MWCNT concentrations using Raman Spectroscopy

3.5.7. Turbiscan

The stability of the presumably dispersed COOH-MWCNTs was assessed with Turbiscan Lab Expert type stability analyser manufactured by Formulacion (France). The backscattering (BS) of a pulsed near-infrared light ($\lambda = 880 \text{ nm}$) scanned the samples from the bottom to the top. It measured the percentage of transmission through the samples as a function of the height of the tube, in order to quantify the rate of destabilisation [99].

Turbiscan accounts for all the processes taking place in the sample (particle agglomeration and settling process). The larger the shift in measurement, the more unstable the solution is.

In this study, two COOH-MWCNTs solutions of 10 ppm were placed into cylindrical glass tubes and submitted to analysis by the Turbiscan Lab Expert type stability analyser. Turbiscan was used to scan along the height of the different dispersed COOH-MWCNT sealed in the tubes at two different temperatures for 24 h.

3.5.8. Phosphorus 31 Nuclear Magnetic Resonance

Phosphorus 31 Nuclear Magnetic Resonance (P-NMR) is used to determine the presence of phosphorus of a chemical compound. The samples were sent to Durham for analysis.

3.5.9. Transmission Electron Microscopy

Transmission electron microscopy (TEM) is a scattering spectroscopy imaging technique that is able to depict the morphology of the carbon nanotubes at the sub-nanometre scale. For this study, TEM images were obtained on a FEI Titan Themis Cubed 300 operated at 300 kV. The COOH-MWCNTs sample was prepared by suspending a small amount of powder sample in methanol, followed by ultrasonication for 5 min. One drop of this suspension was placed on a carbon-coated copper grid for TEM analysis.

Energy Dispersive x-ray Spectroscopy (EDX) was used to detect elemental characteristics within the sample. It provides information about the composition of the substrate being analysed.

3.5.10. Dynamic Light Scattering

Particle size distribution and zeta potential were analysed using Malvern Zetasizer Nano ZEN1600.

The Zetasizer uses Dynamic Light Scattering (DLS) to determine the sizes of particles in suspension in aqueous solution. DLS assesses the size of

particles by light scattering. Suspended particles naturally undergo Brownian motion. The larger the particle, the slower the Brownian motion will be. Thus, DLS uses light scattering to monitor particles Brownian motion to determine the particle size [100]. The procedure projects a monochromatic light beam onto a solution containing particles, when the beam hits the particles in Brownian motion, wavelength of the light varies. This variation is linked to the size of the suspended particles. DLS periodically refers to measurements and interprets light scattering data on a microsecond timeframe [101].

The Zetasizer measures zeta potential by measuring the electrophoretic mobility of charged particles due to an applied electric field. The velocity of the particle under electrophoresis depends on the Zeta potential, electric field strength, dielectric constant and viscosity of the medium. Zeta potential is related to electrophoretic mobility by the Henry Equation:

$$U_E = \frac{2\varepsilon z f(ka)}{3\eta} \quad (3.3)$$

Where U_E is the electrophoretic mobility in m/s, z is the zeta potential in Volts, ε is the dielectric constant, η is dielectric constant, η is viscosity (Pascal seconds), and $f(ka)$ is the Henry's equation.

3.6. Conclusion

The following chapters 4, 5 and 6 outline the results gathered from the materials, reagents, tests, procedures and characterisation equipment described above in Chapter 3.

Chapter 4 Adsorption of Poly Phosphino Carboxylic Acid onto Carboxylated Multiwalled Carbon Nanotubes (NAST2)

4.1. Introduction

A major factor in squeeze treatment is the need for an effective adsorption of the scale inhibitor (SI) within the reservoir rock porous media. This ensures a lengthy squeeze lifetime [49]. The NAST methodology was created with the aim to increase the adsorption of SI and to offer an extended squeeze lifetime to protect the well against scale formation. This method is separated in two main steps:

- Step1/NAST1 is about injecting and adsorbing COOH-MWCNTs onto a rock surface porous media.
- Step2/NAST2 is solely about the adsorption of PPCA onto COOH-MWCNTs.

This chapter solely focuses on Step2/NAST2 in static conditions, to gain a fundamental study of the interaction of COOH-MWCNTs and PPCA. Previous work [6] has already shown that COOH-MWCNTs offered far greater SI adsorption than reservoir rock in simplistic conditions – experiments were done with distilled water, simplistic brine and at room temperature. With respect to this study, the aim is to further understand the interaction between PPCA and COOH-MWCNTs. The experiments were all done in Nelson Forties Formation Water (NFFW) and at 50°C, unless stated otherwise. This chapter provides a study of the adsorption rate of PPCA SI onto COOH-MWCNTs, an investigation on the effects of various pH values on the SI adsorption efficiency, and a presentation of the differences in SI adsorption for various COOH-MWCNT and PPCA concentrations. The adsorbing capabilities of the COOH-MWCNTs are also analysed by fitting a Langmuir isotherm (section 4.2.5). The C18-Hyamime method was used to measure the concentration of PPCA SI before and after the experiments.

Phosphorus-Nuclear Magnetic Resonance (P-NMR) was also conducted to show the presence of phosphorus on the COOH-MWCNTs and examine the hypothesis that PPCA adsorbs onto COOH-MWCNTs. The summary of experimental results of this chapter are illustrated in Figure 4-1.

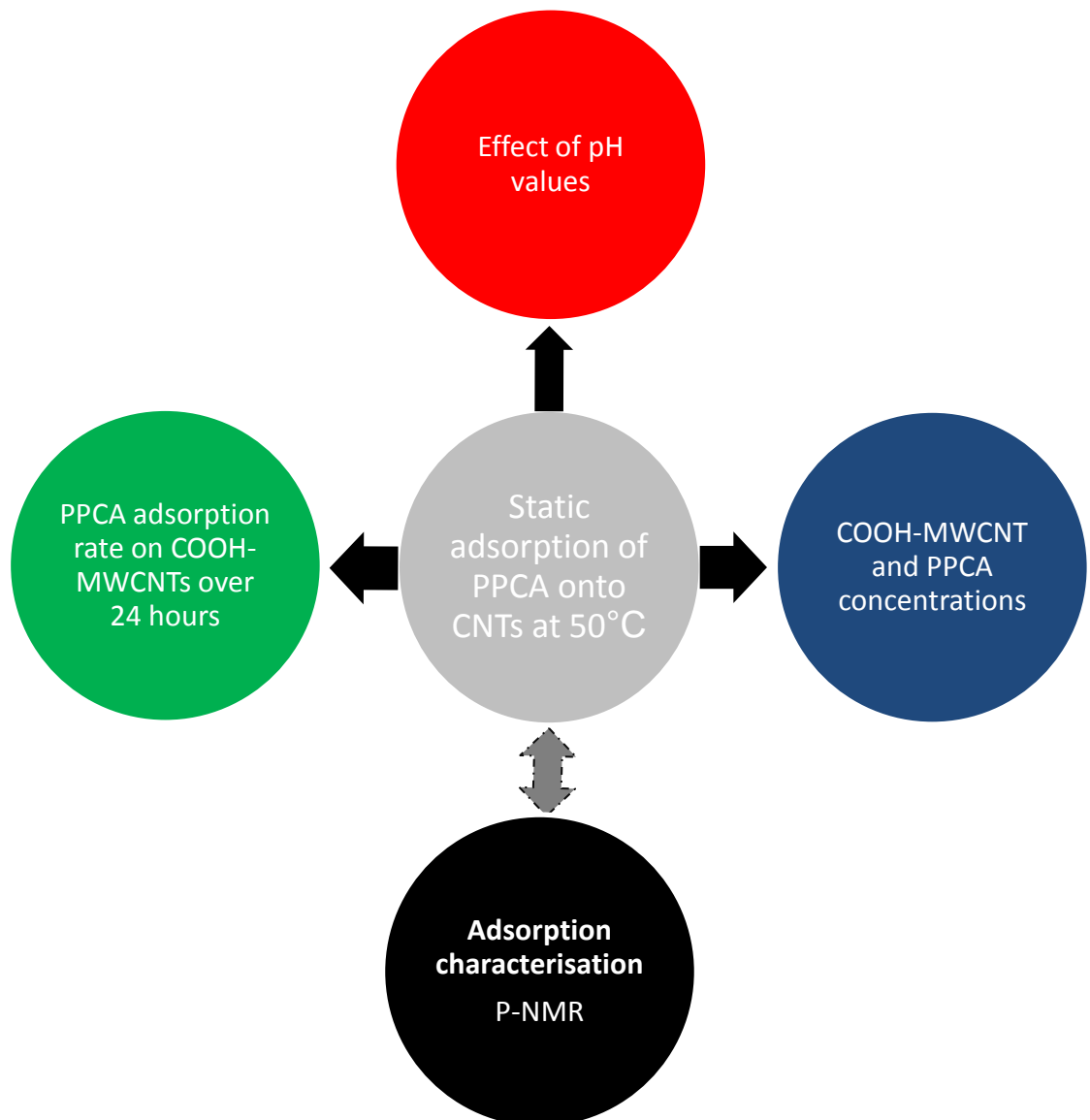


Figure 4-1 Overview of the experimental work carried to investigate the interaction of PPCA on CNTs being studied

4.2. Adsorption Data

Adsorption of scale inhibitors on the COOH-MWCNTs was quantified by C18-Hyamime method; P-NMR helped confirming the adsorption behaviour of PPCA onto COOH-MWCNTs.

Results from sand pack experiments (presented in Chapter 5) show that the average amount of COOH-MWCNTs retained onto the rock matrix ranges between 4 to 10 mg, and the pore volume is approximately 10 mL. Based on the aforementioned, the static adsorption experiments were designed using various masses of carbon nanotubes ($m = 4, 6$ and 10mg) at a fixed volume ($V=10$ mL) of scale inhibitor solution.

Experiments were performed at 50°C . The stock solution was prepared using the synthetic Nelson Forties Formation Water Composition (NFFW). The composition of the brine is discussed in 3.1.1.

The experiments were carried at the following range of concentrations: 100, 500, 1000, 2500 and 5000 ppm of PPCA. This allowed a better study of the adsorption process of PPCA on COOH-MWCNTs. After 6 hours at the respective temperature, the solutions are taken and measured by the C18-hyamime method.

4.2.1. Adsorption of Polyphosphino Carboxylic Acid with Complex Brines onto COOH-MWCNTs in Comparison to Sand

A static adsorption test was performed and the results were compared to Farooqui's [29] [59] study. Both tests were run at the same temperature and same pH value ($\text{pH}=6$), the adsorbent-adsorbate mass to volume ratio was different, 10 g of sand in 80 mL of PPCA and formation water for Farooqui et al. [29] against 10 mg of COOH-MWCNTs in 10 mL of PPCA and formation

water in this study. Both water chemistries have the exact same composition and PPCA concentration was 1000 ppm.

Figure 4-2 shows the comparison of results of adsorption of PPCA (mg/g) on COOH-MWCNTs and rock. Approximately 1 mg/g PPCA adsorption was observed by Farooqui [59] while 350 mg/g of PPCA adsorption was seen for the NAST methodology. This data shows how much more efficient COOH-MWCNTs are at retaining PPCA in comparison to silica sand in the same conditions.

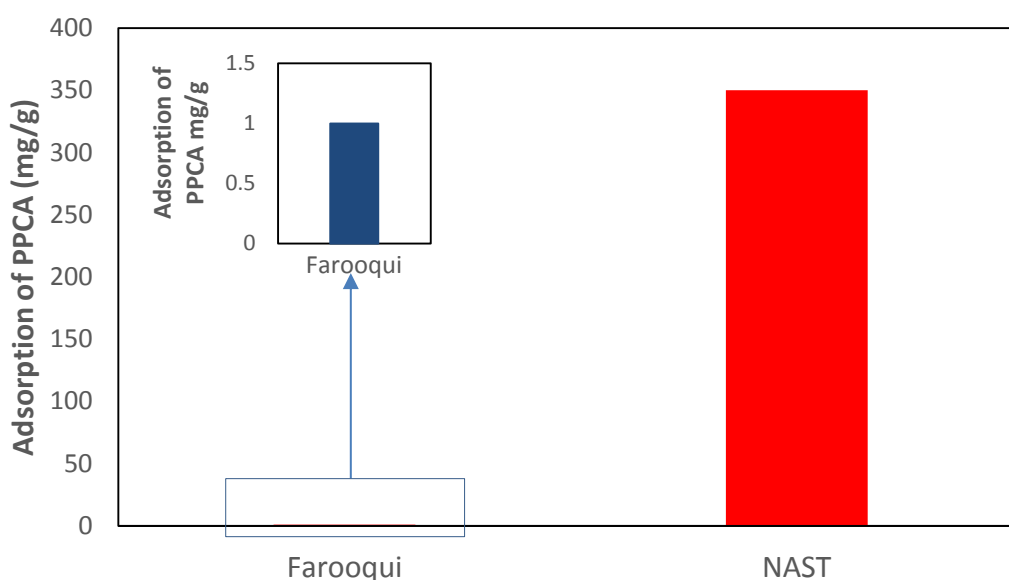


Figure 4-2 Comparison of results between adsorption of PPCA on COOH-MWCNTs and rock by Farooqui et al. [29]

The experimental results show the efficiency of COOH-MWCNTs for adsorbing PPCA. PPCA adsorption is also enhanced by the presence of cations, such as calcium [29]. PPCA is known to be poly-anionic, meaning that the polymer dissociates into anions and associates with cations, such as calcium [29, 102]. COOH-MWCNTs are also known for having affinities with electrolytes such as calcium [103]. In the case of this study, a COOH-MWCNTs - calcium cation complex may form and attach to PPCA, leading to enhanced adsorption of PPCA. This proposal has discussed in detail by Ghorbani [6]. These experimental results also confirm the conclusions from

Ghorbani [6], COOH-MWCNTs have a very high adsorptive affinity for scale inhibitor.

4.2.2. The Rate of Adsorption of PPCA on COOH-MWCNTs

The PPCA adsorption rate on COOH-MWCNTs has been determined by measuring C18-hyamine from samples taken at set time intervals. Samples were taken before and after adding the COOH-MWCNTs to the solution. Figure 4-1 shows a normalised adsorption of PPCA onto COOH-MWCNTs. Concentrations are normalised to the stock solution (at zero time here). Samples were extracted at 0.5, 1, 2, 10, 16, 20 and 24 hours. The concentration of COOH-MWCNTs injected was 40 mg in 100 mL of a 5000ppm PPCA solution diluted in brine.

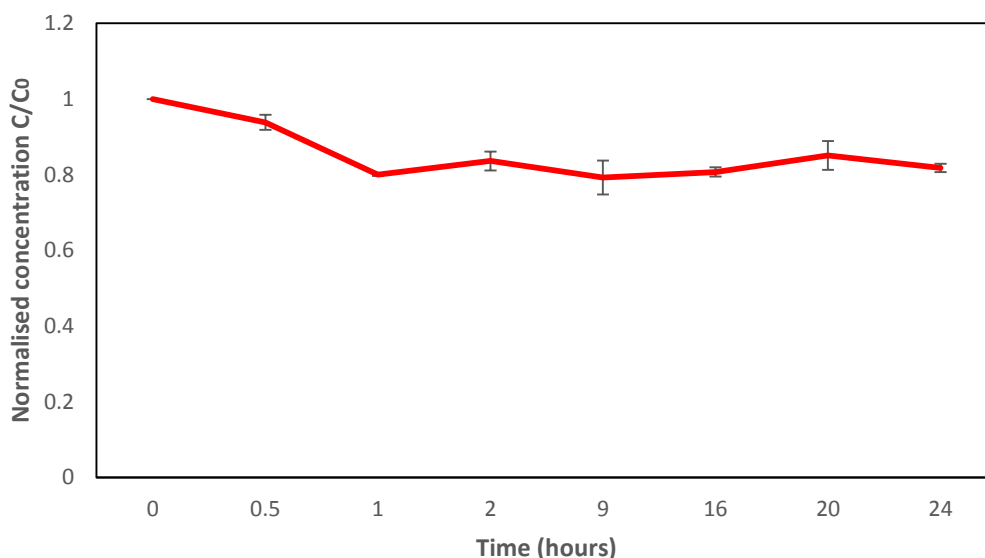


Figure 4-3 PPCA adsorption onto COOH-MWCNTs within 24 hours at 50°C

Figure 4-3 indicates that after 0.5hr, based on calculations, 47% of the final adsorption (850 mg/g in this experiment) was obtained. After a 1 hour, adsorption of PPCA on COOH-MWCNTs had reached a pseudo-equilibrium (~ 1800 mg/g), as all available sites on COOH-MWCNTs were probably

occupied by PPCA. This is indicative of a fast saturation, meaning that a shut in period could be reduced in a realistic application with the NAST methodology. However, actual reservoir performance will be affected by pore sizes, geometries and available functional sites. Hence, dynamic tests will be discussed in Chapter 6.

4.2.3. Adsorption of PPCA on CNTs at Various pH Values

Solution pH value can affect the protonation state of the PPCA as well as the physicochemical properties of the adsorbent, by creating defects and carboxyl sites. This will influence the adsorptive nature of the carbon nanotube. Indeed, the adsorption of PPCA on COOH-MWCNTs is hypothesized to be dependent on the availability of defects and availability of carboxyl sites on the carbon nanotubes [7]. Figure 4-4 shows a plot of the adsorption of PPCA on COOH-MWCNTs over three pH values. The data is plotted in ppm to reveal the quantity adsorbed at each pH value.

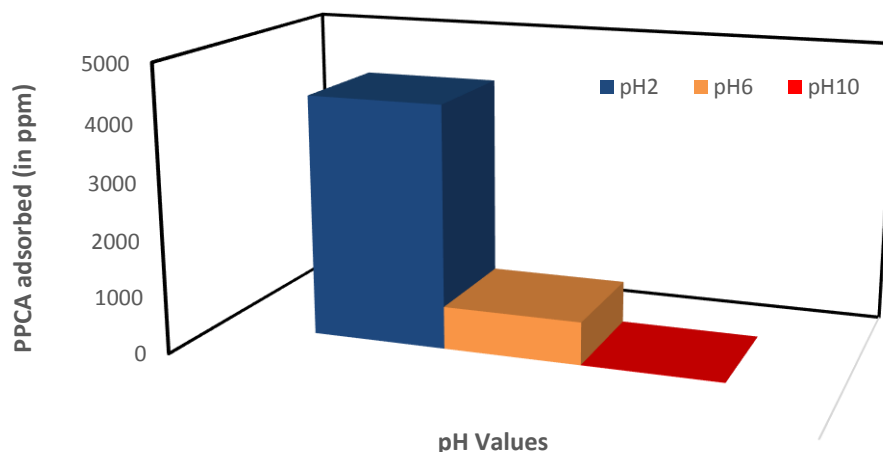


Figure 4-4 Adsorption of PPCA on CNTs over three pH values with 4 mg of CNTs in 10 mL of a 5000 ppm PPCA solution

Figure 4-4 suggests that at pH2, CNTs are able to adsorb more PPCA than pH6 and pH10. At pH 6, CNTs are capable of adsorbing substantially more PPCA.

In a more acidic environment (pH 2), there is a higher content of -COOH functional groups on COOH-MWCNTs [104], suggesting that there are more defects and edges on the nanotubes. These defects and edges may increase the specific surface areas of the carbon nanotubes and consequently may significantly increase the adsorption of PPCA [104]. Also, the decrease of the pH leads to neutralization of the charge on the surface. As the pH value decreases below the point of zero charge (PZC) of the adsorbing materials (COOH-MWCNTs), the positive charge density increases and adsorption capacity of anions (negatively charged ions) increases. PPCA is a poly anionic inhibitor. The PZC is pH 3.3 for COOH-MWCNTs [105, 106]. As a general guide, adsorption by electrostatic attraction is accomplished in the pH interval between the isoelectric point (IEP), typically close to the PZC, and the point of zero charge (PZC). Thus the increased adsorption of PPCA seen at pH 2 is explained by maximum electrostatic attraction expected close to the PZC [107]. Thus based on these explanations, this explains the high adsorption of PPCA by COOH-MWCNTs at pH2. The data herein seem to indicate that at this point adsorption is triggered by physical electrostatic interaction and a hydrogen bonding interaction between the negatively charged PPCA species and the positively charged protonated carboxylated groups at the surface of the COOH-MWCNT [103, 108].

CNTs have an overall negative surface charge at pH 4 to 10 [109]. At pH6, COOH-MWCNTs have a slightly negative surface charge. Negatively charged surface sites become available for calcium ions to adsorb onto MWCNTs, thus changing the surface charge towards a more positive (at least, less negative) value. The complex formed between COOH-MWCNTs and calcium ions is aiding the adsorption of the poly-anionic inhibitor PPCA onto the COOH-MWCNTs, as was demonstrated by Ghorbani [6]. Adsorption of PPCA on the COOH-MWCNT is also happening from the available -COOH functional sites present on the nanomaterial.

At solution pH 10, both CNTs and PPCA are highly negatively charged, and electrostatic repulsion may become a dominant counter- action force, resulting

in low to no PPCA adsorption. The results of this section are discussed in section 7.1.

4.2.4. Static Adsorption - Adsorption of Various PPCA Concentration on Different Masses of COOH-MWCNTS

Static adsorption tests were performed in order to assess the adsorption of PPCA onto the COOH-MWCNTs. Experiments were performed at 50°C. The stock solution was prepared using a synthetic formation water - see composition in section 3.1.1. For these tests, the experiments were designed using three masses of carbon nanotubes ($m = 4, 6$ and 10 mg) at a fixed volume ($V=10$ mL) of scale inhibitor solution. These masses and volume were selected because of the results from sand pack and core flood experiments (see Chapter 5) show that on average the COOH-MWCNTs staying retained to the rock matrix is between 4 to 10 mg and the pore volume of 10 mL.

The experiments were carried at the following range of concentrations: 100, 500, 1000, 2500 and 5000 ppm of PPCA. After 6 hours of being subjected to the treatment temperatures, the solutions were taken and measured by the C18-hyamine method. Figure 4-5 demonstrates that higher adsorption on COOH-MWCNTs is related to higher PPCA concentrations. Also, the higher the COOH-MWCNTs concentration, the more PPCA is adsorbed onto it.

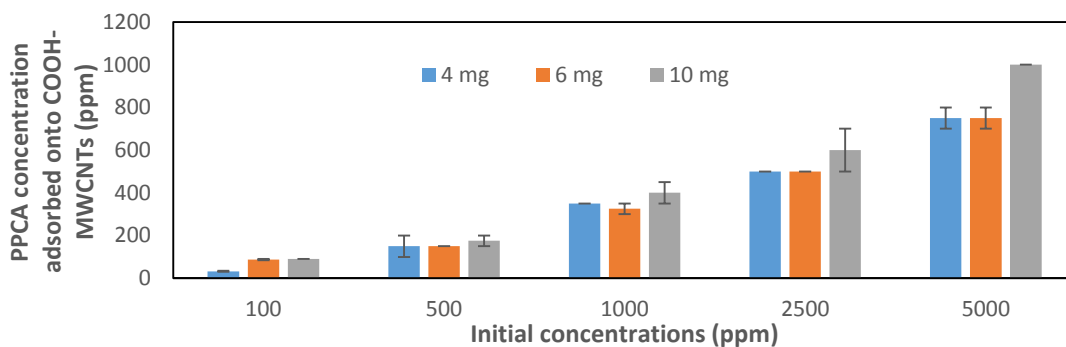


Figure 4-5 Change in PPCA concentration from 100 to 5000 ppm with various CNT masses 4, 6 and 10 mg

On the other hand, the data is shown as a mass of PPCA adsorbed per grams of COOH-MWCNTs (in mg per gram). It can be observed that the lower the mass of CNT to volume of PPCA (m/V) ratio, the higher the adsorption efficiency. This aligns with scale inhibitor adsorption theory [29, 49]. This likely occurs because 4 mg of COOH-MWCNTs is more efficiently dispersed than 10 mg in such a volume. Figure 4-6 shows the adsorption isotherm of PPCA in milligrams per grams of COOH-MWCNTs (mg/g).

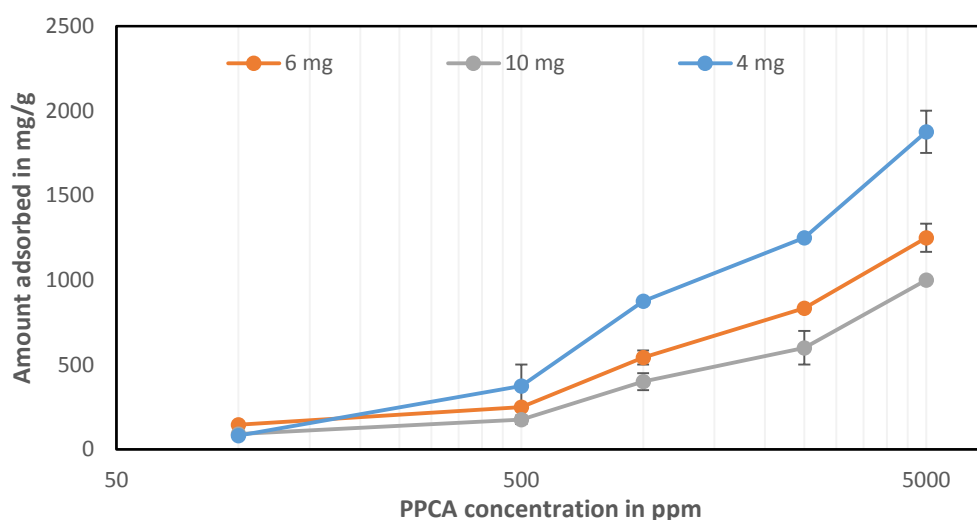


Figure 4-6 Apparent PPCA adsorption onto different CNT masses at 50°C.

4.2.5. Freundlich Isotherm Fittings

Using the measured PPCA amount adsorbed onto COOH-MWCNTs in Figure 4-6, it was possible to fit these data to the Freundlich adsorption model to fit the various mass-to-volume (m/V) ($m = 4, 6$ and 10 mg, $V = 10$ mL) ratios at 50°C. This provides a better understanding of the adsorption properties of COOH-MWNTs with PPCA.

The isotherm model was used to fit adsorption data as a quantitative comparison of the results. The following equation was fit to data in a manner designed to observe the data against model values:

$$\log\left(\frac{X}{M}\right) = \log(K) + \frac{1}{n}\log Ce \quad (4.1)$$

where X is mass of PPCA (mg), M is mass of COOH-MWCNTs (g), Ce is the equilibrium concentration (mg/L), and K (mg/g) and n are Freundlich equation constants.

4.2.5.1. Freundlich Isotherm Fittings – 4 mg of COOH-MWCNTs

The Freundlich equation was fitted to describe the data given by:

$$\log\left(\frac{X}{M}\right) = 0.25 + \log Ce \quad (4.2)$$

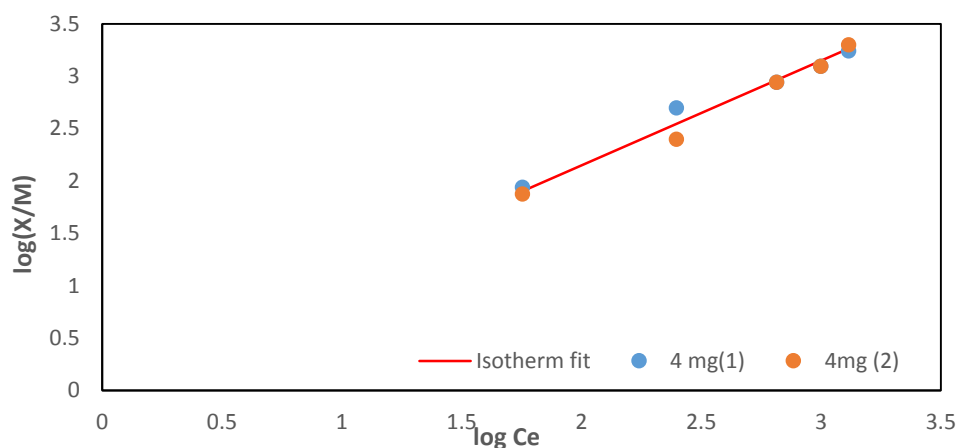


Figure 4-7 Freundlich isotherm fit for adsorption data with 4 mg of CNTs as adsorbent

The adsorption isotherm has a correlation coefficient of 0.99 with the experimental data. The Freundlich model fits the experimental results very well. This isotherm assumes that adsorption of PPCA on CNTs is a multilayer adsorption [110].

4.2.5.2. Freundlich Isotherm Fittings – 6 mg of COOH-MWCNTs

The Freundlich equation as described in equation 4.3 was fitted to describe the data given by:

$$\log\left(\frac{X}{M}\right) = 1.7144 + 0.32 \log C_e \quad (4.3)$$

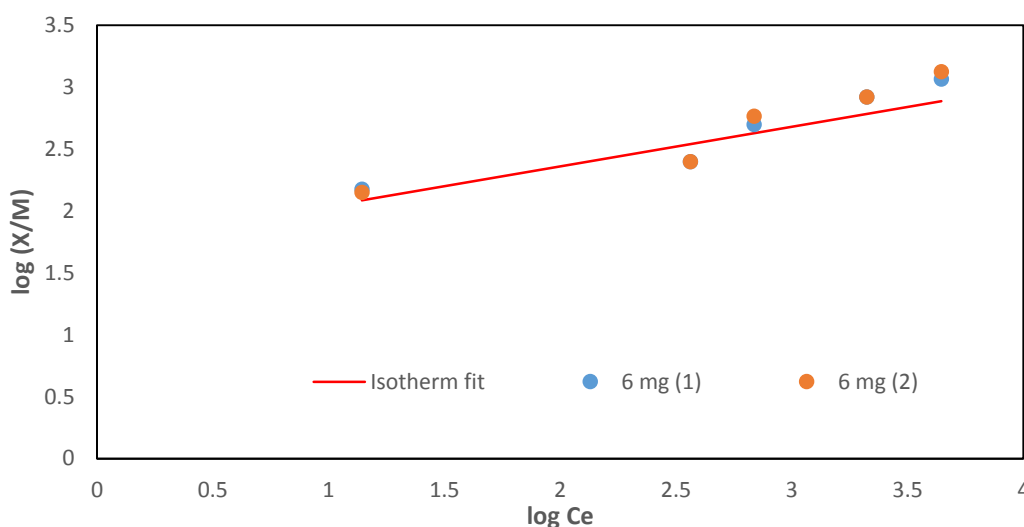


Figure 4-8 Freundlich isotherm fit for adsorption data for 6 mg of CNTs as adsorbent

The adsorption isotherm displays a correlation coefficient of 0.93 with experimental data. As it can be seen, this provides a decent fit for a specific adsorbent mass (6 mg of COOH-MWCNTs). The fit is not as good as that for 4 mg of adsorbent; this variation can be explained by the fact that the higher the mass-to-volume ratio, the less likely are the chances of observing a good dispersion, leading to less adsorption sites available on COOH-MWCNTs for the adsorption of PPCA.

4.2.5.3. Freundlich Isotherm Fitting for 10 mg of COOH-MWCNTs

The Freundlich equation as stated in equation 4.4 was fitted to describe the data given by:

$$\frac{X}{M} = 1.4648 + 0.61 \log C_e \quad (4.4)$$

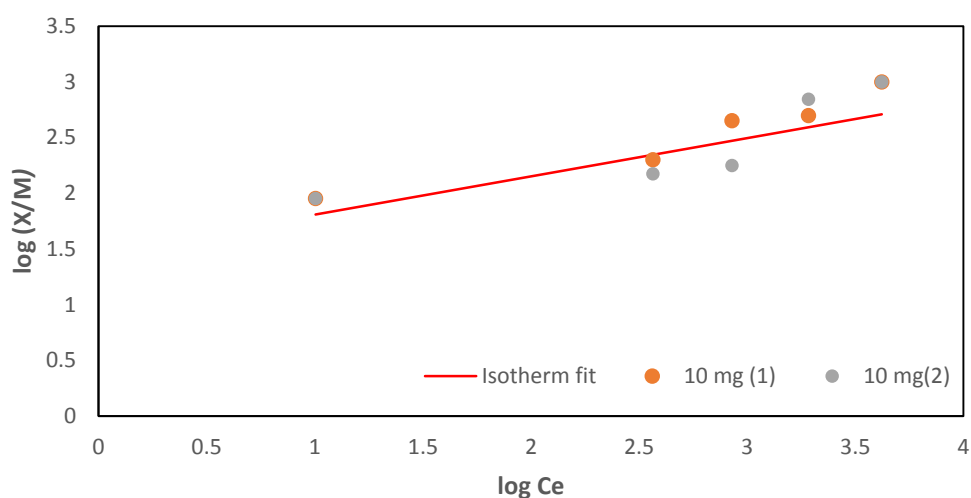


Figure 4-9 Freundlich isotherm fit for adsorption data with 10 mg of CNTs as adsorbent

The adsorption isotherm has a correlation coefficient of 0.82 when compared to experimental data. As can be seen, this provides an average fit, for the specific adsorbent (10 mg of COOH-MWCNTs). The fit is not as strong as for 4 and 6 mg of adsorbent, as shown in Figure 4-8. This indicates that the higher the mass-to-volume ratio, the less likely it is that a good dispersion should be observed, leading to less adsorption sites available

4.2.6. Phosphorus Nuclear Magnetic Resonance

According to the NAST methodology, one of the main objectives is for PPCA to adsorb on the COOH- MWCNTs surface. COOH-MWCNTs adsorb PPCA

more efficiently than sand and release the PPCA at a slower rate [6]. P-NMR confirms the presence of PPCA onto the COOH-MWCNTs. Therefore, static adsorption tests have been performed in order to reinforce the theory. Figure 4-10 shows a peak at 42.2 ppm, this indicates the presence of PPCA onto the sample.

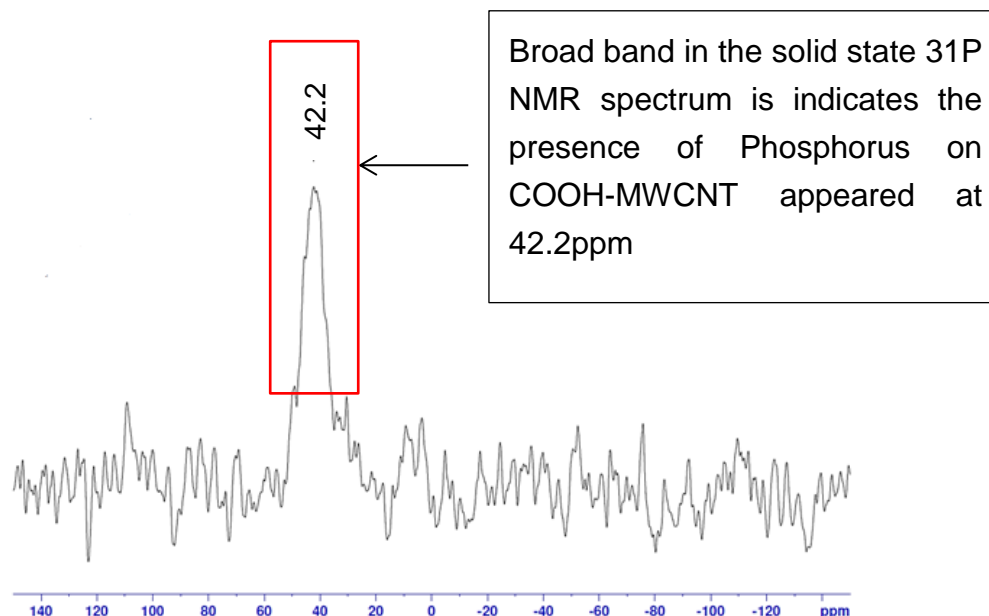


Figure 4-10 Phosphorus bonding indicating the presence of PPCA

4.3. Conclusion

Scale inhibitor adsorption within the reservoir formation is the main factor governing the lifetime of a scale inhibitor squeeze treatment. The large surface area of COOH-MWCNTs make them a good candidate as adsorbent for polymeric scale inhibitor. This chapter quantified PPCA SI adsorption rate on COOH-MWCNTs. Specifically, it identified the effect of variation on environmental values with pH values. It also evaluated, by using Freundlich adsorption isotherms, the influence of mass of COOH-MWCNTs on PPCA adsorption in a set volume. Further analysis confirmed presence of PPCA on COOH-MWCNTs. This study has broadened the knowledge on the interaction between COOH-MWCNTs and PPCA in brine.

The key conclusions from this chapter are described below:

1. COOH-MWCNTs were able to adsorb 350 times more PPCA than sand in mg/g (from section 4.2.1).
2. The adsorption of PPCA with COOH-MWCNTs reaches equilibrium quickly and could potentially lead to a shorter shut in time in oilfield application (from section 4.2.2).
3. At pH 2, PPCA retention is substantially enhanced thanks to the protonation onto the carbon nanotubes. At pH 10, COOH-MWCNTs substantially lose their adsorbing abilities, because they are deprotonated (from section 4.2.3).
4. PPCA adsorption increases with more COOH-MWCNTs but the efficiency reduces because of solution nanoparticle agglomeration (section 4.2.4).
5. Freundlich adsorption isotherm fits the experimental results reasonably well (section 4.2.5).
6. Phosphorus NMR is reinforcing the proposal of Phosphorus attachment onto COOH-MWCNTs (section 4.2.6).

Chapter 5 Transport and Retention of COOH-MWCNTs and their Effects in Porous Media (NAST1)

Step1/NAST1, the focus of this chapter, is about injecting and attaching carboxylated multiwalled carbon nanotubes (COOH-MWCNTs) onto a rock porous media to create a surface that is capable of stronger polyphosphino carboxylic acid (PPCA) adsorption in comparison to an untreated rock [6]. Based on this argument, the drive is to manage the deep placement of these nanomaterials in the porous media without causing substantial formation damage. Recent studies have looked into the transport of COOH-MWCNTs in porous media. It has been concluded that movement of colloids in porous media rely on the colloid surface charge, straining and adsorption sites available due to surface heterogeneity of rock [111-113]. For the application of this study, a rock surface charge functionalisation is necessary before injecting the CNTs. It allows the rock surface charges to be homogeneously changed to ensure a permanent adsorption of COOH-MWCNT onto a rock, with a silane coupling agent.

In this chapter, the transportability and retention of the carbon nanotubes is assessed through a sand pack column and a consolidated core, to simulate the transport in a reservoir-like porous media. Another aspect assessed is the effect on permeability impairment/reduction on a range of consolidated cores. Ideally, a NAST treatment would be done without substantially decreasing the permeability which would lead to slower production. Although the primary focus of this chapter is to solely attach COOH-MWCNT onto the rock matrix, there are also important aspects to be aware of, such as an efficient dispersion of the nanoparticles.

The dispersant selected was polysorbate 80, also known as Tween 80. It is quite commonly used in literature [87, 114]. 3-Aminopropyltriethoxysilane was chosen to treat the rock surface to react and retain the COOH-MWCNTs nanotubes. Figure 5-1 shows an overview of the chapter.

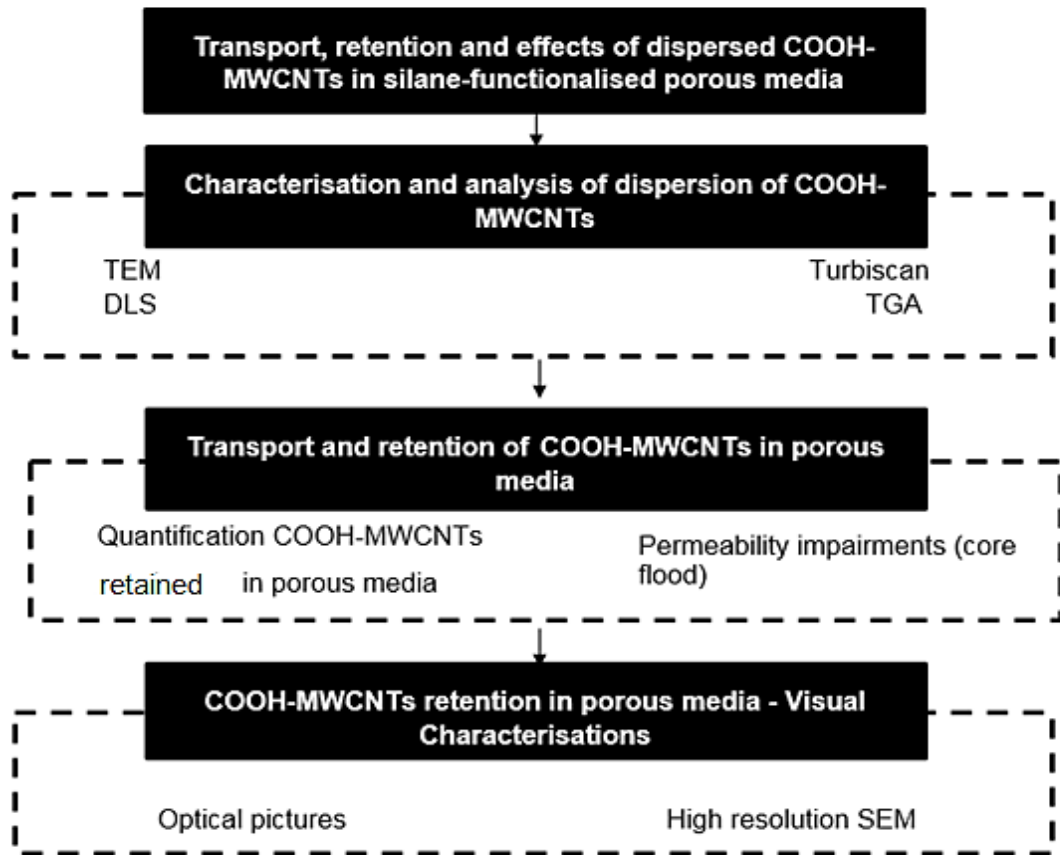


Figure 5-1 Overview of the chapter

5.1. Overview

Previous research [6] focused on developing a methodology whereby COOH-MWCNTs can be covalently attached onto a rock surface for downhole oil and gas applications. However, there were gaps in the methodology that were investigated and optimised in the study herein. This includes the dispersion and the effective placement of the COOH-MWCNTs in the porous media. The COOH-MWCNTs were assessed by Transmission Electron Microscopy (TEM)/ Energy Dispersive X-ray spectroscopy (EDX) and ThermoGravimetric Analysis (TGA) to investigate impurities in the COOH-MWCNTs and their thermal stability. An organic dispersant, Tween 80, was selected. Tween 80 is considered a non-toxic surfactant. Its potential toxicological effects on porous media has been assessed and they all

concluded that Tween 80 has little to no effects on the porous media [115]. The dispersion stability of the COOH-MWCNTs was assessed by Dynamic Light Scattering (DLS) and by using a stability analyser known as “Turbiscan Lab” manufactured by Formulation (France). The COOH-MWCNTs in solution were detected and quantified by Ultraviolet-visible spectrophotometry (UV-Vis) and Raman spectroscopy. Both methodologies are described in the methodology chapter in section 3.5.3 and 3.5.6. The quantification methods of COOH-MWCNTs allowed the amount of COOH-MWCNTs retained in the porous media to be estimated using mass balance calculations. The pressure measurements of various sandstones were done to assess the permeability impairment caused by the nanoparticles. The shift in pore sizes and pore volume was assessed by Nuclear Magnetic Resonance (NMR). The COOH-MWCNT adsorption onto rocks was also assessed with High Resolution SEM (HR-SEM) to understand how the COOH-MWCNTs interact with the rock pores. This provides a reference illustration for retained COOH-MWCNTs onto a rock surface.

5.2. Characterisation of COOH-MWCNTs

5.2.1. Transmission Electron Microscopy of Carboxylated Carbon Nanotubes

TEM images were obtained on a FEI Titan Themis Cubed 300 operated at 300 kV. The COOH-MWCNTs sample was prepared by suspending a small amount of powder sample in methanol, followed by ultrasonication for 5 min. One drop of this suspension was placed on a carbon-coated copper grid for TEM analysis.

Figure 5-2 A shows the TEM/EDX analysis of the COOH-MWCNTs used for this study. The image clearly depicts the impurities present in the carbon nanotubes, which are intercalated within rolled graphene sheets.

Figure 5-2 B was analysed with EDX which revealed green areas representing carbon, and red areas show the metallic impurities representing cobalt.

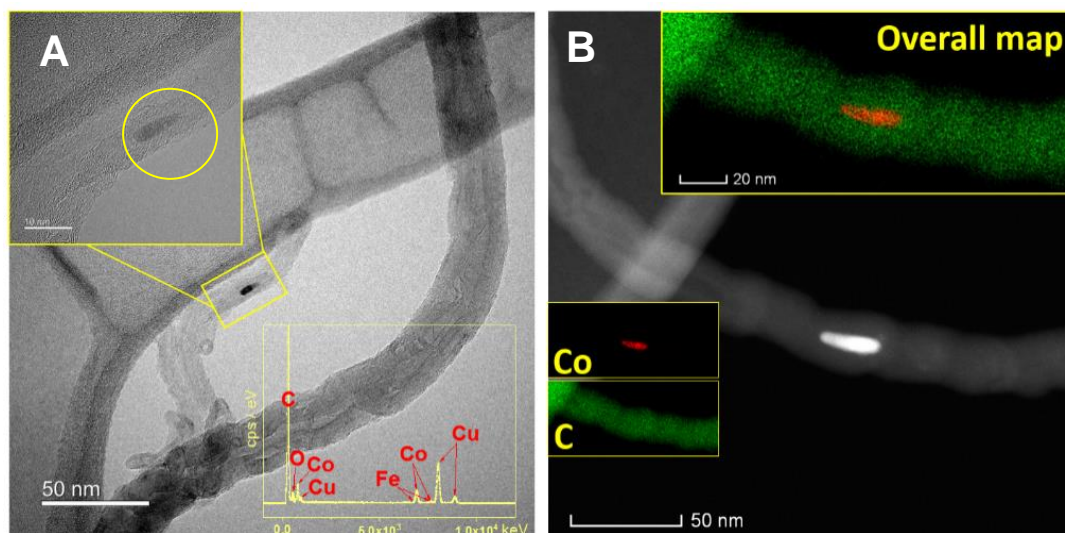


Figure 5-2 TEM images (A) circle indicates residual metal catalyst impurity marked within the nanoparticle. Nanoparticles overlaying one another are also visible, however impurities were no detected. EDX peaks represent elements within the nanoparticle, except for iron from the TEM grid (B) EDX detected impurities within the nanoparticle (cobalt and carbon)

A further characterisation of the CNT materials for determination of metal impurities composition is described in Table 5-1. The spectrum from EDX analysis can be seen in Figure 5-2 (A).

Table 5-1 Compositions of individual metal catalysts nanoparticles present in COOH-MWCNTs based on TEM/EDX analysis

Element	C	O	Fe	Co
Mass Fraction (%)	96.54	2.32	0.05	1.08

5.2.2. Thermogravimetric Analysis Results of 95% pure Carboxylated Multiwalled Carbon Nanotubes

As proven by the TEM data, the COOH-MWCNTs have a few impurities. TGA is another approach to study the purity of the COOH-MWCNTs and also to assess the thermal stability of the nanoparticles. This technique of thermal analysis is subjected to a controlled increase in temperature in which the variation of sample mass is determined as a function of temperature. The analyses of COOH-MWCNT powder were carried out in air, whereby the residual at the end of burning during thermal oxidation represents the remaining metallic impurities. The experiment carried was performed at temperatures ranging from 25 to 1000°C and a heating rate of 40°C/min.

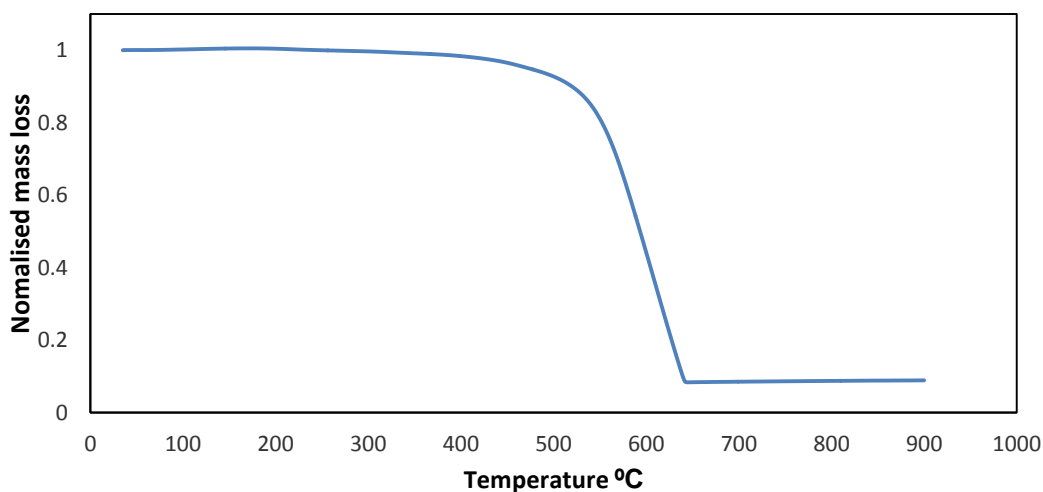


Figure 5-3 TGA of COOH-MWCNTs in air

The thermogravimetric experiments carried show that on the 1st stage, from 0 to 200°C, the sample is stable. From 200 to 400°C, weight loss is due to the decarboxylation of the carboxylic groups present onto the CNTs walls [116]. From 400 to 500°C, the weight loss can be justified by the elimination of the hydroxyl groups [116]. From 500°C onwards, degradation is explainable by the thermal oxidation of the MWCNTs matrix [116].

The remains are assumed to be metal oxides such as cobalt oxides, iron oxides or copper oxide. The presence of these two metal oxides was also discussed in the TEM results in section 5.2.1. The mass remaining is equal to 4.86 % which is approximately equivalent to the manufacturer's data. However, TEM data in section 5.2.1 states that the impurity was found to be of 1.08% Cobalt catalyst and 0.05% Iron catalyst. The difference in impurity measurement between TGA and TEM is most likely due to the sample size difference. EDX only analyses the composition of one or two nanoparticles. While a crucible used for TGA experiments weighed the mass of impurities remaining for an initial 8 mg of COOH-MWCNTs in a crucible before combustion. This could explain why the TGA results are a better match to the manufacturer's data.

5.2.3. Dynamic Light Scattering and Size Distribution

In order to minimise the likelihood of agglomeration, a low CNT concentration is chosen [117]. It will help prevent blockages within the porous media. It is unhelpful to have nanoparticles that are no longer in the nano range and become larger entities [117].

In Figure 5-4, the hydrodynamic particle size distribution of a 20 ppm COOH-MWCNT concentration dispersed in 1.5% Tween 80 and distilled water at room temperature. Most COOH-MWCNTS detected are within 200 nm to 1000 nm (0.2-1 μm) range, which may indicate that most COOH-MWCNTs are individually dispersed. Also, there is a small quantity (<3%) of carbon nanotubes detectable within 4 to 5 μm . The seller stated that the length of a nanotube is between 0.5 to 2 μm Cheaptubes Inc (VT, Cambridgeport).

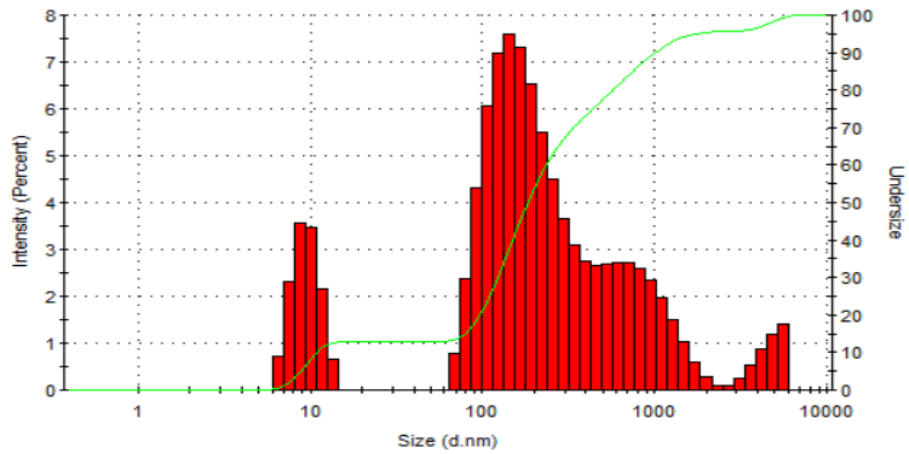


Figure 5-4 COOH-MWCNT hydrodynamic particle size distribution at 25°C

When it comes to a dispersion at 50°C, most COOH-MWCNTS detected fall within the 200 nm to 700 nm (0.2-0.7 μm) range. There is a small quantity (<1%) of carbon nanotubes detectable within 4 to 5 μm which explains the higher average particle size distribution. Figure 5-5 shows a 20 ppm COOH-MWCNT concentration dispersed in 1.5% Tween 80 and distilled water at 50°C.

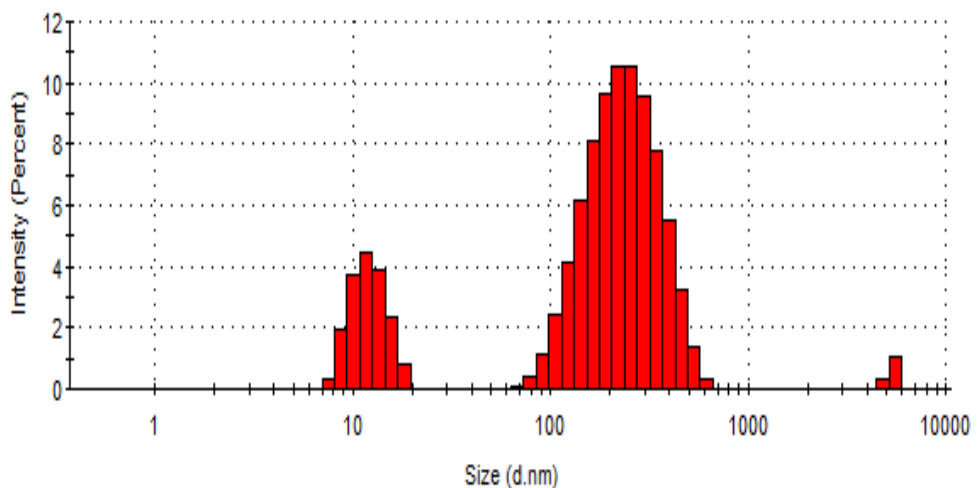


Figure 5-5 COOH-MWCNT hydrodynamic particle size distribution at 50°C

Overall, the average particle size distributions do not change much through the two temperature changes from 25° C to 50°C.

In Table 5-2, the measured zeta potential at room temperature and 50°C indicate that the dispersed COOH-MWCNTs were negatively charged across both temperatures. The change in temperature had little effect on the surface charge of this solution. However, at this range of zeta potential values (ζ), further investigations are required and are carried in section 5.2.4 to ensure a stable dispersion for an efficient injection in porous media.

Table 5-2 COOH-MWCNT zeta potential at 25°C and 50°C

Mean zeta potential (mV)	
Room Temperature 25°C	50°C
-13.1	-13.5

5.2.4. Stability Analyser – “Turbiscan Lab”: Assessment of Stability of COOH-MWCNTs solution with time

The “Turbiscan Lab”, a solution stability analyzer, is used to assess the stability of the dispersed COOH-MWCNTs over a period of time. The apparatus is described in the Methodology chapter in section 3.5.7.

At 25°C, Figure 5-6 shows that the dispersion of COOH-MWCNTs is very stable over the course of 24 hours. There are few changes in backscattering variation, staying within a range of 1.5%. This indicates that there is no obvious particle agglomeration or migration in the solution.

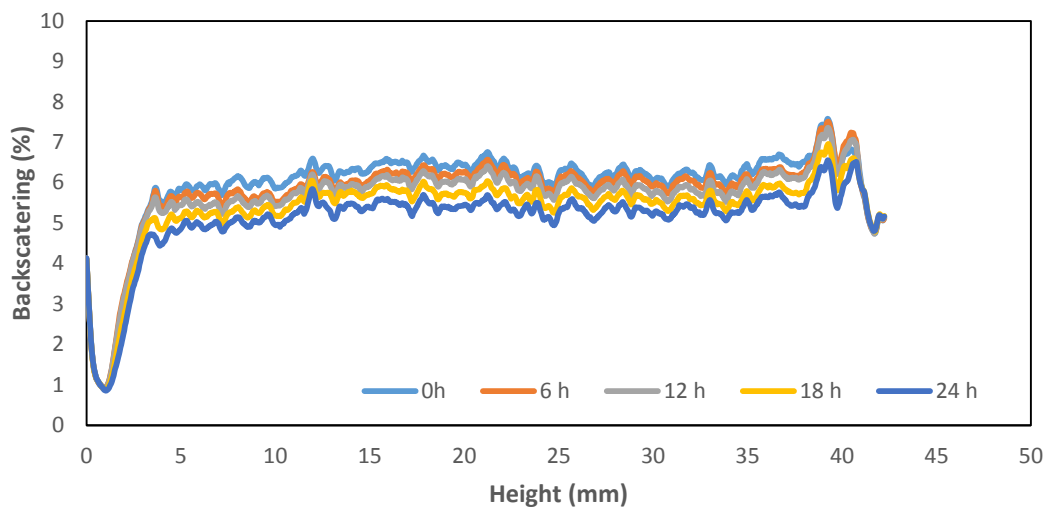


Figure 5-6 Stability analysis of Tween 80 dispersed COOH-MWCNTS analysed by Turbiscan at room temperature

At 50°C, Figure 5-7 shows that the dispersion is very stable over the course of 24 hours. There are very few to no changes in backscattering percentage over the course of 24 hours, indicating no obvious particle agglomeration or migration in the solution.

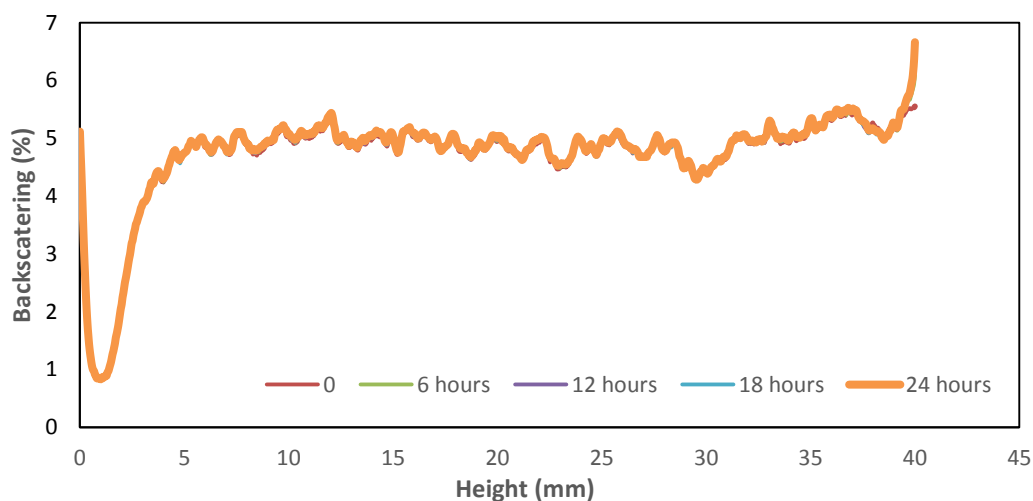


Figure 5-7 Stability analysis of Tween 80 dispersed COOH-MWCNTS analysed by Turbiscan at 50°C

The previous zeta potential results seem to indicate that the dispersion could possibly be unstable. However, the Turbiscan results show otherwise and this agrees with theories that the stability of the dispersed COOH-MWCNTs in Tween 80 is maintained by steric interactions rather than electrostatic interactions [86]. The stability of the solution is important to ensure a steady injection in the sand pack and coreflood experiments.

5.3. Step 1/ NAST 1: Injection and Retention of COOH-MWCNTs in porous media

Nanotechnology, especially nanoparticles suspension has received attention for application in new enhanced oil recovery systems [30, 60, 118, 119]. As a reminder, the aim of this chapter is to assess NAST1. In this section, the transport and retention of COOH-MWCNTs on porous media is being analysed. To the author's knowledge, there has not been previous research evaluating particle retention in a silane functionalised porous media.

Mass balance calculations were possible by measuring the concentrations of effluent of COOH-MWCNT with UV-Vis as a function of pore volumes (PV). This permitted the amount of nanoparticles retained in the porous media to be determined. The porous media was composed of silica sand and clay (more details about minerals used in sand packs are available in section 3.2.1) and a description of the set up can be seen in section 3.4.5. The methodology of NAST1/Step1 described in 3.4.8 is used for this experimental work. All experiments of this section were carried at 50°C.

5.3.1. Transport and Retention of Dispersed COOH-MWCNTs in Silane-functionalised Sand Pack Porous Media

Sand pack experiments were performed to assess the retention of the carbon nanotubes. To consider the repeatability, the experiment was assessed twice. Figure 5-8 displays the change in the normalised effluent COOH-MWCNTs

concentration ratio of the concentration coming in over the concentration coming out (C/C_0) as a function of pore volumes (time). If the concentration ratio (C/C_0) reaches 1 over a period of time at a steady rate (expressed in pore volumes in the graph), then it has reached saturation, meaning no adsorption sites are available.

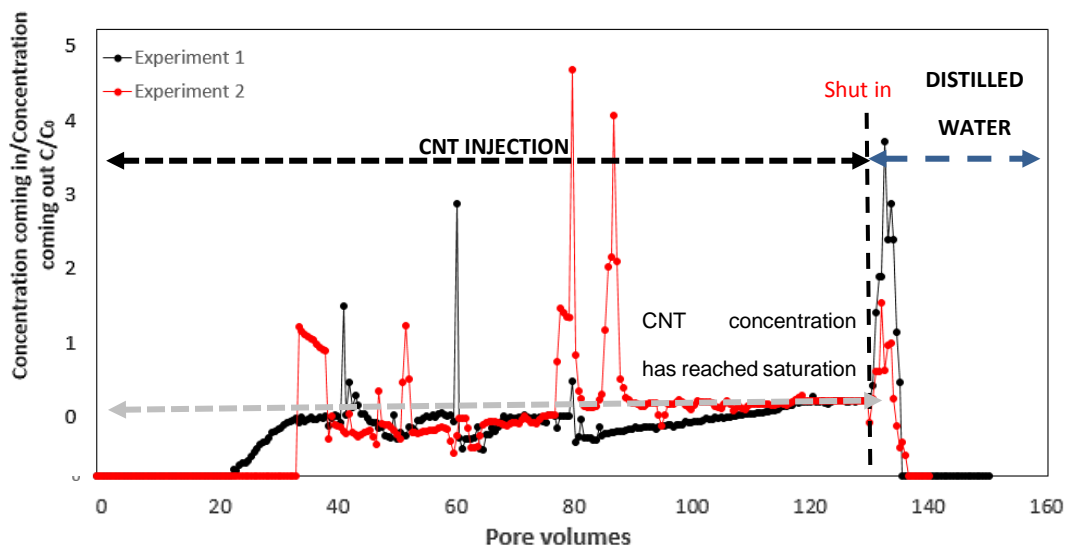


Figure 5-8 Breakthrough profiles of dispersed COOH-MWCNTs in transport experiments 1 and 2 at 50°C. Data were experimentally obtained.

There were no COOH-MWCNTs detected either by Raman (detection limit at 0.5 mg/L) or UV-vis Absorbance (detection limit at 2 ppm) between 0 to 22 PVs and 0 to 36 PVs for experiment 1 and 2, respectively. This result reinforces the theory that the porous medium is strongly adsorbing the COOH-MWCNTs because of silane functionalisation. The nanoparticles started breaking through at 22 (experiment 1) and 36 PVs (experiment 2) respectively but took until 100 pore volumes for experiment 1, and 120 PVs for experiment 2, to reach full breakthrough, meaning at this point, the COOH-MWCNT solution saturated the porous media.

The presence of peaks in Figure 5-8, indicate the release of accumulated COOH-MWCNTs which were strained and log jammed (both these terms are defined in 2.3.4) in certain pores in the porous media and were blocking

access to some adsorption sites. These deviations also lead to modifications in the physical properties of the porous medium (pore sizes, permeability impairment).

When both experiments were saturated, they were shut in for 12 hours. The following step consisted of injecting 20 pore volumes of distilled water to remove the unretained COOH-MWCNTs.

From the results in Figure 5-8, cumulative mass adsorbed of COOH-MWCNTs within porous media is plotted as a function of pore volumes in Figure 5-9.

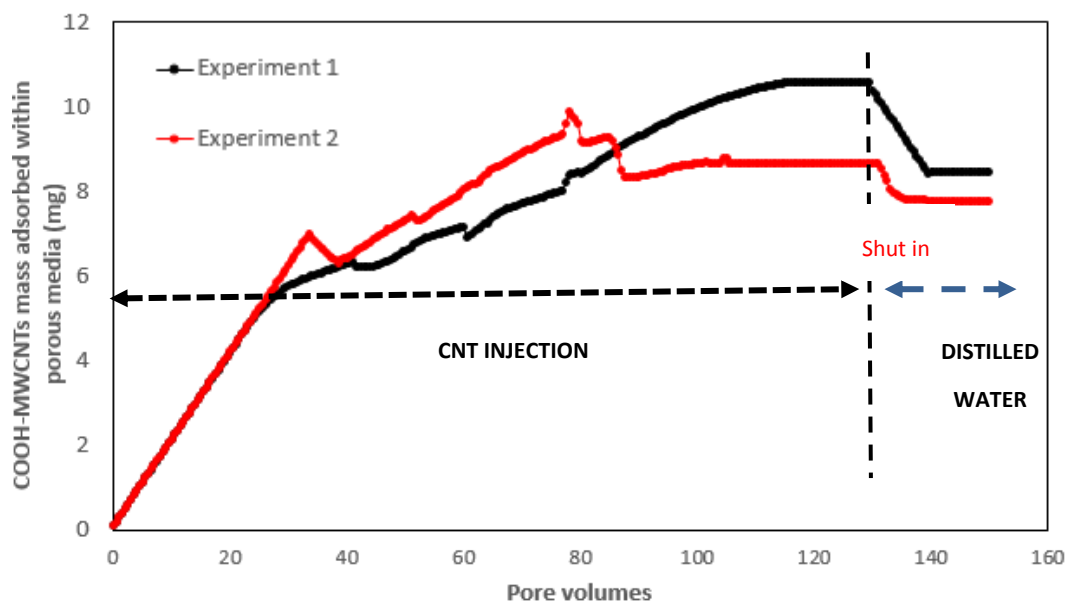


Figure 5-9 Cumulative mass adsorbed obtained from transport experiments 1 and 2 at 50°C in sand pack porous. Data were experimentally obtained.

For transport experiment 1, the mass of CNTs adsorbed per pore volume steadily increased up to 22 pore volumes, then cumulative adsorption rate slowed in response to the release of carbon nanotubes off the column. The peaks illustrated in Figure 5-9, at points 40, 60 and 80 pore volumes show little mass losses in Figure 5-9. During the distilled water flush, a loss of 0.93 and 0.75 milligrams of COOH-MWCNTs is calculated for transport experiment

1 and 2, respectively. Consequently, there is 7.85 mg (experiment 1) and 8.46 mg (experiment 2) of COOH-MWCNTs retained within the porous media by the end of the experiment.

Table 5-3 shows the cumulative mass adsorbed in milligrams in the transport experiments performed in sand packs. Experiments ended with a similar number of carbon nanotubes retained within the porous media. This is considered as evidence for good repeatability of the experiment.

Table 5-3 COOH-MWCNTs retained in sand pack porous media

Rock ID	CNTs adsorbed at shut in (mg)	CNTs adsorbed at postflush (mg)
Transport and retention experiment 1	10.35	8.68
Transport and retention experiment 2	8.45	7.75

5.3.2. Optimisation of Transport and Retention of Dispersed COOH-MWCNTs in Silane-Functionalised Sand Pack Porous Media

It can be seen in Figure 5-9 that COOH-MWCNTs desorb out during the distilled water flush. The final mass of COOH-MWCNTs adsorbed in sand packs is approximately equal to 8.21 ± 0.46 mg. Based on mass balance calculation, this implied that this mass was reached between 60 to 80 pore volumes, as illustrated in Figure 5-10. It was therefore desirable to examine the effect of lower injection volumes.

In Figure 5-10, conducting the shut in at 80 pore volumes was attempted.

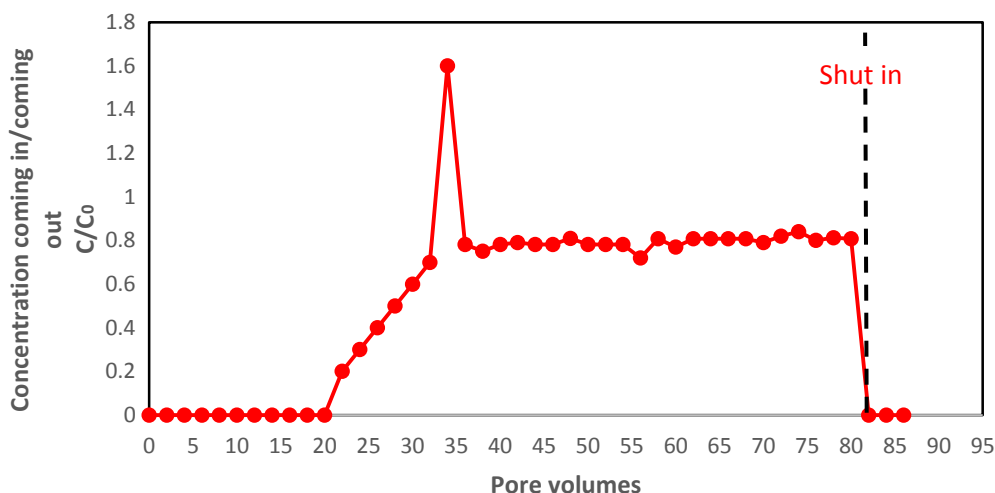


Figure 5-10 Breakthrough profiles of dispersed COOH-MWCNTs in optimised transport experiments at 50°C. Data were experimentally obtained.

As expected in Figure 5-10, the core did not reach saturation, and it reached a pseudo equilibrium at $C/C_0 = 0.80$. Consequently, this resulted in no substantial COOH-MWCNTs flowing out the column, after shut in. During the distilled water flush stage: a small number of COOH-MWCNTs were detected by Raman (limit of detection = 0.05 mg/L) for 2 pore volumes, but below the limit of quantification.

Using the results in Figure 5-8, cumulative mass adsorbed of COOH-MWCNTs within porous media is plotted as a function of pore volumes in Figure 5-9.

As seen from Figure 5-11, a lower PV injection does not affect the retention within the pack. It resulted in 7.1 mg of COOH-MWCNTs adsorbed in sand pack. There is a difference of 1.11 mg, in comparison to sand pack experiments shown in Figure 5-7. This data could lead to shorter injection period for the carbon nanotubes in a realistic application. Also, it is ideal that the release of carbon nanotubes into the nature is limited due to their toxicity [120]. Therefore a shorter nanoparticle injection may be a safer option.

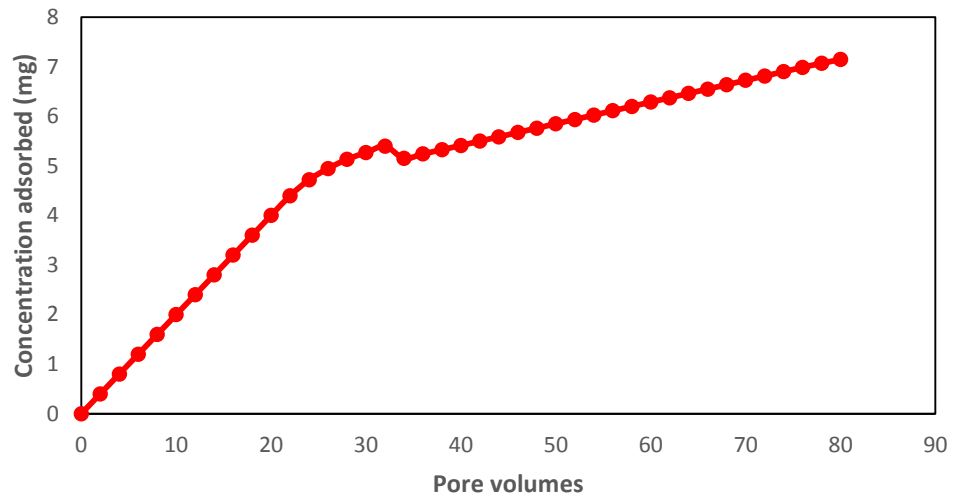


Figure 5-11 Mass gain of COOH-MWCNTs retained during injection in porous media at 50°C

A comparison of mass gained in transport experiments and optimized transport is shown in Table 5-4.

Table 5-4 COOH-MWCNTs retained in sand pack porous media: Optimised vs regular system

Rock ID	CNTs adsorbed at shut in (mg)	CNTs adsorbed at postflush (mg)
Transport experiment 1 and 2	9.4 ± 0.95	8.21 ± 0.46
Optimised transport experiment 2	7.6	7.1

5.4. Effect of COOH-MWCNTs on the Permeability of the Porous Media

COOH-MWCNTs have shown potential for increasing oil recovery for various applications [60, 121]. Due to their small size nanoparticles can pass through a range of reservoir pores. Injecting particles through a silane functionalised core or a reservoir will lead to particle retention and this will affect the permeability of the rock. Particle retention can occur through various mechanisms such as log-jamming, straining or adsorption onto rock surface. As a reminder, for the successful application of the NAST methodology, the effective placement of carbon nanotubes in the porous media is an important step. In order to perform this step, the porous media is pre-treated with silane to enhance the retention of carbon nanotubes onto the porous media.

The retention behaviour of the COOH-MWCNTs in a silane functionalised porous media can play a major role in oil recovery by, potentially changing reservoir permeabilities. During the injection process, ideally, the pressure difference would have a minimal deviation from start of test to the end, this would indicate very little damage to the core. It is important for permeability impairment in reservoir properties to not exceed a certain extent to prevent other major oilfield issues such as a reduced oil production in real life applications.

The transport and retention of COOH-MWCNTs was assessed in four different silane-treated cores of various permeabilities, ranging from moderate to low permeability. The core plugs had average dimensions of 13.23 mm length, 14.01 mm width and 15.04 mm height. The setup shown in Figure 3-16 was used, and Omega PX409 pressure gauge was installed to record the differential pressure. All cores were injected with a dispersed COOH-MWCNTs solution (concentration of 10 ppm) for a period of 5 hours. The pressure difference across the core was recorded during the entire injection process. Examination of permeability impairment was conducted by comparing the flow ability of brine before and after COOH-MWCNTs injection.

Optical analysis was also performed in order to support the observed reduction in permeability that occurred during flooding with CNTs.

5.4.1. Effect of Nanoparticle Injection on Differential Pressure in Rock Cores

The experiment consisted of injecting COOH-MWCNTs into various silanised rocks, to assess which rock to select to test NAST with a core flood, without excessively raising the pressure difference in a silanised porous rock. Figure 5-12 shows the pressure difference profiles amongst all the rocks tested.

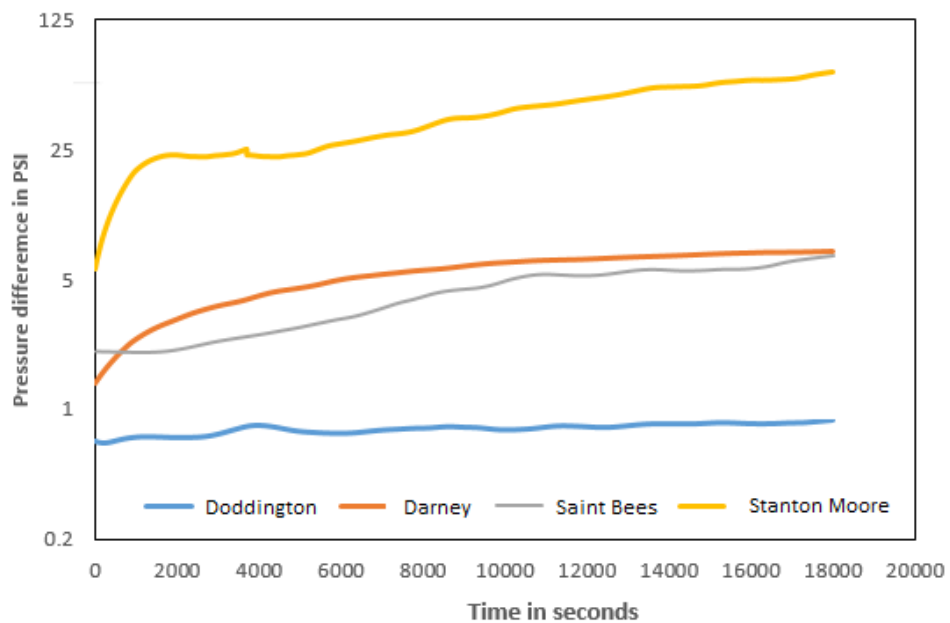


Figure 5-12 Differential pressure graph of CNT injection into all rocks

The differences in the profiles demonstrate that the pressure difference in the Doddington rock has smoothly increased from 0.4 PSI to 0.9 PSI (2.75 to 62.05 KN/m²). While Darney and Saint Bees had a similar profile, the pressure difference in both cores increased more drastically.

The Stanton Moore pressure drop has severely increased overtime going from 7 to 68 PSI (48.26 to 468.843 KN/m²), this indicates severe pore blockages by the nanoparticles.

This data indicates that NAST operates well with a high permeability rock such as Doddington, it highly modifies the properties of Saint Bees and Darney which are initially moderate and low permeability rock respectively. It looks fully incompatible with a rock such as Stanton Moore which originally has a low permeability rock. A more detailed explanation of the rock selection of core flood is described in section 5.4.2.

5.4.2. Permeability Impairment due to COOH-MWCNT Injection in Various Sandstone Cores

From results in Figure 5-12, the injection carbon nanotubes increased the differential pressure to a great extent, especially for the Stanton Moore rock core. The Doddington rock had the smallest shift during the injection. It was therefore desirable to examine the permeability impairment due to the retention of the nanoparticles in porous media. As seen in Table 5-5, all rocks displayed a severe permeability reduction. Oil and gas regulations do not allow a permeability reduction higher than 20%.

Table 5-5 Permeability post and pre-experiment of Doddington rock sample

Rock ID	Pre injection mD	After injection mD	Permeability impairment
Doddington	51	12	76.40 %
Darney	48	0.8	98.30 %
Saint Bees	2.5	1	60.00%
Stanton Moore	0.93	0.46	50.53%

Differences in permeability impairment show that Doddington has a final permeability of 12 mD, which theoretically is acceptable for oil and gas productions. However, regulations do not allow a realistic application to have permeability impairment higher than 20% [40, 47, 122, 123]. In all the other rocks tested, the final permeability was between 1 to 0.8 mD and had a permeability impairment higher than 20%. From optical inspection presented in section 5.4.3, it seems that CNTs blocked most of the pores pathways of the cores. If the test, was scaled up to a coreflood, the low permeability may have been a problem, so in order to prevent issues that come with low permeability rocks, Doddington was chosen. The permeability impairment is an area that will receive attention in future work.

This data set indicates, that as of today, NAST is compatible with high permeability rocks. But this is an area that can be improved if lower concentrations are chosen for example.

5.4.3. Optical Inspection of Retention of COOH-MWCNTs

Optical inspections were performed on each rock samples after the effects on permeability were assessed. It is observed that the colour of inlet of has changed to black as COOH-MWCNTs were attempted to be injected into the core. The analysis done in this section makes it achievable to support the observed reduction in permeability that took place during flooding with nanoparticles.

5.4.3.1. Optical Inspection of Retention of COOH-MWCNTs: Doddington rock core

Doddington is a pink, medium grained sandstone. It has an average composition of 69% quartz, 5% feldspar, 2% iron oxide; 5% clay and exhibit a porosity of 19% [93]. Figure 5-13 shows the Doddington rock sample before and after injection of the carbon nanotubes in the porous media.

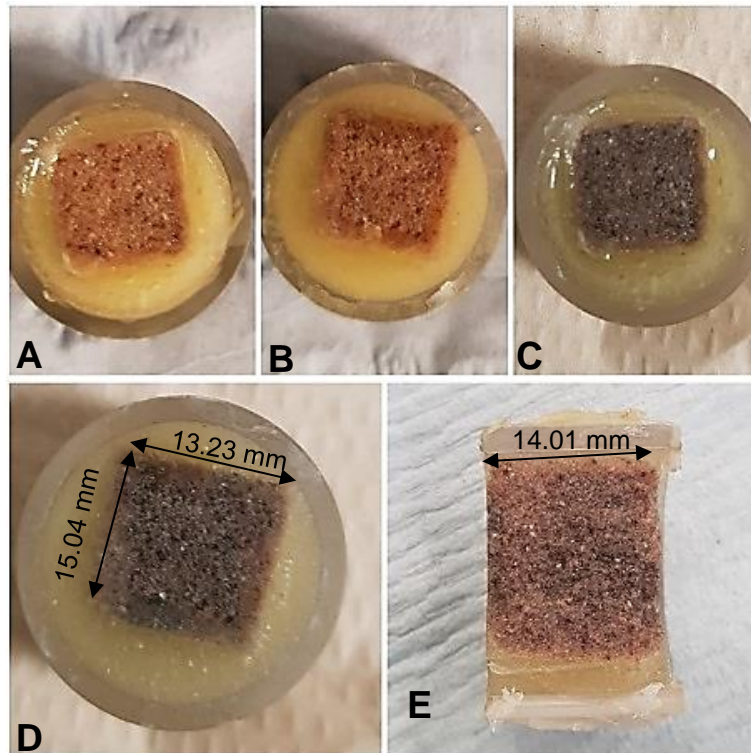


Figure 5-13 Doddington profiling A) Inlet before injection B) Outlet after injecting C) Inlet post injection D) Outlet post injection E) Cross section

It was observed that the COOH-MWCNTs deposition was reasonably uniform in this rock sample. It can also be reinforced that a homogenous dispersion of COOH-MWCNTs into the core was achieved from the uniform colour of the inlet. The outlet colour has also uniformly turned black, which suggests that CNTs have been transported the core evenly.

5.4.3.2. Optical Inspection of Retention of COOH-MWCNTs: Darney rock core

Darney is a yellow-buffed coloured, medium grained sandstone. It has an average of 73.5 % quartz composition, 1.5% feldspar, 1 % iron oxide, 6% clay and average porosity of 18% [93]. Figure 5-14 shows the Darney rock sample before and after injection of the carbon nanotubes in the porous media.

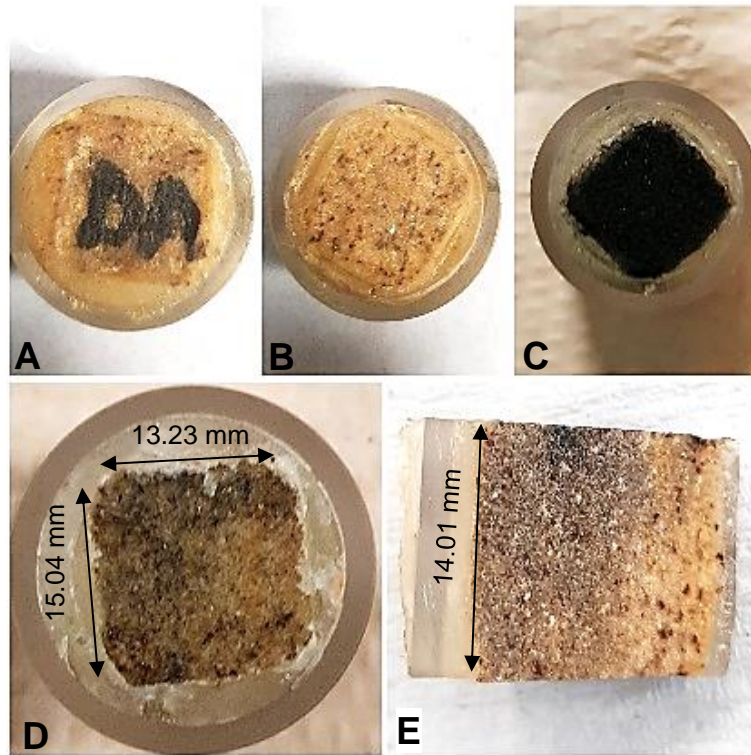


Figure 5-14 Darney sandstone profiling A) Inlet before injection B) Outlet after injecting C) Inlet post injection D) Outlet post injection E) Cross section

In Figure 5-14, it can be seen that a homogenous dispersion of COOH-MWCNTs into the core occurred from the uniform colour of the inlet. Figure 5-14 D and E suggests that a large number of the particles were strained and blocked a few pore pathways, explaining why there was such a high permeability impairment, see Table 5-5 for more details. The outlet colour of core has partially turned black, which suggests that a certain number of CNTs have gone through the core unevenly.

5.4.3.3. Optical Inspection of Retention of COOH-MWCNTs: Saint Bees rock core

Saint Bees rock is a red coloured sandstone which has an average of 69% quartz, 2% feldspar, 5% iron oxide, 5% clay and 19% porosity [93]. Figure 5-15 shows the Saint Bees rock sample before and after injection of the carbon nanotubes in the porous media.

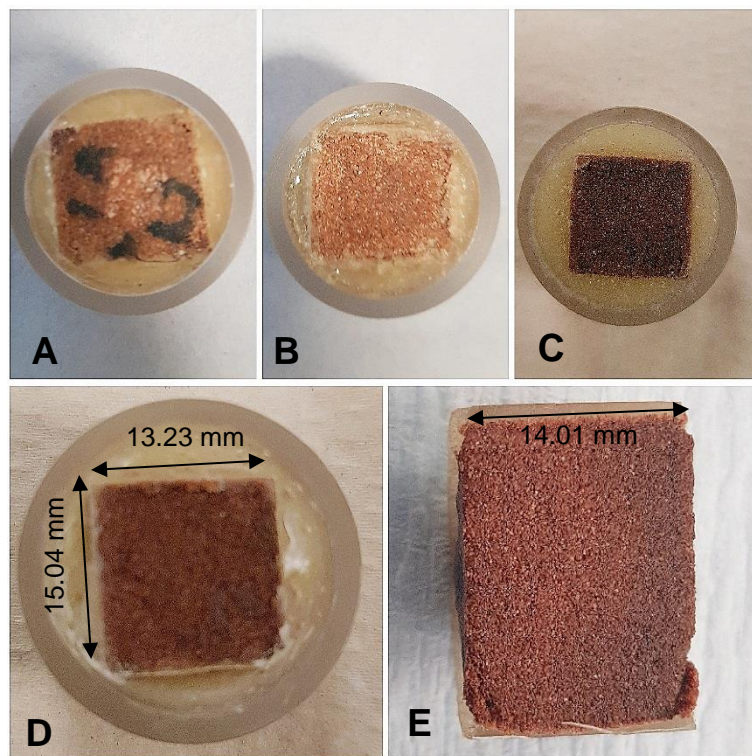


Figure 5-15 Saint Bees sandstone A) Inlet before injection B) Outlet after injecting C) Inlet post injection D) Outlet post injection E) Cross section

Figure 5-15 shows that the COOH-MWCNTs did not manage to go further than the upper half of the sandstone porous media. Most likely due to high amount of pore blockages. The Raman analysis was unable to detect any peaks indicating that the COOH-MWCNTs were not able to break through from the sandstone.

In Figure 5-15 C, it can be seen that a homogenous dispersion of COOH-MWCNTs into the core occurred from the uniform colour of the inlet. However, Figure 5-15 D and E suggests that a large number of the particles were entrapped in the porous media and never broke through. This was confirmed by Raman analysis as it was unable to detect any peaks that would indicate that the COOH-MWCNTs were able break through from the sandstone. The retention of the nanoparticles within the media explains why there was such a high permeability impairment, see Table 5-5 for more details. The outlet colour of core has not turned black, which suggests that CNTs have only gone through a certain distance in the core.

5.4.3.4. Optical Inspection of Retention of COOH-MWCNTs: Stanton Moore Rock Core

Stanton Moore is a fine grain sandstone, it has an average porosity of 14%. It is a sandstone that is composed of 73.5% quartz, 3.5% feldspar, 2% iron oxide and 7% clay [93]. Figure 5-16, shows the Stanton Moore rock sample before and after injection of the carbon nanotubes in the porous media.

In Figure 5-16 C, it can be seen that a homogenous dispersion of COOH-MWCNTs into the core occurred from the uniform colour of the inlet. At the inlet, it can be observed that the COOH-MWCNTs deposition was reasonably even in this rock sample, which indicates that many pores were blocked. However, Figure 5-16 D and E suggests that no particles had managed to penetrate the rock core. This was confirmed by Raman analysis as it was unable to detect any peaks that would indicate that the COOH-MWCNTs were not able break through from the sandstone. The retention of the nanoparticles within the inlet of the media explains why there was such high permeability impairment, see Table 5-5 for more details. The outlet colour of core has not turned black, which suggests that CNTs have not gone through the core.

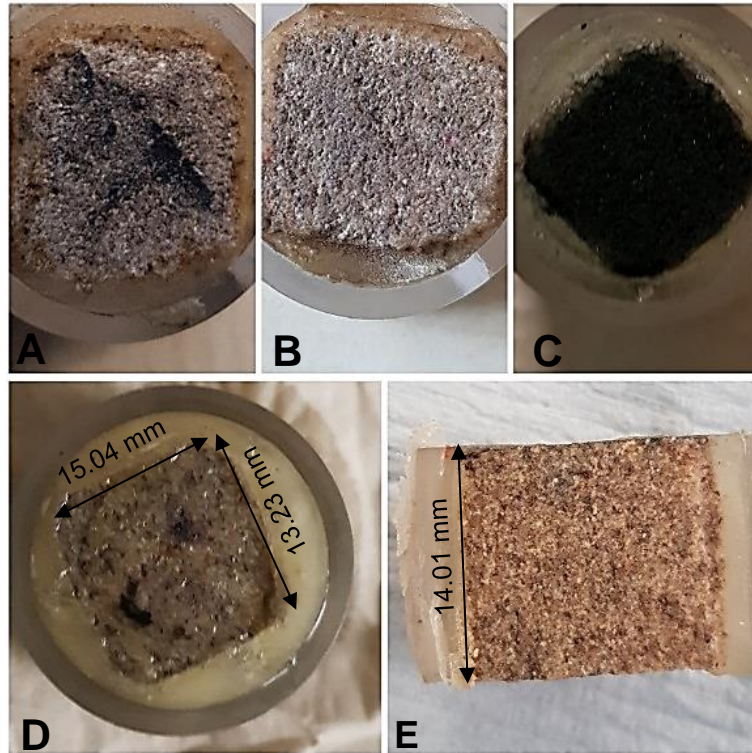


Figure 5-16 A) Inlet before injection B) Outlet after injecting C) Inlet post injection D) Outlet post injection E) Cross section

5.5. Core flood: Injection and retention of COOH-MWCNTs

A coreflood experiment was carried out to study the transport and retention of COOH-MWCNTs in porous media as well as and most importantly the retention of scale inhibitor. The latter will be discussed in the next chapter (Chapter 6).

Permeability impairment tests allowed to select this rock for the core flood experiments. Doddington rock was selected as it offered the smallest pressure difference deviation from start of test to the end. It also had the highest permeability post injection and retention of COOH-MWCNTs.

The coreflood was conducted in a Hassler style of coreflood with a confining pressure of approximately 1000 PSI (6894.76 KN/m²). The experiment details are described in section 3.4.6.

5.5.1. Transport and Retention of COOH-MWCNTs in core flooding

In Figure 5-17, the analysis of the concentration of COOH-MWCNTs coming off the core flood is monitored as a function of pore volumes. This data provides information on the release rate of the nanoparticles off the silane-functionalised rock.

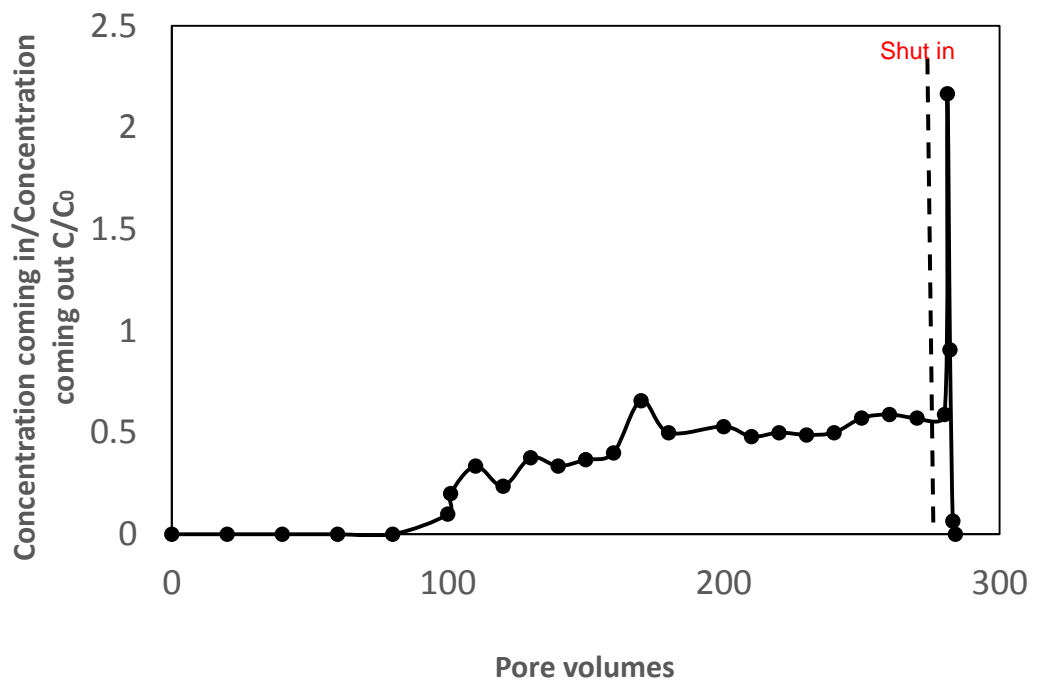


Figure 5-17 Breakthrough profiles of dispersed COOH-MWCNTs core flood experiments at 25°C performed to evaluate the impact of silane functionalisation on COOH-MWCNT transport and retention. Data were experimentally obtained.

From Figure 5-17, the nanoparticles broke through at 80 pore volumes. This was followed the concentration of solution coming off kept increasing until it reached a pseudo-steady release at 80% breakthrough around 170 pore volumes. The core never reached full breakthrough, meaning that it never saturated, so the injection was stopped at 280 pore volumes. In the postflush

period, only 3 PVs had nanoparticles within them. The fact that the solution did not saturate, is supported by the optical inspection in Figure 5-19.

Figure 5-18 shows the cumulative mass gain as a function of pore volume. This data gives information on the number of nanoparticles adsorbed onto the core.

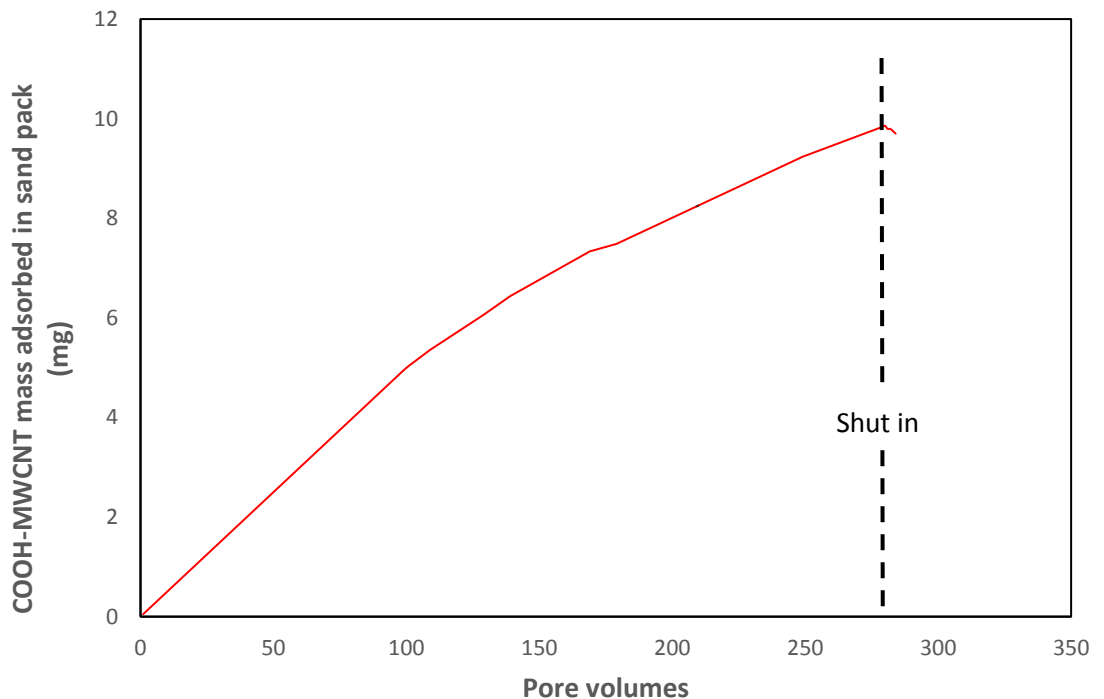


Figure 5-18 Mass gain of COOH-MWCNTs retained during injection

There is 9.9 mg of COOH-MWCNTs retained within the core after 280 PVs of injection. There is obviously more retention than a sand pack because the rock formation is tighter. A minimum amount of 0.5 mg was lost during the postflush.

5.5.2. Permeability Impairment due to COOH-MWCNT Injection in Coreflood

As seen in Table 5-6, COOH-MWCNTs retained within the core experienced quite a high change in permeability. The final permeability is 14.5 mD which is theoretically within an acceptable range for oil and gas productions. However, as mentioned earlier, oil companies would not allow changes exceeding 20% to occur in a real conditions. In future work, a more controlled permeability change is required in order to design the tests for the field.

Table 5-6 Doddington core permeability pre and post CNT injection.

Pre injection mD	After Postflush mD	Permeability impairment (%)
190	14.5	92

Figure 5-19 shows a picture of the core before and after the COOH-MWCNTs injection.

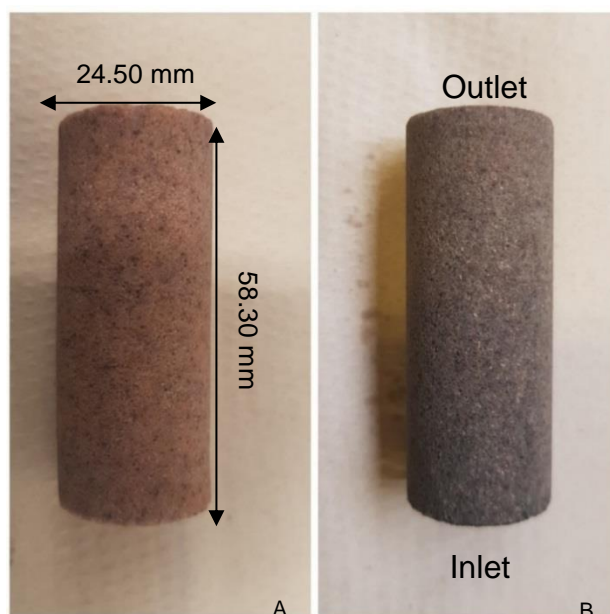


Figure 5-19 a) Before CNT injection b) After CNT injection.

5.5.3. Petrophysical Nuclear Magnetic Resonance

Figure 5-20 illustrates the pore size distributions of the core obtained by NMR relaxation of water where relaxation time T_2 directly corresponds to the pore size of the rock. The y-axis represents the normalised signal of each pore to accumulative signals. Larger T_2 represents bigger pore sizes and the normalized signal amplitude indicates the pore size distributions. The pore size distribution of the Doddington rock core was measured before and after the coreflood tests. The graph illustrates a clear change in pore size distribution, it is clear that most pores were reduced by retention of COOH-MWCNTs on sand SI. Furthermore, the pore volume decreased from 5.65 to 5.21 mL, representing a 7.7% pore volume reduction.

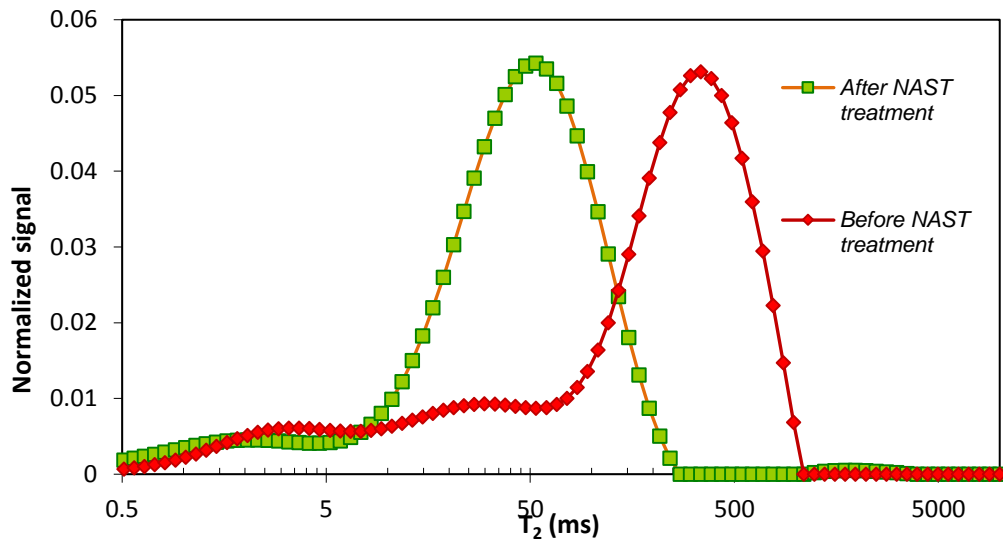


Figure 5-20 Pore size distribution of core before and after experiment

5.5.4. Scanning Electron Microscope Results of Bonded COOH-MWCNTs onto the Doddington Rock Porous Media

The SEM pictures support the observed impairment in permeability that occurred during flooding with nanoparticles. Pictures also demonstrated the successful retention of COOH-MWCNTs w prior silane functionalisation process.

Figure 5-21 show pictures of the Doddington rock core, after the injection of COOH-MWCNTs within the rock. Pictures taken from various area of the core are taken.

Figure 5-21 A, B and C show three SEM images of the core inlet at different magnifications. Figure 5-21 A illustrates that the carbon nanotubes are clearly attaching on the pore walls without blocking the pore. This goes in line with the NMR data (Figure 5-20), that pores sizes are reduced by the retention of COOH-MWCNTs in porous media. Figure 5-21 B shows COOH-MWCNTs bundled and attached along the pore pathway, the deposition of the COOH-MWCNTs in the porous media seems to be multilayer one. Figure 5-21 C is a higher magnification of Figure 5-21 B, from this, it can be seen that the COOH-MWCNTs attached to the surface, however there are still sites available for adsorption, as there some uncovered areas.

In Figure 5-21 D and E, SEM pictures are taken from a cross section of the core. In Figure 5-21 D shows a flat rock grain covered with COOH-MWCNTs. The deposition is random. However, an overall uniform coverage was gained, which is one of the aims of the NAST methodology. In comparison to the inlet, there is evidence for less agglomeration. Figure 5-21 B shows attached COOH-MWCNTs onto the rock walls, and agglomeration of COOH-MWCNTs inside a pore throat. This supports the notion that pore throat size are also affected in a rock such as Doddington.

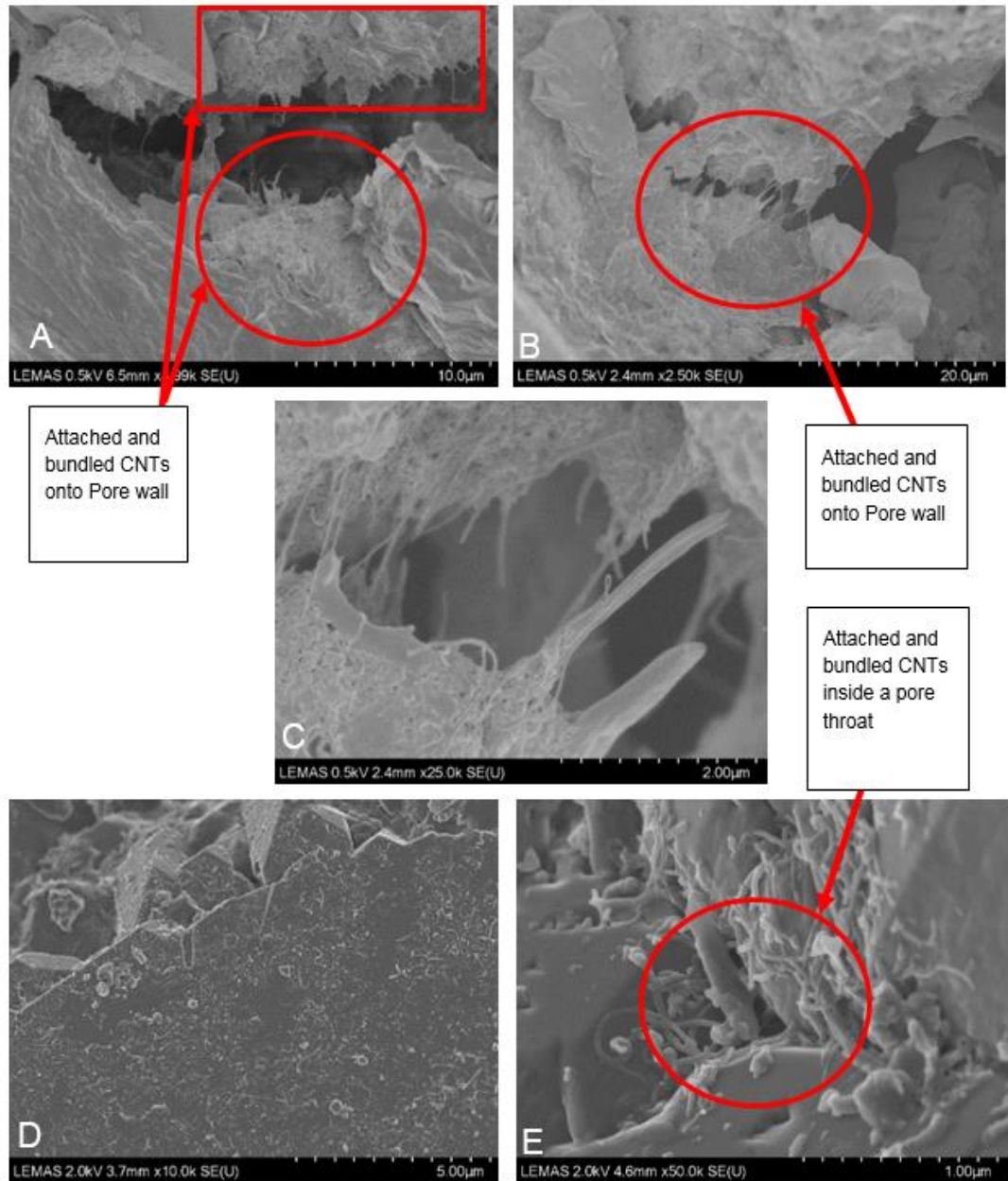


Figure 5-21 Doddington SEM pictures A) Rock Inlet B) Rock inlet within a pore pathway C) Magnification to illustrate deposition of CNTs within pore pathway D) Cross section of core showing an uniform deposition of COOH-MWCNTs E)COOH-MWCNTs deposition in front of a pore pathway

In order to substantiate the fact that CNTs are attached onto rocks in Figure 5-21, Figure 5-22 shows the bare surface of a doddington rock without any COOH-MWCNTs attached to the surface.

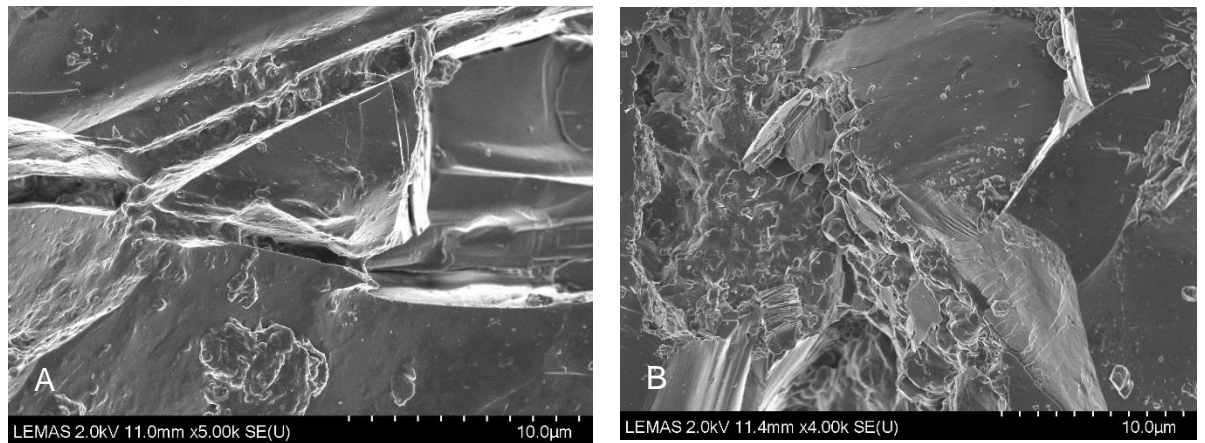


Figure 5-22 A and B - Doddington SEM pictures without CNTs attached to the rock surface

5.6. Conclusion

This chapter assesses the first part of the NAST methodology in dynamic flooding experiments. Specifically, it investigates the successful attachment of COOH-MWCNTs onto rock surfaces, and their effect on permeability. Pore blockages are unwanted. In order to maximise the prevention of this, first of all, the COOH-MWCNTs have to be well dispersed and the solution must remain stable for a span of at least 24 hours. This was successfully proven with the DLS and stability analyzer data. Then, to ensure the successful attachment of the COOH-MWCNTs in porous media, the rock must be reactive, so it was treated with (3-aminopropyl) ethoxysilane. The silane coupling agent creates a functional group which bonds with COOH-MWCNTs.

Data from permeability tests, NMR pore size distribution and SEM pictures have all shown that transport and retention of COOH-MWCNTs affect reservoir properties. It is necessary to conduct additional experiments to build upon the achieved results to minimise permeability impairments for a potential realistic application. The data set presented herein gives an initial understanding of the effect of COOH-MWCNTs in a silane functionalised porous media.

Chapter 6 Inhibitor Dynamic Testing of the NAST methodology

NAST 1 and NAST 2 have been separately studied in Chapter 4 and Chapter 5. NAST 1 focuses on the transport and retention of COOH-MWCNTs onto the rock surface. This process modifies the rock surface in order to increase its reaction to scale inhibitor (SI) and thus improving the adsorption and desorption of the aforementioned. NAST 2 involves the adsorption of PPCA onto the COOH-MWCNTs. The feasibility of NAST in dynamic experiments has been previously demonstrated by Ghorbani [6]. The focus of the study is to carefully assess the NAST methodology at 25°C and 50°C and better studying the retention and desorption processes of PPCA under this methodology. Comprehensive sand pack and core flood data were experimented in order to extend the understanding of this novel methodology. Experiments were performed using sand packs and core flood experiments. The sand pack is a simplified version of a core because it is a replication of the sandstone formation. Furthermore, it is easily reproducible, and it is a highly permeable media allowing to prove concepts before getting into core tests. In order to obtain a core, a cylindrical rock sample is cut from the oil reservoir, a process that normally occurs during the drilling operation. Then the sampled core is used for flooding experiments by placing the core in a core holder and pressurising the outer surface to simulate the reservoir pressure condition.

Figure 6-1 represents a schematic representing an adsorption/desorption curve illustrating the effluent concentration of SI as the volume of fluid injected, this is usually stated in terms of the pore volume (PV) in the core. The red and blue lines denote the concentration of SI during the injection of SI into the core and post-flush, respectively, at every PV. The vertical green line indicates where post-flush was started and the horizontal one shows the concentration of SI during main treatment [6]. Squeeze treatment or a coreflood test is conducted until the effluent concentration reaches MIC [6]. A result can be

extrapolated from the return curve, which is a calculation of the mass of SI remaining in the core. Hence, the surface area (SA) below the green line represents the total mass of SI injected in the core and SA below red and blue curves indicate the mass ejected during main treatment and post-flush, respectively [6]. Therefore, the cumulative mass of SI remaining in core at each PV injected can be obtained by subtracting the mass ejected from mass injected [6].

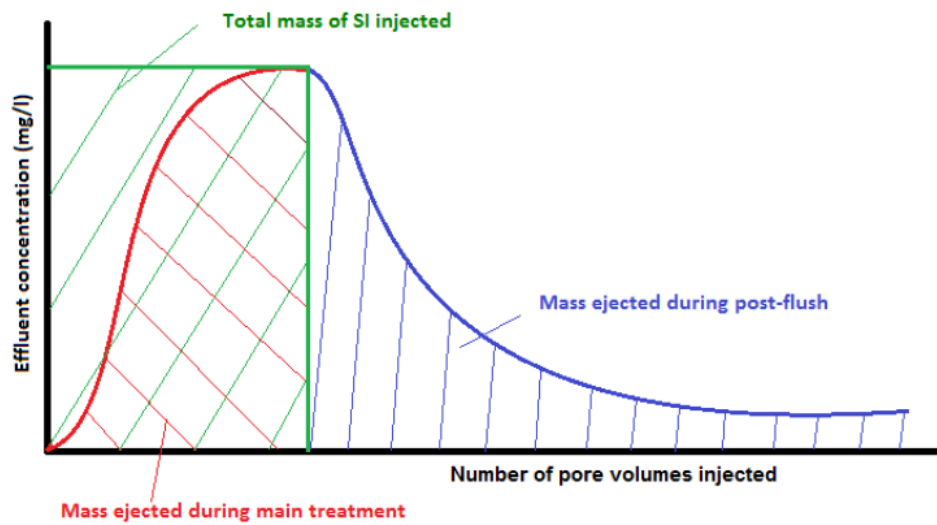


Figure 6-1 Schematic of adsorption and desorption curve of effluent concentration of flooding experiments

The scale inhibitor PPCA was prepared in a standard NFFW brine, described in 3.1.1. The C18-hyamine method was used to measure the concentration of the scale inhibitor, see section 3.4.5 for the methodology. Induced Coupled Plasma Mass Spectroscopy (ICP-MS) was used to investigate the behaviour of elements such as calcium.

6.1. Experimental Details

In this chapter, sand pack and core flood experiments were done at 25 and 50°C. However previous research was mostly done at room temperature.

In a chronological order, the following experiments were conducted to give a methodical approach to study the adsorption of PPCA onto silica against the NAST methodology. Due to time limitation, only one NAST coreflood experiment was carried out.

1. Sand pack flood: Conventional PPCA flood against NAST PPCA flood at room temperature (25°C).

These tests were designed in order to assess NAST with a realistic brine. This enabled to test NAST with a complex brine and evaluate whether it functions under these conditions.

2. Sand pack flood: Conventional PPCA flood against NAST PPCA flood at 50°C and against NAST PPCA re-squeeze NAST at 50°C.

These tests assessed NAST squeeze lifetime within more realistic conditions, and re-injection of scale inhibitor was tested for the first time.

3. Core flood: Conventional PPCA against NAST PPCA flood at 25°C and against NAST PPCA flood re-squeeze at 25°C.

These tests allowed to test the methodology with a rock core and the improved methodology developed throughout the research project via the use of the sand pack experiments.

6.2. Results

Coreflood and sand pack methodologies have been tested to assess the methodology of the NAST methodology in the laboratory. Every experiment was designed to understand the adsorption and desorption mechanism by comparing results from the NAST methodology to the conventional methodology. A few experiments had a scale inhibitor re-injection, also known as re-squeeze. This helped better assess one of the long term benefits of this methodology.

6.2.1. Sand Pack Flood: NAST VS Conventional PPCA flood at 25°C

This section provides a comparison of the conventional and NAST sand pack flood at a single flow rate, 20 mL/hr. Steps for the NAST and conventional methodology are described in section 3.4.8.1. The main treatment uses 5000ppm PPCA in NFFW brine; whereas all post flush uses NFFW brine at 20 mL/hr. The main treatment, shut in and post flushes were conducted at 25°C.

6.2.1.1. Comparison of Conventional and NAST Methodologies in Sand Pack Flood at 25°C

Figure 6-2 displays the effluent concentration of PPCA (ppm) as a function of the pore volumes injected. The results of NAST and conventional tests are compared to understand the efficacy of the novel methodology. There were two experiments, for each methodology tested, thus allowing variability to be assessed (expressed as errors bars). The experiment was flushed up to 50 pore volumes to first investigate the adsorption and desorption mechanism of the NAST methodology.

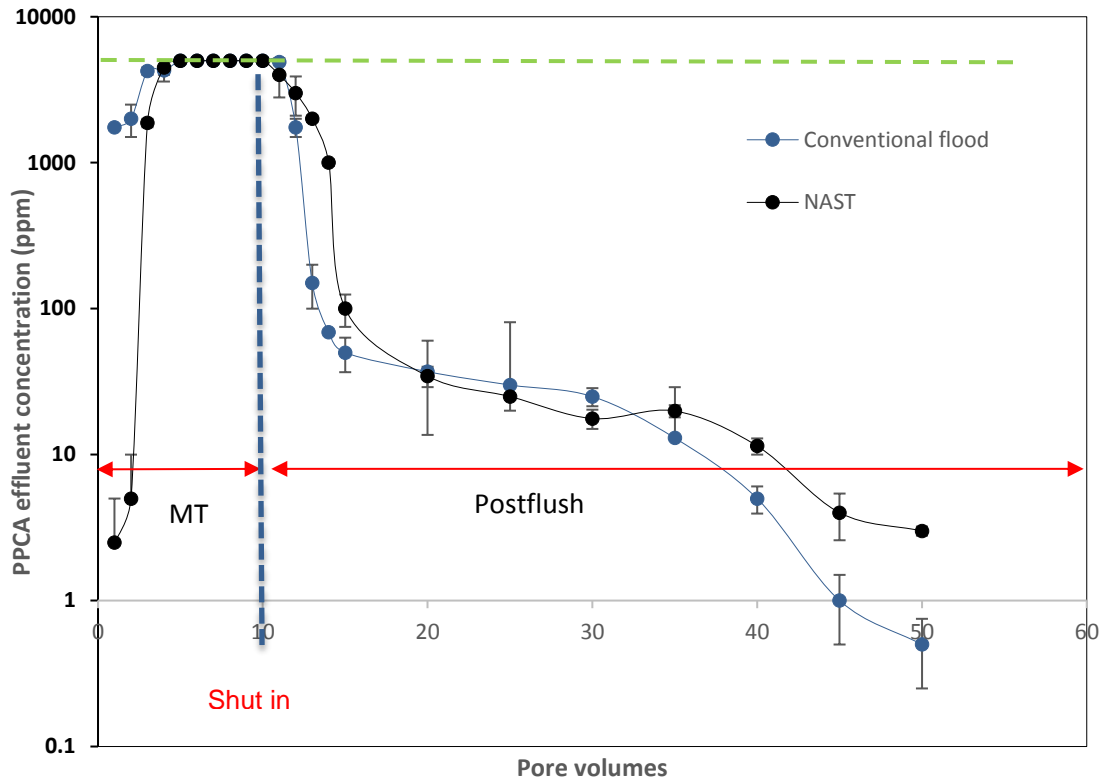


Figure 6-2 Sand pack experiments comparison of conventional method and NAST at 25°C effluents concentration as a function of PV

Figure 6-2 indicates that NAST has a steeper reach to saturation than the conventional method. This indicates a strong adsorption rate and is due to the presence of the carbon nanotubes that have changed the affinity of the rock. It can be seen that for the NAST methodology experiments, the first two pore volumes equalled 0.005% and 0.007% of the stock solution. While the conventional method had 35% and 40% of the stock solution for the first two pore volumes. From the 5th to 10th PV, SI effluents stabilised at their stock concentrations; which indicate that the chemical was fully saturated in the sand pack system. At this point, shut in is performed.

After shut in, when flow recommences, a drop in SI was observed for the first pore volume of post flush for the NAST methodology. This is indicative of a high retention in the porous media due to COOH-MWCNTS and cations (further detailed in section 6.2.1.3.). This extra adsorption was not observed with the conventional method.

The post flush period was carried out from 10 PV until 50 PV of brine injection. By the end of the flush period, the conventional experiment SI concentration had dropped below the Minimum Inhibitor Concentration (MIC), 1 ppm, at 50 PVs. At the same pore volume, the NAST methodology sand pack was able to desorb the inhibitor above MIC. This highlights the superiority in desorption performance from the NAST methodology. Repeatability of the experiments reinforce the presented results.

6.2.1.2. Mass Balance of Adsorbed Inhibitor on Sand Pack: Comparison of NAST and Conventional Method

The tests presented in Figure 6-2 were originally designed to assess the mechanism of SI adsorption and desorption. Hence, in order to better understand the system, cumulative mass of SI adsorbed is calculated. This will provide information on the adsorption mechanisms.

Figure 6-3 displays the mass of PPCA remaining in the core in mg. Higher adsorption and a more steady release of PPCA can be observed for the NAST methodology. These results show that the presence of COOH-MWCNTs has clearly enhanced the affinity of PPCA with the porous media. Mass balance calculations have revealed that by the end of the post flush period, a large number of PPCA was still adsorbed within the media. This indicates that the NAST methodology had the potential to desorb the inhibitor for a longer period than the conventional method.

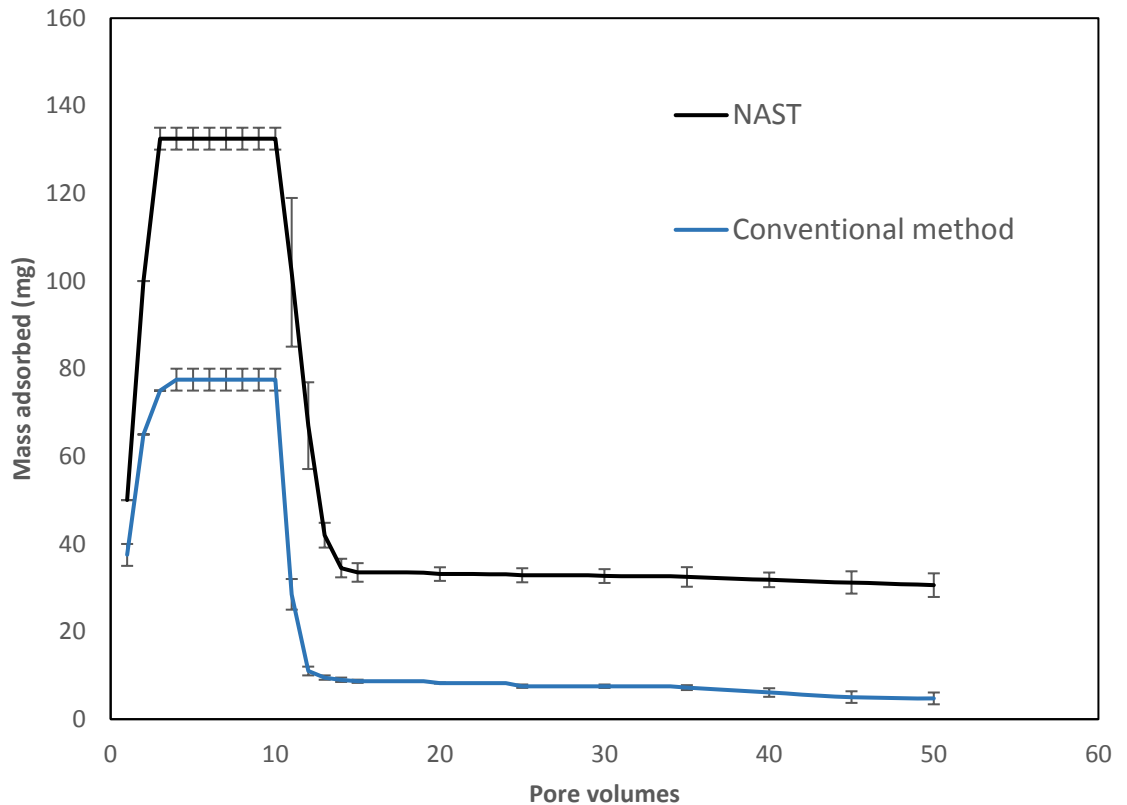


Figure 6-3 Mass of SI adsorbed onto sand pack as a function of PV (NAST vs Conventional)

6.2.1.3. Ion Monitoring of Calcium during Flushing Period

Calcium also plays a role in SI retention. This was investigated for the NAST methodology. In Figure 6-4, they were monitored by ICP for this experiment. After the shut in, at the initial release of the first post flush, the calcium is reduced from 2000 ppm to 150 ppm. This indicates the associated bonding between SI and Ca to form a complex [29]. COOH-MWCNTs are also known for having a bridging effect with calcium ions [103]. This also plays a role in the successful retention of the scale inhibitor as was demonstrated by Ghorbani [6].

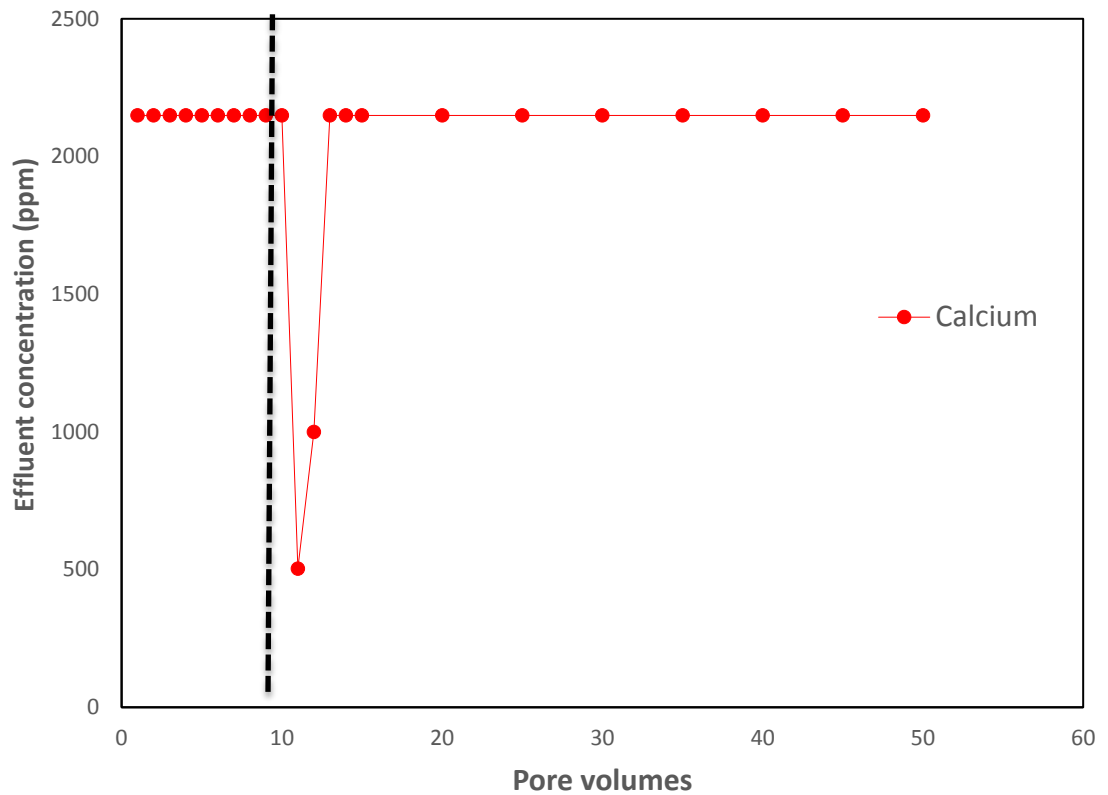


Figure 6-4 Monitoring of calcium with ICP as function of pore volumes injected

6.2.2. Sand Pack Flood: Conventional, NAST and NAST re-squeeze in sand pack flood at 50°C

This section represents a comparison of the conventional and NAST sand pack flood at a single flow rate, 20 mL/hr. Steps for the NAST and conventional methodology are described in section 3.4.8.1. The main treatment uses 5000ppm PPCA in NFFW brine; whereas all post flush uses NFFW brine at 20 mL/hr. The main treatment and post flushes were conducted at 25°C.

6.2.2.1. Comparison of Conventional, NAST Methodologies Adsorption and Desorption Curves in Sand Pack Flood at 50°C

Figure 6-5 displays the effluent concentration of PPCA (ppm) as a function of the pore volumes injected. The results of NAST, NAST re-squeeze, conventional tests are compared to examine the effectiveness of the novel methodology. There were two experiments, for each methodology tested, thus producing estimates of variability (errors bars). The experiment was flushed until the inhibitor was below MIC (1 ppm). For the first time, the re-squeeze abilities of NAST have been tested.

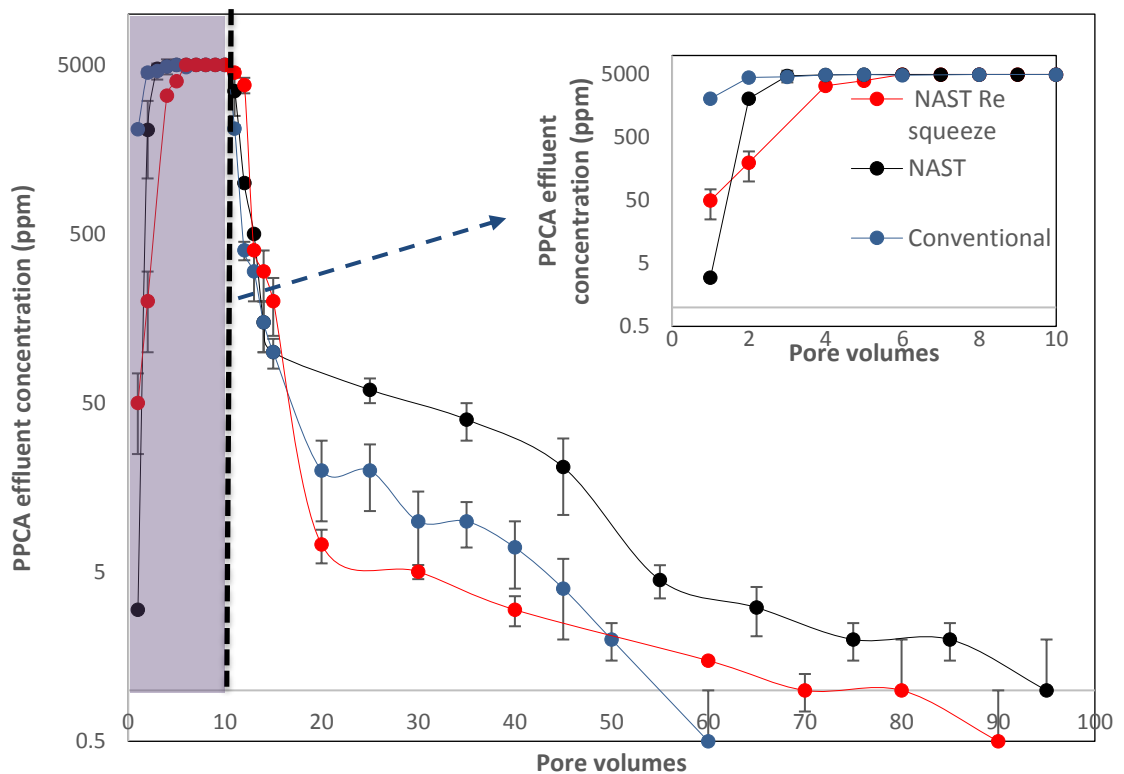


Figure 6-5 Sand pack experiments comparison of conventional method, NAST and NAST Re-squeeze at 50°C effluents concentration as a function of PV. The faded area is being magnified to show the adsorption rate of each experiment.

Figure 6-5 indicates that NAST has a steeper reach to saturation in comparison to the conventional method, a closer examination can be seen in the magnified area of the graph. The graph indicates a strong adsorption rate because of the presence of the carbon nanotubes that have changed the affinity of the rock porous media. It can be seen that for the NAST methodology experiments, the first two pore volumes were 0.006% and 40% of the stock solution, while the conventional method had 40% and 90% of the stock solution released for the first pore volumes. From the 3rd to the 10th PV, SI effluents stabilised at their stock concentrations; which indicate that the chemical was fully saturated in the sand pack system. At this point, shut in is performed.

When the flow resumes, post shut in, the NAST methodology outperforms the lifetime of the conventional method by 37%. The NAST re-squeeze test has been shown to be successful. It demonstrates a stronger adsorption rate than the conventional method and a slower desorption rate in comparison to the conventional squeeze treatment. It outclasses the conventional method lifetime by 33%.

6.2.2.2. Mass Balance of Adsorbed Scale Inhibitor on Sand Pack: Comparison of Conventional, NAST and NAST re-squeeze methodologies

In order to substantiate the adsorption and desorption results, cumulative mass of SI adsorbed is calculated. This provides information on the adsorption and desorption mechanisms.

Figure 6-6 displays the mass of PPCA remaining in the core in mg. Higher adsorption and a more steady release of PPCA can be observed for the NAST methodology. These results show that the presence of COOH-MWCNTs have enhanced the affinity of PPCA with the porous media. Re-squeeze is also displaying a greater PPCA affinity to the porous media than the conventional treatment.

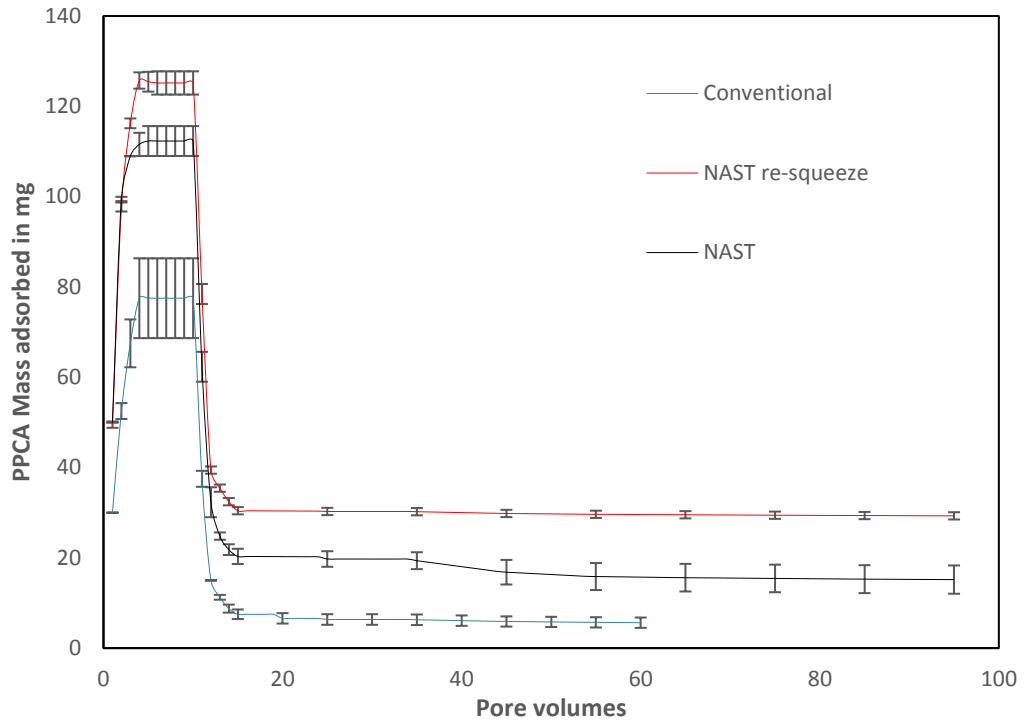


Figure 6-6 Mass of SI adsorbed onto sand pack as a function of PV (NAST vs Conventional vs NAST re-squeeze)

These results demonstrate irreversible retention as there is still a large amount of PPCA attached within the core at the end of the postflush, for both the NAST and NAST re-squeeze methodologies. This type of behaviour has already been observed by Ibrahim et al. [49], as well as Kerver et al. [124]. Methods have to be found to desorb the extra amount of PPCA adsorbed, thus further enhancing the performance of NAST squeeze treatments. It can be concluded that NAST and NAST re-squeeze methodologies are more effective than the conventional method at retaining PPCA. The re-squeeze methodology has shown to retain to more PPCA very likely due to the fact that during the NAST postflush period, calcium has bridged with the carbon nanotubes and the porous media. This helped attach more PPCA during the re-squeeze period.

6.2.3. Coreflood: Conventional Flood vs NAST and NAST Re-squeeze at 25°C

Results from the coreflood experiments are reported in this section. The main treatment used 5000ppm PPCA in NFFW brine at 20 mL/hr flow rate; whereas all post flushes used NFFW brine at 20 mL/hr. The main treatment and post flushes were conducted 25°C. Core flood experiment was done in order to compare the conventional methodology with NAST and NAST re-squeeze methodologies in a more realistic environment.

Before the dynamic experiment was conducted, the cores were characterized, see Table 6-1.

Table 6-1 Core flood characterisation

Core ID	Pore volume	Porosity (%)	Permeability (mD)
Conventional flood	5.16	17.46	185
NAST and Re-squeeze	5.65	18.68	193

6.2.3.1. Core flood: Comparison of Conventional, NAST methodologies adsorption and desorption curves in core flood at 25°C

Figure 6-7 displays the effluent concentration of PPCA (ppm) as a function of the pore volumes injected. The results of NAST, NAST re-squeeze, conventional tests are compared to understand the effectiveness of the novel methodology. There was only one experiment performed for each methodology. The experiment was flushed until the concentration of PPCA

was below MIC (1 ppm). For the first time, the re-squeeze abilities of NAST have been tested in a core flood.

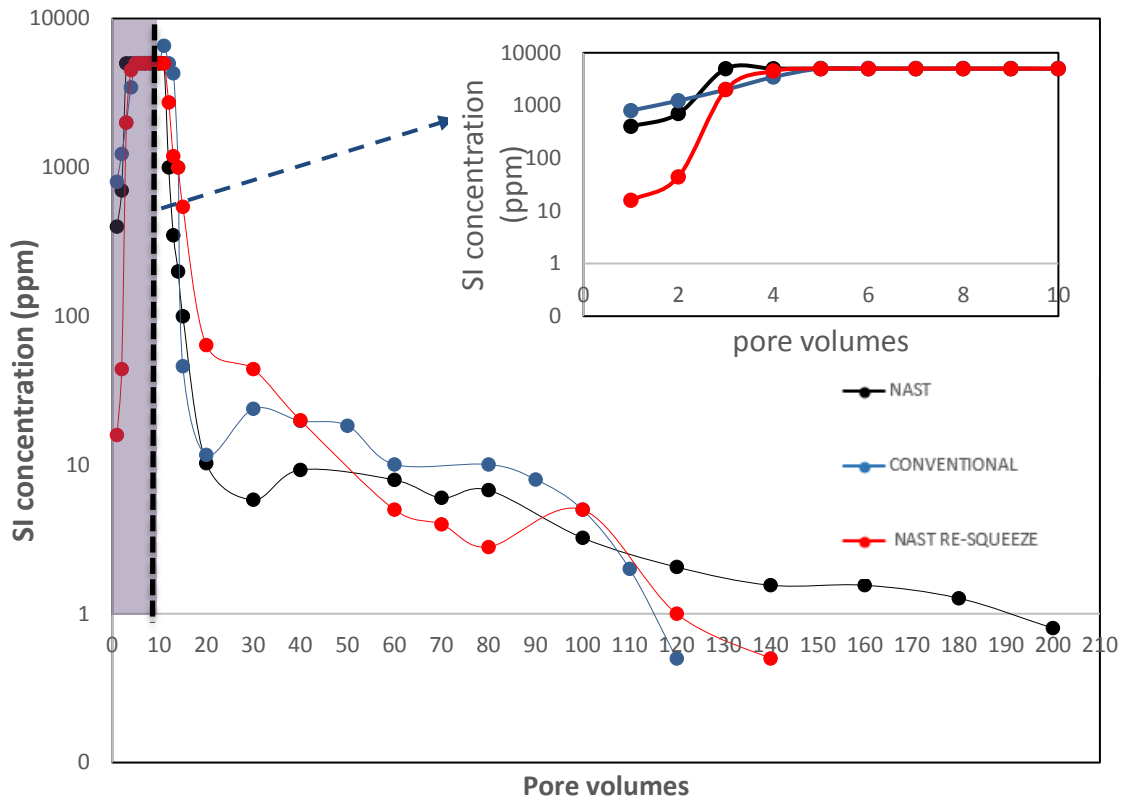


Figure 6-7 Core flooding experiments comparison of conventional method NAST and NAST Re-squeeze at 50°C effluents concentration as a function of PV. The faded area is being magnified to show the adsorption rate of each experiment.

Figure 6-7 clearly illustrates that the NAST methodology produced high and strong adsorption rate during main treatment and a more controlled and slower and longer desorption during production (post-flush). The NAST methodology was applied to the coreflood test with complex brine (NFFW) composition and the results were compared to commercial coreflood tests.

At the end of the postflush period, the SI dropped below 1ppm at 200 pore volumes, which is a significantly better performance than the conventional squeeze which dropped at 120 pore volumes. NAST desorption lifetime outperformed the conventional method by 40%.

In the case of NAST re-squeeze, Figure 6-7 clearly illustrates high and strong adsorption. It offers a faster adsorption rate during main treatment and a controlled and slower desorption during post-flush. It outperforms the conventional method (desorption lifetime is 15% longer) but underperforms in comparison to the initial NAST treatment. Standard squeeze methodologies have all mentioned that a re-squeeze is expected to show improved performance over the initial conventional squeeze [50, 55]. However, data from literature actually is lacking to prove this hypothesis. In case of the NAST methodology, understanding the underlying reason why this happens will aid the design of a method to tackle the issue.

NAST enhanced adsorption kinetics to PPCA has been shown by Ghorbani [6], and data herein reinforces these previous findings. Results agree with those found in sand pack experiments. Also, this suggests that the sorption behaviour of the COOH-MWCNTs inside the consolidated core at 1000 PSI (6894.76 KN/m²) confining pressure is similar to sand pack behaviour which has no confining pressure. This shows that sand packs are good precursor experiments to do before coreflood tests.

6.2.3.2. Mass Balance of Adsorbed Scale Inhibitor in Core: Comparison of Conventional, NAST and NAST re-squeeze performances

This test was originally designed to assess the mechanism of SI adsorption and desorption. Hence, in order to better understand the system, the cumulative mass of SI adsorbed is calculated. This will provide information on the adsorption mechanisms.

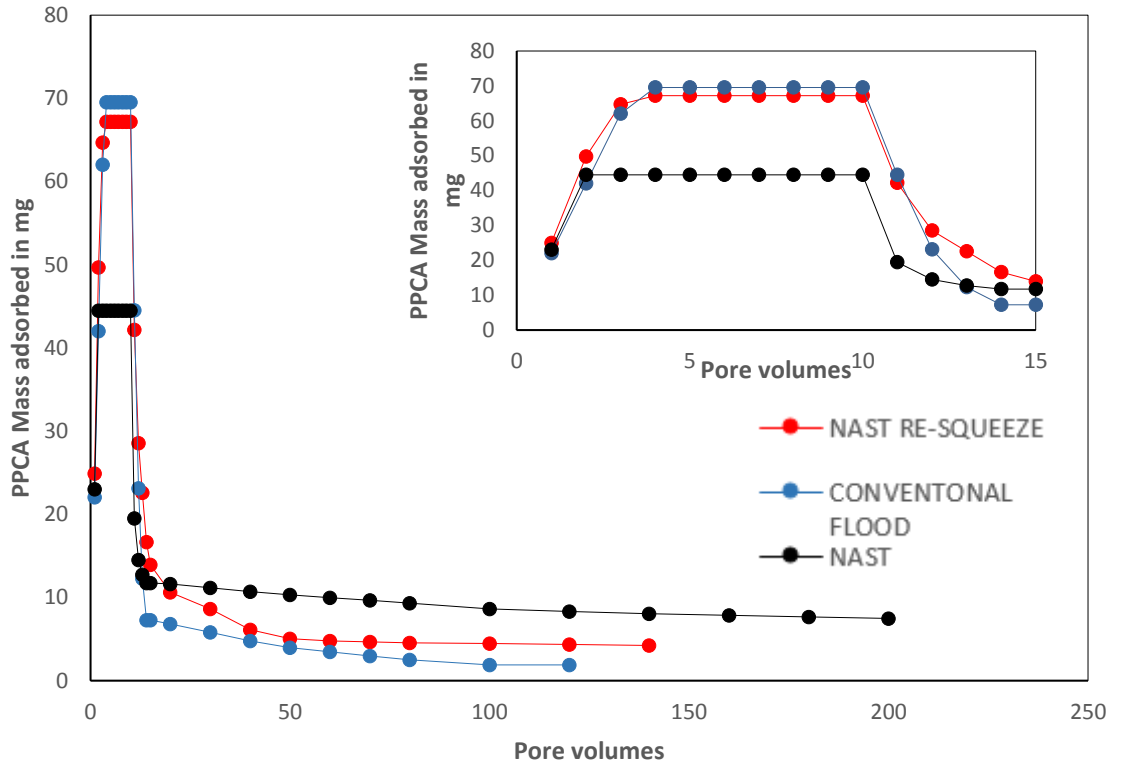


Figure 6-8 Mass of SI adsorbed onto core floods as a function of PV (NAST vs Conventional vs NAST re-squeeze)

In Figure 6-8, the results show better adsorption of PPCA with the NAST process and a striking difference in desorption. It demonstrates better retention during SI injection leading to higher and quicker adsorption, which end up offering in a longer squeeze lifetime. At shut in, which is performed at 10 PV, significantly less PPCA was in the core in comparison to the conventional method. This is evident in the inset of Figure 6-8. This highlights that in the presence of retained COOH-MWCNTs, the consolidated core is subjected to less surface area available due to the presence of the nanoparticles which very clearly blocked a few pathways (see section 5.5.4 for more details) [125]. This could explain why more scale inhibitor is able to be retained at shut in within the conventional method. However, the presence of COOH-MWCNTs in the core is showing an enhanced retention of PPCA,

as there is 7.89 mg of PPCA attached at the end of the NAST flush while 1.89 mg of PPCA was left in the conventional flush. Thus, it can be concluded the mechanism of adsorption is as important if not even more as the amount retained during adsorption period [42].

In terms of the NAST re-squeeze abilities, the results show better adsorption of PPCA within the NAST re-squeeze process and a better adsorption and desorption profile than the conventional method. The reason why it may be able to retain substantially more PPCA at shut in than NAST may be due to the postflush period, the calcium and potentially other cations had the chance to deposit and attach more onto to the rock surface and COOH-MWCNTs. In this case it is only beneficial for the squeeze treatments as it will help adsorb more PPCA.

Nevertheless, mass balance calculations show that there is still some unreturned inhibitor from mass balance calculations, this was also found for the NAST floods. If the amount that is still retained can be desorbed off the column, this means that NAST can potentially offer a greater lifetime. Finding a method to desorb the extra inhibitor is key.

6.3. Conclusion

The quantity of SI present at shut in was found to be significantly higher in most cases for the NAST floods. However, it was not the case for the core flood experiments. This highlights the notion that the amount of SI adsorbed is only one factor that affect the length of a squeeze lifetime. The mechanics of how SI is adsorbed is as important as how much is adsorbed.

In Figure 6-4, during the early post flush period, a significant drop in calcium profile was observed in the effluents. From this, it is clear that some complex interaction is happening between SI, COOH-MWCNTs, and calcium ions.

Comparing the conventional flood to the NAST flood, it was found that the effluent SI concentrations were able to desorb higher than MIC for a longer

period than for the conventional treatments. All conventional floods show lower return effluent concentrations over the main flow back period compared to NAST floods. This provides strong justification as to why the industry should at least consider the application of NAST squeeze treatments, although care must be taken to prevent excessive CNT injection, or formation damage in the injection process.

It is believed that the experiments reported in this thesis represent one of the most comprehensive data set of NAST experimental SI work executed to date.

Chapter 7 Discussion

Scale formation naturally occurs in oil and gas applications. One of the best approaches to prevent its formation is by the injection and retention of polymeric scale inhibitors such as PPCA. The squeeze treatment of scale inhibitors is the most efficient and widely used method to prevent scale formation [126]. An effective and successful squeeze treatment relies on the adsorption and desorption of the chemical specie. Improving squeeze treatment efficiency has been extensively researched in the past [7, 50, 55, 96, 127, 128]. Even recently new methodologies have been proposed such as using additives [42, 129, 130], this methodology works by adsorption of a charged additive onto the rock prior to application of the scale inhibitor. In addition, the use of nanoinhibitors [119, 125, 131-133] have been developed to increase squeeze lifetime, this approach places the synthesized nanoparticles with inhibitor deep into the rock formation. The Nanotechnology Assisted Squeeze Treatment (NAST) methodology is an innovative methodology that was originally created by Ghorbani et al. [6] and this method looked at enhancing the adsorption of polymeric scale inhibitor PPCA with the use of COOH-MWCNTs. This methodology has shown great potential to enhance the adsorption of the scale inhibitor. Thus, the aim of this research is to answer some questions about the feasibility of NAST in dynamic and complex conditions as well as further study the mechanisms of adsorption of scale inhibitor on COOH-MWCNTs [6].

As a reminder, the NAST methodology is divided in two main steps: Step1/NAST1 and Step2/NAST2.

- Step1/NAST1 is about injecting and adsorbing COOH-MWCNTs onto a rock surface porous media.
- Step2/NAST2 is solely about the adsorption and desorption of PPCA onto COOH-MWCNTs.

Figure 7-1 illustrates a breakdown of the NAST methodology process.

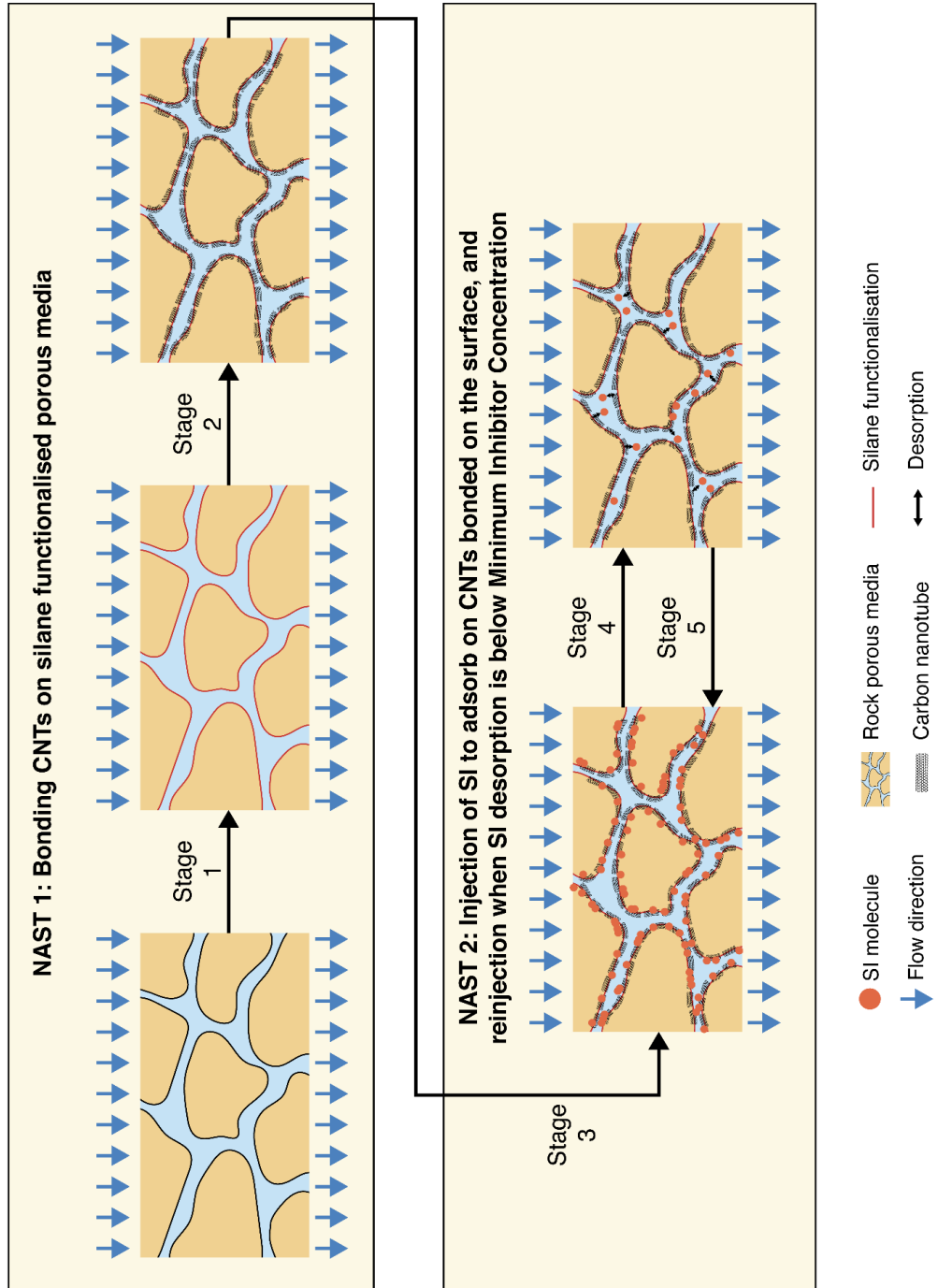


Figure 7-1 NAST methodology process. Stage 1: Silane functionalisation of rock surface. Stage 2: Delivering CNTs to bond to rock. Stage 3: Pumping SIs to adsorb on the CNTs. Stage 4: Resume production. Stage 5: Re-injection of SIs when SI desorption is below MIC.

The objectives of the work presented in this thesis were to develop a study of the adsorption of PPCA on COOH-MWCNTs by the use of methodologies such as adsorption isotherm fittings, by analysing the effects of varying environmental factors such as pH values or by the use of P-NMR to further confirm interaction of PPCA with CNTs. Also, obtaining an initial understanding on the effects of transport and retention of COOH-MWCNTs on porous media were assessed by the use of permeability impairment characterisations via the use of pressure gauges, petrophysical NMR, SEM and mass balance calculations obtained from the effluents concentrations. Lastly, squeeze treatment simulations were performed in order to understand the adsorption and desorption of polymeric scale inhibitor in dynamic conditions by the use of sand pack, core flooding experiments and concentration measurements by the use of the C18-hyamine method.

From the results presented in Chapter 4, 5 and 6, an understanding of adsorption of PPCA on COOH-MWCNTs has been developed. The effects transportation and retention of COOH-MWCNTs on reservoir properties have been assessed. To conclude, dynamic scale inhibitor squeeze were performed and all data obtained will help assessing the performance of NAST treatments against a laboratory conventional squeeze methodology.

The discussion is divided into three main areas:

- Studying the adsorption of PPCA on CNTs.
- The effect of nanoparticles transport and retention and its effects on reservoir properties.
- Squeeze performances of the NAST methodology.

7.1. Studying the Adsorption of Scale Inhibitor on CNTs

Step 2/NAST2 focuses on the adsorption of PPCA on COOH-MWCNTs. Various factors are to consider as the full adsorbing potential of CNTs is

unknown. The subject of this part of the discussion is to further understand the adsorption of SI on CNTs. This was achieved by the using adsorption isotherm fittings, by analysing the effects of varying environmental factors such as pH values or the practice of P-NMR to further confirm interaction of PPCA with CNTs.

Ghorbani in his thesis has already proved that adsorption of PPCA onto COOH-MWCNTs is achievable and is more effective than on rock [6]. However, most of the tests were done with simplistic brine. Thus, within this study the concept had to be proven with complex brine (formation water) and higher temperatures. Figure 4-1 illustrates the effectiveness of carbon nanotubes to retain PPCA in comparison to sand. 350 mg/g adsorption of PPCA was observed within NAST in comparison of 1 mg/g of PPCA adsorption with sand by Farooqui et al. [29]. The main observation is that COOH-MWCNTs are able to adsorb PPCA in realistic brine and moderate temperatures, and this is more effective than silica in these conditions.

The initial static adsorption results were very promising. Understanding how fast equilibrium is reached is another key step for NAST. Indeed, reaching equilibrium, implies that the shut in can be very fast. This would lead to a faster return to production. A conventional squeeze would have a shut in period of 12 to 24h, to retain most of the scale inhibitor onto the rock surface. One day off production represent a financial loss of the order of millions going away for a company [108]. With the NAST static adsorption test, equilibrium was reached within an hour. This displays a possibility for NAST to firstly offer a longer squeeze lifetime and a great adsorption mechanism and all this will come with a shorter shut in period which would substantially cut down production losses due to the shut in. This has not been proven in dynamic experiments, so further research is required.

Effects of various pH in adsorption of PPCA on COOH-MWCNTs were studied in section 4.2.3. The overall conclusion is that adsorption decreases, as the pH gets higher.

At pH2, the inhibitor adsorption is maximised due to increased hydrogen bonding onto the MWCNTs and a decreased level of electrostatic repulsion with the COOH-MWCNTs surface (see Figure 7-2). Indeed, decreasing of the pH leads to neutralization of the charge on the surface, and as pH value decreases below the point of zero charge (PZC) of the adsorbing materials, the positive charge density increases and adsorption capacity of anions increases [105, 108, 134]. PPCA is poly anionic inhibitor. The PZC is pH 3.3 for COOH-MWCNTs [105, 108, 134], thus based on these explanations, this explains the substantially high adsorption of PPCA at pH2 [105, 108, 134].

Also, pH2 oxidizes the COOH-MWCNTs, indeed Cho et al.[135] demonstrated that the surface oxidation degree of COOH-MWCNTs had significant effects on their capacity to adsorb molecules. The oxidation leads on creating edges and defects on the COOH-MWCNTs which offer more available adsorption sites.

At pH6, COOH-MWCNTs have a slightly negative surface charge. So, negatively charged surface sites become available for Ca^{2+} to adsorb onto MWCNTs, thus changing the surface charge towards a more positive (at least, less negative) value and capable of increasing the adsorption of the poly-anionic inhibitor PPCA onto the COOH-MWCNTs [108, 134]. Physical electrostatic interaction is also triggered by the hydrogen bonding interaction between the negatively charged PPCA species and the positively charged protonated carboxylated groups at the surface of the COOH-MWCNT composite [71, 103, 108].

At pH10, the hydrogen bonding disappears, and the COOH-MWCNTs are completely deprotonated. COOH groups become COO^- after deprotonation. With CNTs and PPCA solution all negatively charged, electrostatic repulsion become a dominant action force, resulting in low to no PPCA adsorption onto CNTs [104, 134].

The large difference in adsorption capacity at these three pH values, as observed in this study, is consistent with expectations based on deprotonation

of carboxylic groups on the surface of MWCNTs at higher pH values [71].

A summary of the possible reaction on COOH-MWCNTs in an acidic and alkaline environment is illustrated in Figure 7-2.

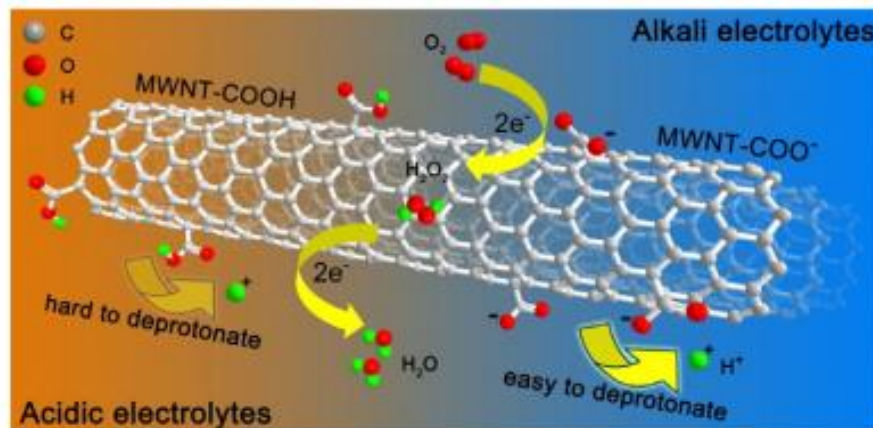


Figure 7-2 COOH-MWCNTs in acidic and alkaline environment [104]

In the case of NAST, physical electrostatic adsorption and a hydrogen bonding process seem to be the dominant adsorption mechanisms. Without a doubt, these two adsorption mechanisms are caused by the strong electrostatic interaction between the negatively charged PPCA species and the positively charged protonated carboxylated groups at the surface of the composite [109, 136, 137]. The calcium and other cations also modify electro-chemical properties of COOH-MWCNTs surface through electrostatic interactions and may complex with the inhibitor to aid adsorption [105, 138]. This trend of conclusions has similar agreements with Sorbie et al. on their studies on rock and inhibitor [108].

In most reservoirs, the water pH is near neutral, so for a “greater” enhanced adsorption with the COOH-MWCNTs, a combination of NAST and precipitation squeeze is a more achievable methodology. In a precipitation squeeze treatment, scale inhibitor are retained as a solid or a gel-like phase [29]. Factors which affect this process depend on the physical conditions such as inhibitor interactions with cations (Ca^{2+} in particular), pH and temperature

[29]. Precipitation squeeze treatment are particularly effective at high temperatures ($>95^{\circ}\text{C}$), which notably were not assessed in this study. Previous results [6] have shown that the interaction between calcium cations and PPCA is occurring within the NAST methodology. In this study, this was demonstrated in dynamic experiments (Figure 6-4). This highlights that precipitation squeeze is a squeeze methodology that could be combined with NAST if operated in the right conditions. This is an area that is worth investigating. One of the great reassurances with this novel method, is the fact that previous scale inhibitors theories with rock are also compatible with NAST. Hydrogen bonding and cations (Ca^{2+}) bonding are mainly responsible for inhibitor/rock interaction, and it appears to be a similar interaction with inhibitor/COOH-MWCNTs [108].

Effects of various COOH-MWCNTs mass over various PPCA concentrations were assessed and fitted to Freundlich adsorption model. According to the R-squared values of the regression analyses presented in Table 7-1, Freundlich models fitted the experimental isotherm equilibrium data reasonably well, with R^2 values > 0.82 . Freundlich isotherms represent an empirical model employed to describe equilibrium on a heterogeneous surface; they do not assume a monolayer capacity as in the case of the Langmuir model [110]. Freundlich isotherm suggests the presence of different bonding sites on the adsorbent which is in agreement with the chemical structure of COOH-MWCNTs. Carboxylate $-\text{COOH}$ can participate in the PPCA bonding process. The value of $1/n$ (Freundlich model) can be used to predict bonding affinity between the sorbent and the sorbate [139]. From Table 7-1, values of n for 4 mg of adsorbent is suggesting a better bonding interaction between PPCA and the active sites of COOH-MWCNTs. This is likely explainable by the fact that the higher the mass of COOH-MWCNTs to volume of PPCA solution the less likely a good nanoparticle dispersion should be observed, leading to less adsorption sites available. Most importantly, the nature of the isotherms for all 3 MWCNTs concentrations showed and confirmed a very high affinity with PPCA.

Table 7-1 Isotherm parameters of PPCA adsorption on various CNT mass

Freundlich isotherm			
Mass	$1/n$	$\log K_F$	R^2
4 mg	1	0.25	0.99
6 mg	1.71	0.32	0.93
10 mg	1.46	0.61	0.83

COOH-MWCNTs provide an efficient approach for the adsorption of PPCA. The presence of carboxylic groups on CNTs are believed to be offering additional adsorption sites, and this enhances the nanoparticle adsorption capacity. The mechanism is in line with a good fitting of the experimental data with the Freundlich adsorption isotherm.

Also, the squeeze treatment literature [38, 39, 47, 48, 127], has demonstrated that the mechanism of adsorption/desorption squeeze treatments is associated with the profile of the adsorption isotherm on the reservoir rock. Thus, it can be predicted and analysed by using mathematical modelling for both laboratory experiments and field systems. The good fitting of the adsorption isotherm with the carbon nanotubes in static test raises expectations for being able to model NAST adsorption isotherm for realistic applications. Indeed, creating compatibility tests, with various rock mineralogies bonded with COOH-MWCNTs is definitely an area to investigate to find out if the adsorption of PPCA onto Rock-MWCNTs complex is also predictable under these conditions which are closer to reality.

To further confirm PPCA adsorption on COOH-MWCNTs, A Solid state ^{31}P NMR spectrum investigation was carried. It indicated the presence of

Phosphorus on CNTs with a clear peak at 42.2ppm (Figure 4-10). CNTs are known for having various adsorption mechanisms such as hydrophobic interactions, pi-pi bondings, electrostatic interactions and hydrogen bonds, so many adsorption mechanisms happening simultaneously is not undeniable [140-142].

In the case of NAST, physical electrostatic adsorption that also involves a hydrogen bonding process appear to be the dominant mechanisms. Indeed, these two adsorption mechanisms are caused by the strong electrostatic interaction between the negatively charged PPCA species and the positively charged protonated carboxylated groups at the surface of the nanocomposite [109, 136, 137].

From this study, it can be concluded that PPCA adsorption onto the COOH-MWCNTs may be due to electrostatic interaction, a hydrogen bonding process, and from a surface bonding process due to the presence of calcium cations [72, 108].

7.2. Transport and Retention of Nanoparticles in Porous Media

The main idea of NAST is to assist the rock surface to adsorb the inhibitors more efficiently. Most current nanotechnology methodologies want minimum nanoparticle retention within the rock porous media and nanoparticles [113, 143]. However NAST actually wants a retention of the nanoparticles onto the porous media. The approach taken for this methodology is what makes it innovative.

Our current understanding of the effects of carbon nanotubes and transport in porous media environments is still quite limited. NAST requires the carbon nanotubes to be retained in the porous media, for this reason the rock surface is treated with silane to cause the surface to be reactive to carbon nanotubes.

Therefore, assessing the effect of the retention on the permeability in a realistic core is important in order to refine future tests.

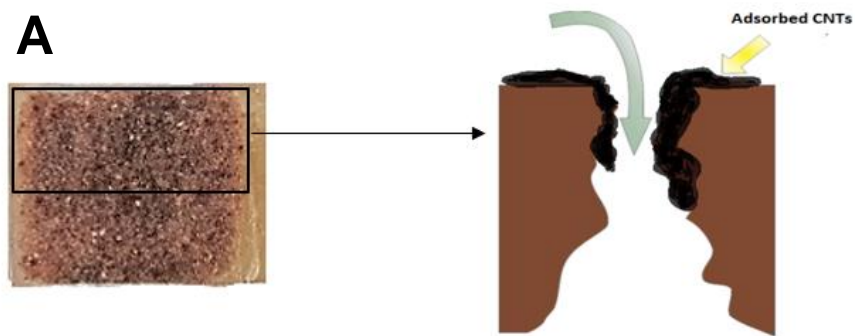
Retention of nanoparticles occur with various mechanisms such as adsorption, straining and log jamming within the porous media. . Permeability impairments is caused by one or multiple phenomena described previously. Adsorption and pore blockages are explained in the literature review in section 2.3.4 for more details.

Effect of nanoparticle injection in a silanised rock porous media was assessed on different rocks with permeabilities ranging from high to low. Experiments carried out examined the rise in pressure difference by injecting COOH-MWCNTs into rock cores. All experiments carried had an increase in pressure difference. Section 5.4.1 reports how differential pressure increases while injecting the nanoparticles within the porous media. The lower the initial rock permeability was, the higher the pressure difference was during the injection process. This is a clear indication that the nanoparticles have a deteriorating effect on the permeability.

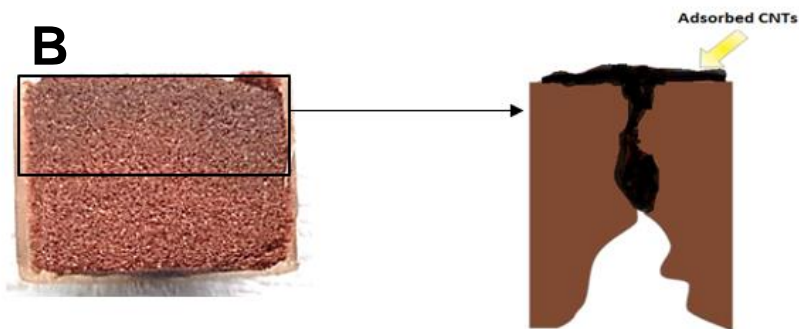
Permeability impairment tests were conducted before and after the injection for each rock. The permeability was measured before and after the injection cycle. It was done to monitor whether the rock itself was damaged or modified by the nanoparticle injection process. It was observed that the most permeable rock (Doddington) was still highly permeable post injection (12.5 mD), while the other rocks ended with really low permeability values (~1-0.8 mD).

Figure 7-3 A shows a rock with high permeability (Doddington), CNTs seem to adsorb pretty uniformly, this type of adsorption should not cause massive problems when production resumes. Figure 7-3 B shows an adsorption of COOH.MWCNTs on a tight pore entrance. This may lead to severe problems when production resumes as it is blocking and jamming the entrance to the pore. This is unacceptable for oil production. Also, optical images from section 5.4.3 have revealed that particles have the tendency to stay trapped and log-

jammed (agglomerate in in a pore) at the inlet, as it is exemplified in Figure 7-3 B. This supports the theory that the permeability reduction occurs with a higher percentage closer to the inlet than the outlet in nanofluid injection in porous media, and this phenomena has also been described in other studies [78, 144-146].



A
High permeability sandstone: Large pores remain partially open even with adsorbed CNTs



B
Lower permeability sandstone: CNTs block and jam pore entry space

Figure 7-3 Illustration of CNT adsorption on porous media. A) A high permeability (rock) have pores still opened after CNT adsorption. B) Lower permeability will have most pores blocked because of CNT adsorption

For all rock tested, rock permeability impairment ranged from 50% to 98%. This magnitude of damage is too high for a potential field application. However, it has been demonstrated that by either reducing nanoparticle concentration, shortening the injection period of nanomaterials, or selecting

smaller sized particles permeability impairment could stay within an acceptable range for oilfield applications [123, 143, 144].

A coreflood experiment was carried out to test NAST. The core used was also characterised before and after experiments. It can be seen that that the pore size distribution has severely changed in section 5.5.3. This is indicating that the physical properties of the rock cores have changed as well. Figure 7-4 illustrates the change in pore size distribution change after the conventional and NAST treatment respectively. The NAST core demonstrated noticeable shifts in term of pore size distributions, most of the large pores became smaller, while almost undetectable changes were observed with the conventional test.

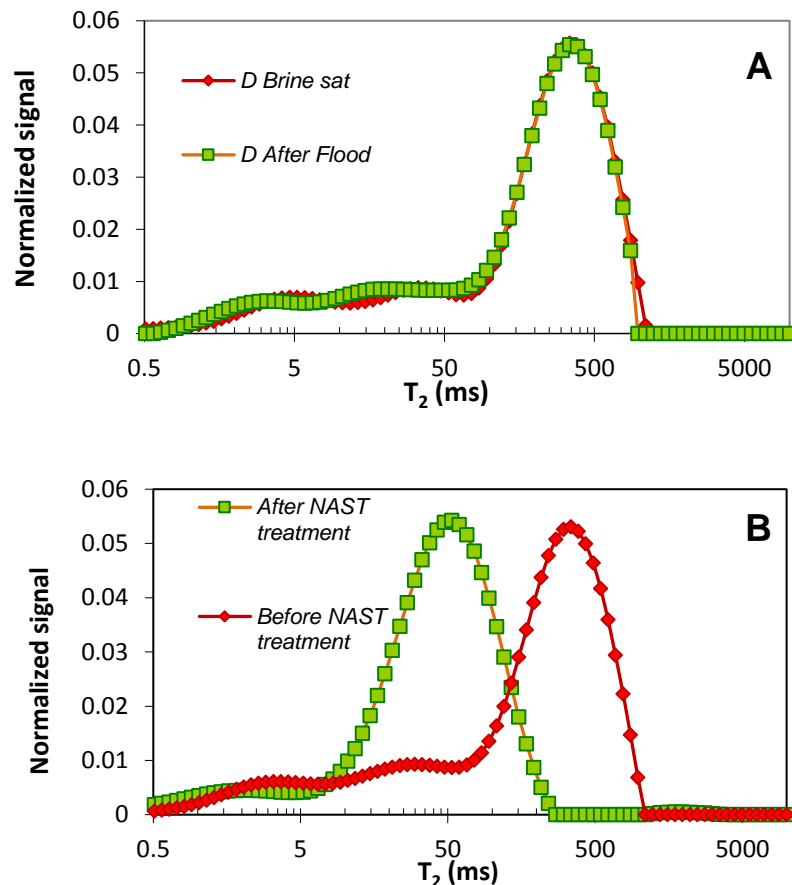


Figure 7-4 Pore size distribution of core before and after experiment. A) Conventional core. B) NAST core

SEM pictures in Figure 7-5 confirm that the pore size was modified in the Doddington core. This substantiates the pore sizes distribution shift observed in the NMR data in Figure 7-4 B. This data also allows validation by illustrating the successful adsorption of carbon nanotubes onto the pore wall with the silane functionalisation. This is a key detail for NAST.

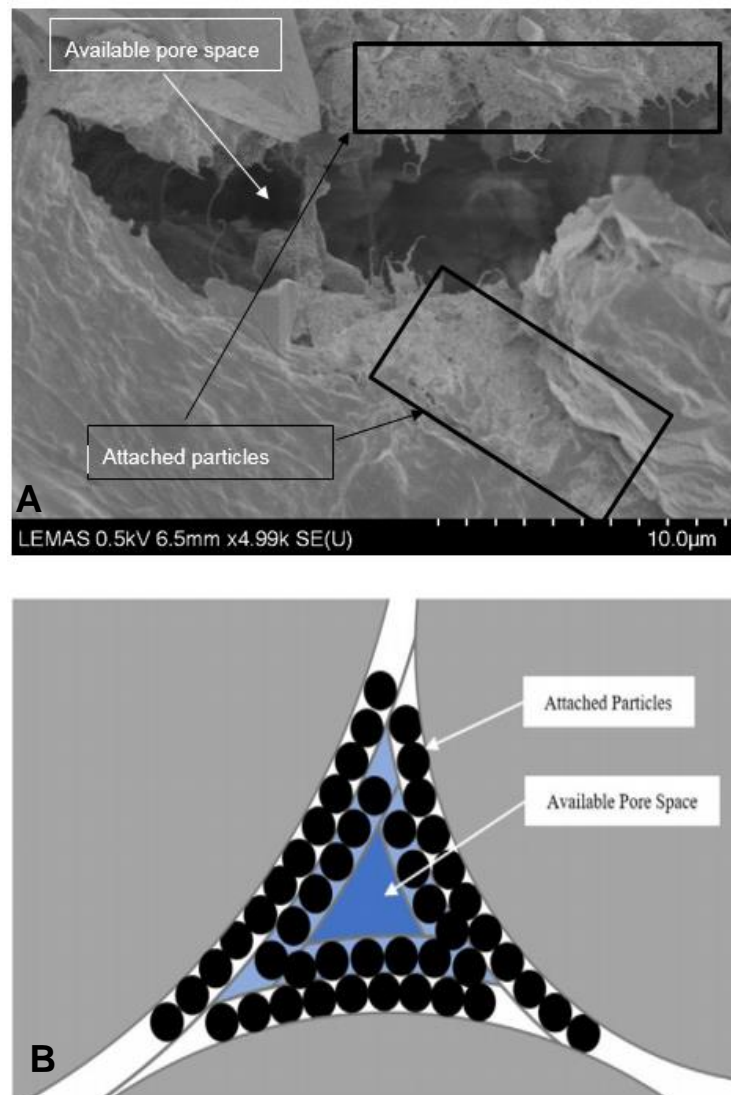


Figure 7-5 A) SEM image of the Doddington core at the end of NAST experiment showing particle deposition onto the pore wall. B) An adsorption schematic is also shown to prove that adsorption theory is matched by experiment.

In term of porosity shift, there was a variation of 1.45%, and pore volume change of 7.7% after the NAST flood is achieved. While nearly the same porosity was observed for the conventional core. Overall, the permeability experienced a severe drop after NAST flooding, but the change was small after the conventional flood. This supports that the COOH-MWCNTs have a deteriorating effect on rock permeability. The retention inside the rock during the flooding reduces the permeability. The nanoparticles do not cause impermeability, but care has to be taken as a permeability shift of 92% is too high for realistic applications [40, 147, 148]. This clearly shows the importance of optimising the transport and retention of the COOH-MWCNTs to minimise such a high permeability impairment. Table 7-2 summarises the changes in porosity and permeability for NAST and conventional coreflood experiment.

Table 7-2 Summary of formation damage on coreflood after experiments

Core ID	Porosity (%) (Before test)	Porosity (%) (After test)	Perm (mD) (Before test)	Perm (mD) (After test)
NAST	18.68	17.23	193	14.5
Conventional	17.46	17.36	185	181

In the sand pack experiments, the transportability and retention of the COOH-MWCNTs were typically tested using silica sand and clay (silica sand and clay) with a grain size distribution of the grain size distribution of 300 to 100 μm and 10 to 30 μm respectively. The sand pack, which is an unconsolidated media, has a larger pore space around each grain particle .

The core has a tighter formation which suggests a smaller pore space (hence porosity) [125, 133, 149]. It is believed that reduction in the pore space or porosity may lead to a reduction in the transportability of COOH-MWCNTs due to an increase in particle sorption and deposition to formation medium surfaces [133]. Sand packs, within this study, have a porosity of 0.31 while the porosity of the core is tighter with a porosity of 0.17. From the point of view of particle adsorption, the lower the porosity and permeability, the more retention should be observed [125], retaining 8.1 mg and 9.9 mg of COOH-MWCNTs for sand packs and core flood respectively (see Table 7-3)

Table 7-3 Average COOH- COOH-MWCNTs attached in sand pack porous media

Core ID	CNTs retained at shut in (mg)	CNTs retained after post flush	Mass of porous media (g)	Retention (mg/g)
Sand packs	9.4 ± 0.95	8.21 ±0.46	82.85±0.25	0.099±0.055
Core flood	10.4	9.9	66.57	0.1487

This shows that 0.14 mg/g was adsorbed on the core, while 0.099 mg/g in the sand. This data suggests that the core is more efficient to adsorb COOH-MWCNTs. This could be interesting, as it implies that a short injection of carbon nanotubes would have a higher retention rate in a realistic application. Being able to work out an ideal ratio to avoid impairing permeability dramatically and have enough CNTs well deposited by avoiding pore blockages is another area of future investigation.

By analysing the breakthrough graphs of CNTs for sand packs and coreflood in Figure 5-8 and Figure 5-17, beside the different conditions (different confining pressure and temperature) the change from consolidated (rock core) to unconsolidated (sand pack) porous media, dimension difference, it did not indicate a noticeable variation in deposition kinetics. In both cases a long adsorption period has been observed mostly because of the silane functionalised rock surface. Most of the previous literature, with untreated cores indicate release of carbon nanotubes within 0 to 2 PV injected in sand pack experiments [71, 113].

This study has shown that the silane treatment made carbon nanotubes release off the column around 22 PVs for the sand pack experiments, and 80 PVs for the core flood experiment. This supports the successful attachment of carbon nanotubes on the porous media rock walls with the presence of a silane catalyst. Further investigation is needed in this area as the flow of CNTs in silane treated porous media has been studied for the first time.

In term of the NAST methodology application, a uniform deposition without any agglomeration on the surface porous media would be ideal. It has been hypothesised in static adsorption test results that a well dispersed COOH-MWCNTs show a better adsorption efficiency for PPCA. Therefore being able to place COOH-MWCNTs effectively within the porous media will help preventing severe permeability impairment within the rock and will likely lead to a more efficient PPCA retention. This is an area that requires more examination to be optimised.

7.3. Squeeze Performances of the NAST Methodology

Chapter 5 presents novel experimental results for the NAST methodology, tests were carried with unconsolidated (sand packs) and consolidated core. The objective of performing these experiments were as follows:

1. To study adsorption kinetic of PPCA on porous media using the NAST methodology.
2. To evaluate and further understand the mechanism of desorption of PPCA off the porous media using the NAST methodology.

In all floods performed, NAST shows a stronger adsorption rate than the conventional method. Affinity of CNTs and PPCA is once again shown, first with static adsorption tests and now with dynamic experiments. This result also aligns with Ghorbani et al [6]. Figure 7-6 illustrates the high adsorption of PPCA in the core flood experiment.

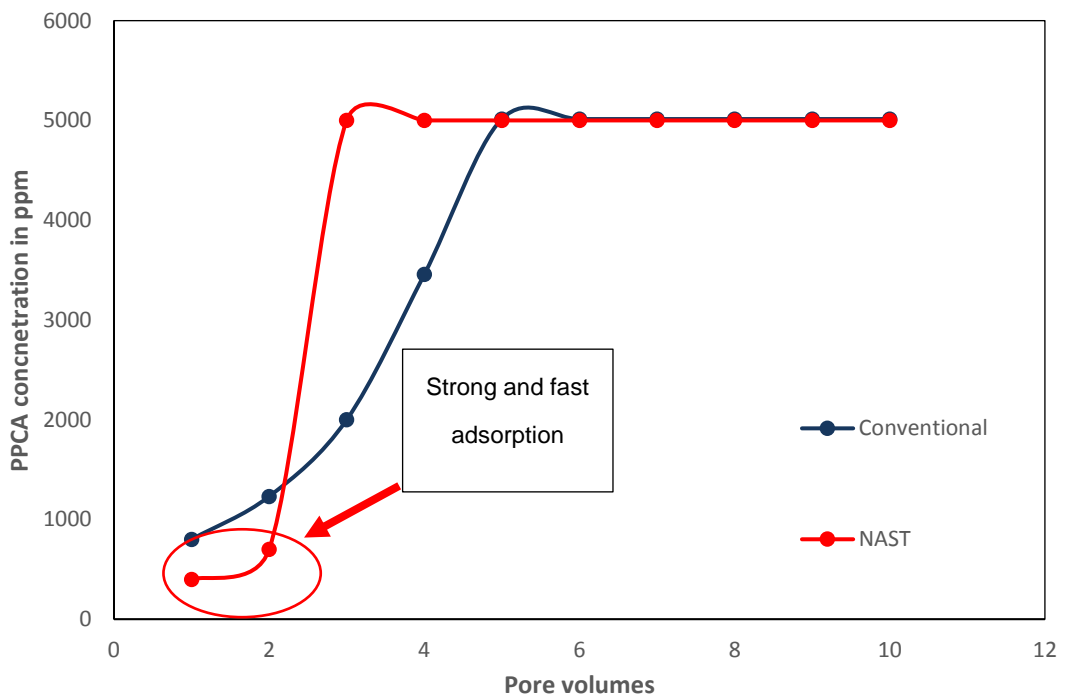


Figure 7-6 Highlight on enhanced adsorption rate with NAST with the coreflood experiment

Experiments conducted in this study, went from dynamic tests which involves sand pack and core floodings. Data from chapter 6 suggests that the sorption behaviour of the COOH-MWCNTs inside the consolidated core at 1000 PSI (6894.76 KN/m²) confining pressure is similar to sand pack sorption behaviour which has no confining pressure.

This is due to properties pertaining to adsorption and surface chemistry as they are not expected to change substantially from sand pack to coreflood. One of the most accurate ways of assessing the efficiency of the retention of a specie onto a surface is to calculate via mass balance calculations the ratio of mass of adsorbent over the mass of adsorbate. In other terms, data is plotted as mass of inhibitor retained over the mass of the porous media.

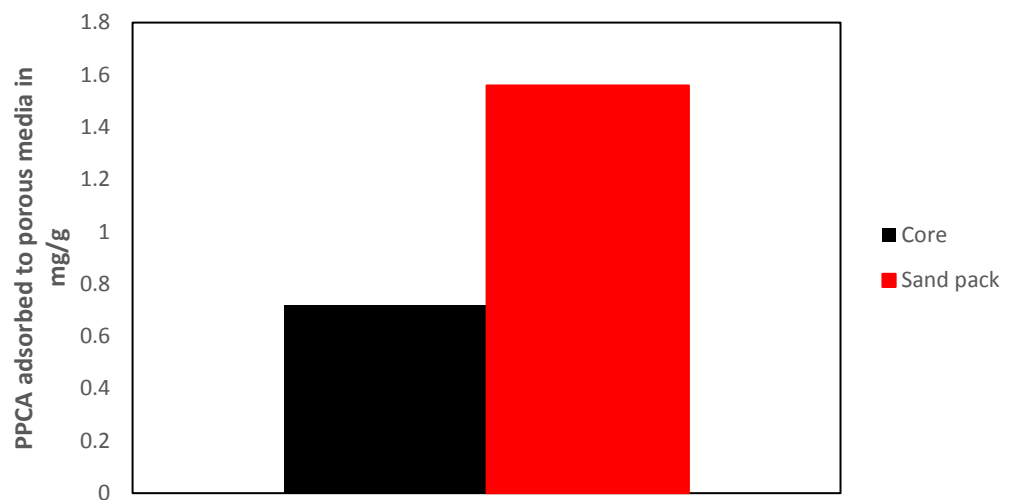


Figure 7-7 PPCA inhibitor adsorbed on NAST core and sand pack porous media at shut in at 25°C.

Figure 7-7 indicates that more PPCA is present in the sand pack at shut in. Sand packs have numerous large pores, leading to a considerable increase in the pore throat size and permeability [125, 150]. These large pores allow the scale inhibitor to migrate through the medium with a reduced interfering force compared to transport in a consolidated core. In a core, the injected inhibitors need to travel through tight formation with a much reduced permeability and pore throat size [118, 125]. This highlights that in the presence of retained COOH-MWCNTs, the consolidated core is subjected to less surface area available due to the presence of the nanoparticles which very clearly blocked a few pathways (See section on formation damage in section 5.5 and 7.3) [125].

As previously mentioned, nanoparticles restrict access to available sites due to pore blocking. This could be the reason why more scale inhibitor is able to be retained within the conventional method in comparison to NAST at shut in. This can be seen in Figure 7-8. It clearly shows that at the end of the postflush period, the presence of COOH-MWCNTs in the core has clearly enhanced the retention of PPCA.

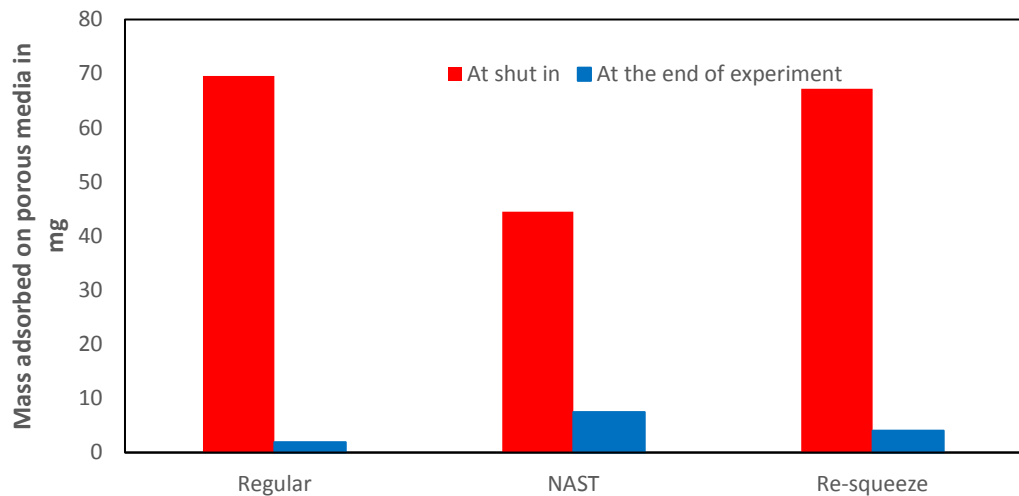


Figure 7-8 Scale inhibitor retained in core flood experiments

Thus, the mechanism of adsorption is as important if not even more as the amount retained during adsorption period [42]. This statement reinforces the belief that COOH-MWCNTs are strong PPCA adsorbent and that the NAST methodology is successful to some extent to the purpose it has been created for.

In term of desorption, NAST consistently outperformed the conventional method. Furthermore, by the end of the flush, mass balance calculations have shown that all NAST flood had a large number of PPCA left within the media. As explained earlier in the discussion, in the static adsorption section, hydrogen bonding may be one of the main interaction between PPCA and COOH-MWCNTs. This type of bond, which could be an intermediate between physisorption and chemisorption [72], is complex to break, hence why it is

necessary to conduct additional studies, as the full potential of NAST is not being utilised.

Another interesting point for NAST, is that it is possible to combine this methodology with other known methodologies that act towards achieving the same goal. For instance, a fraction of the retained COOH-MWCNTs can bridge with cations to create a divalent metal (mainly Ca^{2+}) – COOH-MWCNTs complex, this was proven in section 6.2.1, and also demonstrated by Ghorbani [6]. This complex is able of to create another complex with PPCA to create the commonly known Ca–PPCA complexes to desorb onto the produced water [49, 59, 96]. A proposed mechanism with calcium ions is illustrated in Figure 7-9. This was also discussed in section 7.1.

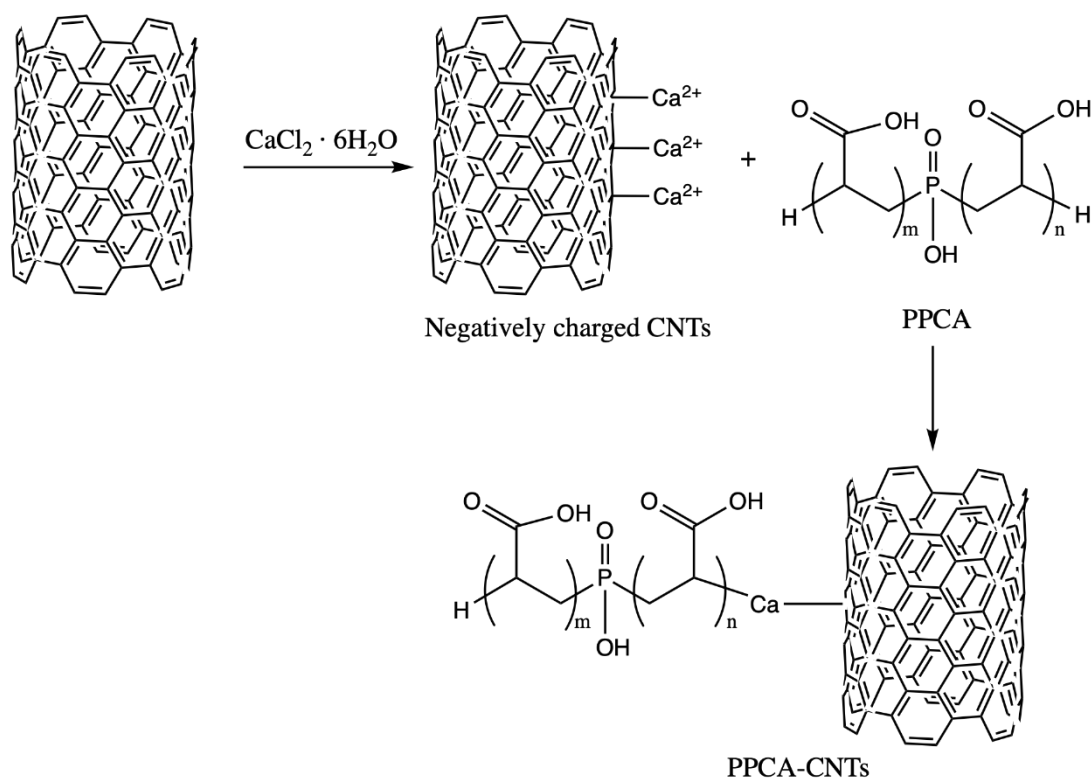


Figure 7-9 Proposed adsorption mechanism with calcium ions, CNTs and PPCA.

The topics researched in this thesis were done in an attempt to better understand the adsorption of PPCA on CNTs. The static adsorption results now help to understand the adsorption on porous media to some extent. Though the PV of the core was of 5.21mL post CNT treatment, it had a PPCA injection of 10 PV which is equivalent of 52.10 mL. Static adsorption tests were done at 10 mL. Results are not directly comparable, but they provide information about the adsorption of PPCA based on the mass of adsorbent. It has been calculated that nearly 10 mg of CNTs were present in the NAST core flood experiment. 10 mg of CNTs was also assessed in static adsorption. It can be seen that that the adsorption of PPCA in mg per gram of CNTs was equal to 1000 mg/g for a 5000 ppm solution of PPCA. According to Ibrahim et al. [49], the true mass adsorbed to a porous media is +3PV post shut in, so the mass retained in the core at this instance is equal to 11.75 mg for 10 mg of CNTs for a 5000 ppm solution that was injected which is equivalent of 1175 mg/g of PPCA adsorbed per gram of CNTs. The plot in Figure 7-10 shows a comparison of both. The higher adsorption observed by 11.75% in the dynamic experiment is likely because the core offered more surface area due to the presence of rock material. This data supports, to a limited extent, that NAST static adsorption results can be used to estimate adsorption in dynamic experiments. It also indicates that the presence of COOH-MWCNTs clearly influence SI retention on a rock.

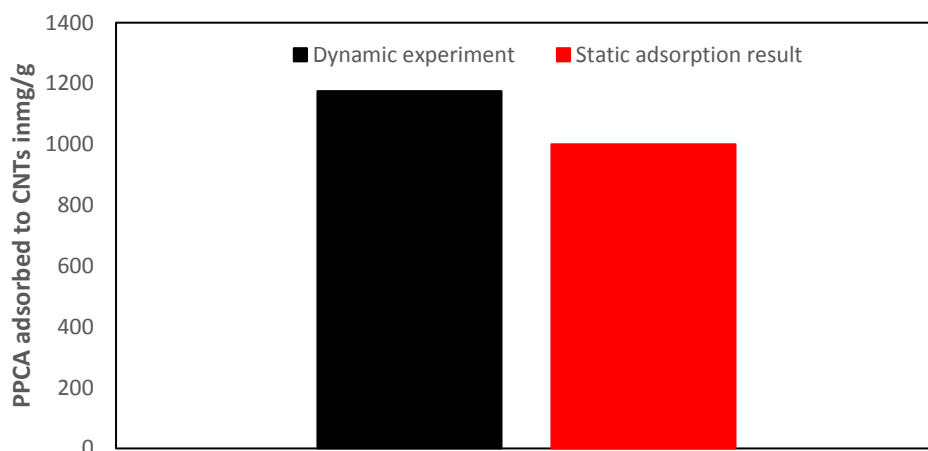


Figure 7-10 A comparison of static and dynamic experiments for adsorption of PPCA on CNTs.

To conclude, NAST adsorption and desorption process have been understood that in the previous study. A better understanding is now available, and NAST has shown to be feasible in complex conditions, with further study, the method could be designed for use in oilfields.

7.4. Relevance of the Research

New data set is now available for this novel methodology. It is designed for squeeze treatment applications, therefore it is important to highlight the relevance to industry and future studies in this field.

Novelty 1: *The findings from adsorption and dynamic tests in formation brine and moderate temperature reveal that the NAST methodology can offer a strong adsorption of PPCA and represents a long-term desorption of the inhibitor*

The fast saturation of PPCA in dynamic and complex conditions is an interesting result for NAST, as it could potentially shorten the inhibitor injection period in a real-world application. This could be used to reduce the use of costly scale inhibitors, and reduce the implementation time of a squeeze treatment.

The long-term desorption offered by NAST is what makes this methodology most promising. Additional work is needed to improve knowledge of exactly why some scale inhibitor remain retained in the porous media at the end of the postflush period. The extra amount of PPCA attached to the porous could be exploited and utilised to prevent scale formation for a longer time period. If optimised, this has the potential of saving oil and gas operator's money.

Novelty 2: *The transportation and retention of COOH-MWCNTs in porous media have shown to be effective in a certain range of permeabilities.*

NAST aim is to deploy the methodology in as many reservoirs as possible ranging from higher reservoir permeabilities to lower permeabilities.

Nanoparticles have the ability to transport effectively in sand packs and moderately permeable core porous media. For a realistic application, sand packs can be representative of fractured reservoirs [125], so this implies that NAST should work in moderately high permeability reservoirs and reservoirs that have been fractured [125]. With respect to lower permeability rocks, the transport and retention of nanoparticles have shown to be very limited to unsuccessful. Further work is needed in this area in order to deploy the technology to as many oil reservoirs as possible.

Novelty 3: Transport and retention of COOH-MWCNTs in a silane functionalised porous media and its effects on porous media

This research provides the first evaluation of the transport and successful retention of COOH-MWCNTs in a silane functionalised porous media. Results have shown to be very repeatable. Further understanding of the retention processes of COOH-MWCNTs in this system will help design an oilfield application for NAST more accurately.

Chapter 8 Conclusion and Future Work

8.1. Summary of the Key Results

The purpose of this study was to understand the behaviour of COOH-MWCNTs and their interactions with PPCA to better understand the adsorption and desorption benefits of the NAST methodology in static and dynamic conditions. Also, the study was partially fulfilled in the purpose of understanding the transport and retention of CNTs in porous media and analyse its effects on porous media.

Outcomes from the adsorption study have furthered the fundamental understanding of the interaction of PPCA with COOH-MWCNTs. The environmental factors such as pH values also make a significant change in PPCA adsorption on CNTs. This work made new discoveries about the effect of mass of CNTs/volume of PPCA. The Freundlich adsorption isotherm has been successfully fitted to match experimentally obtained results. Also, static adsorption results developed in this study used experimentally relevant COOH-MWCNTs concentration which matched, to a limited extent, the adsorption of PPCA on CNTs in dynamic conditions.

Transport and retention properties of COOH-MWCNTs in porous media were investigated using sand pack columns and core flooding apparatus. Findings from the transport studies provide a thorough quantitative analysis of the retention of MWCNTs in a silane-functionalised porous media. To the author's knowledge it is the first time it has been investigated. Data provided within this study assessed transport of COOH-MWCNTs in a range of various rock permeabilities, and it also raised questions about permeability impairment issues, as the physical properties of the rocks are modified to a point where a realistic application may be unacceptable. Additional investigation is recommended to tackle this issue.

The NAST application has proved to change the physical properties of the porous media. COOH-MWCNTs also changes the chemical properties of the porous media. The chemical change has been shown to substantially increase the squeeze performance of PPCA by increasing its adsorption on the porous media. It has been proven that the mechanism of PPCA adsorption within the NAST system also increases PPCA adsorption rate to porous media and desorbs PPCA longer than a conventional methodology. However, irreversible PPCA retention is a phenomenon that has been present in all experiments. Further work is needed in this area; to optimise the potential of the methodology. Another discovery is that NAST methodology performs well at 25 °C and 50°C and with complex brine. It is believed that the experiments reported in this thesis represent one of the most comprehensive and recent data set of NAST experimental SI work.

To conclude, adsorption and desorption process when using the NAST methodology have been further characterised in comparison to the previous study. Experiments were done from less to more realistic experiments, going from static adsorption tests to sand pack and core flooding experiments. A better understanding is now available, and NAST has shown to be feasible in complex conditions, with further study, the method could be designed for use in oilfields.

8.2. Breakdown of the Conclusions

In this chapter the main results are summarised and some recommendations for future work are advanced. Figure 8-1 illustrates the main conclusions of the study for NAST 1 and NAST 2 ranging from static adsorption tests to dynamic tests.

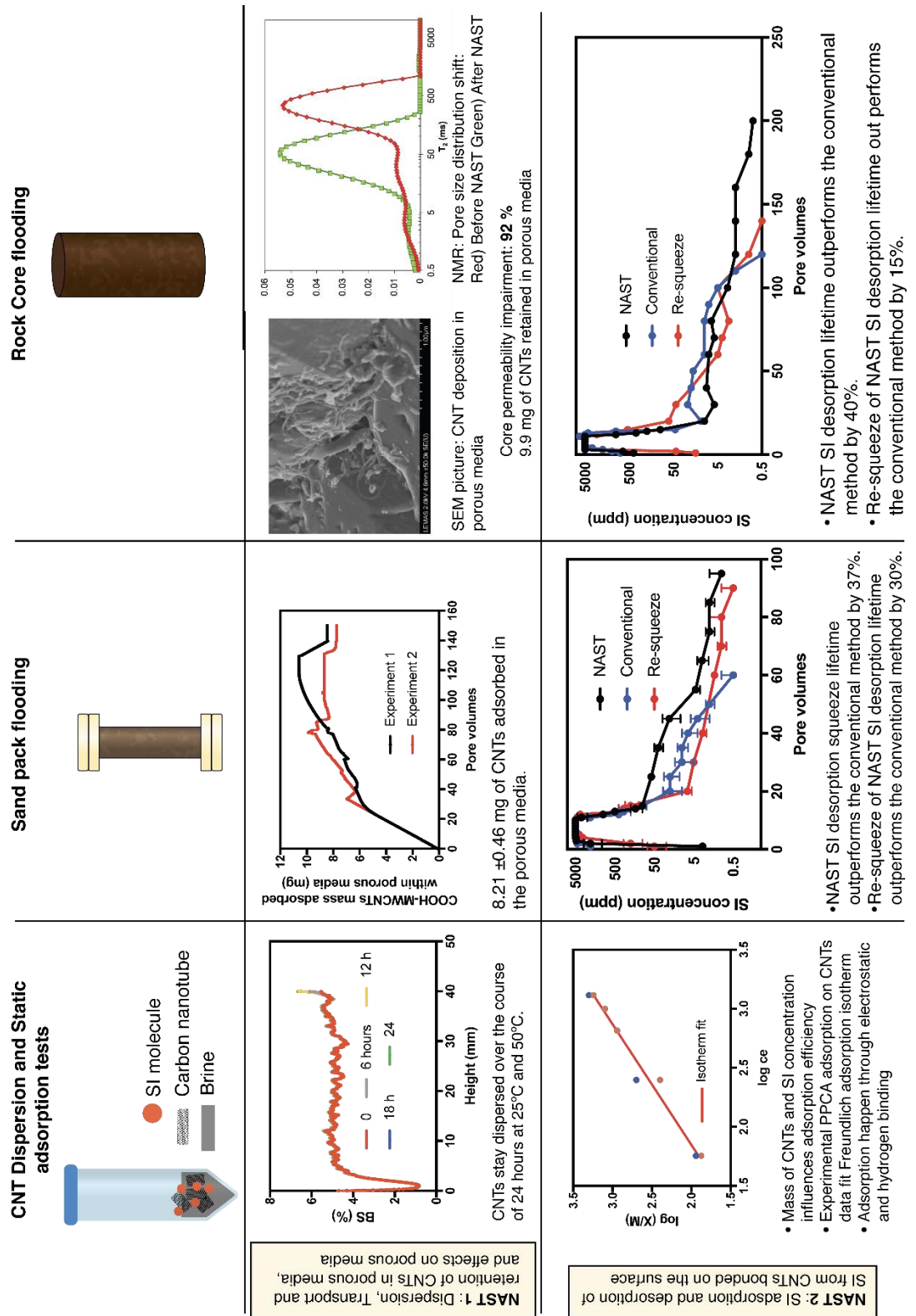


Figure 8-1 Overview of the main conclusions of this study for NAST 1 and NAST2. Ranging from static adsorption tests, sand pack and core flooding experiments.

8.2.1. Step 1/NAST 1: Surface Pre-treatment and CNT Attachment onto Rock

The first steps of the NAST methodology are to pre-treat the surface in order to make it reactive to nanoparticles. The following step is to inject the dispersed nanoparticles into the rock formation. One of the main gaps with the previous study, was the quantification of the COOH-MWCNTs, which has been resolved now.

- Retention of COOH-MWCNTs into the porous media was successful. It was demonstrated that transport and retention of COOH-MWCNTs is applicable for certain rock formations.
- Transport and retention of COOH-MWCNTs is limited along in tight rock formations. In a rock, such as Stanton Moore, it was not able to travel within the rock formation, and it severely affected the pressure difference by blocking pore pathways. This could be dangerous in a realistic application.
- Little desorption of CNTs were detected with Raman, but it was below the limit of quantification.
- Tween 80 has shown to be a promising dispersant for realistic application.
- Care, such as lower CNT concentration, or a shorter COOH-MWCNTs injection have to be taken to prevent severe permeability impairment.
- Successful attachment of CNTs into the rock porous media has been illustrated through SEM pictures.
- Step1 (NAST1) has shown to be successful, but a few areas need to be covered for a potential realistic application. However, the proof of concept is now strong enough for further consideration.

8.2.2. Adsorption of SI onto the CNTs

NAST relies primarily on the ability of the nanomaterials to retain inhibitor better than rock. Thus, a study to understand what mechanisms happening with COOH-MWCNTs was necessary to consolidate the previous developed theories by Ghorbani [6].

- Large amount of PPCA on CNTs was adsorbed in comparison to sand.
- The adsorption of PPCA on CNTs reaches equilibrium within an hour and could potentially lead to a shorter shut in time in oilfield application.
- At pH 2, PPCA retention is substantially enhanced. At pH10, CNTs lose their adsorbing abilities.
- PPCA adsorption increases with more CNTs but the efficiency reduces.
- Experimental data have shown a close fitting to Freundlich adsorption isotherm. These results are encouraging as they show a potential of estimating PPCA adsorption onto COOH-MWCNTs.
- Phosphorus NMR is reinforcing the theory of PPCA adsorption onto CNTs.
- PPCA adsorption on CNTs has shown to work by physical electrostatic adsorption and a hydrogen bonding process.

In conclusion, the knowledge gained in this research advances the understanding of NAST dynamic floods.

8.2.3. Step 2/NAST2: Sand pack and Coreflood Testing of the NAST Methodology

NAST was tested in unconsolidated and consolidated media. The tests were designed to first prove with rock chemistries that NAST was theoretically feasible, the coreflood was an investigation with a real core, which delivered encouraging results to promote future research.

The adsorption rate mechanism of PPCA within the NAST system is stronger than on silica rocks.

- Feasibility of NAST from unconsolidated to consolidated porous media was supported.
- NAST is working with simple rock chemistries (sand pack) and complex rock chemistries (coreflood)
- NAST is effective at 50°C.
- A large amount of PPCA is still retained within the porous media, after postflush, very likely due to hydrogen bonded PPCA with CNTs.

NAST aim was to extend squeeze lifetime which it does successfully. Further investigations were carried from Ghorbani's work. With the advances done with this research, further tests are required to be able to assess the methodology to a realistic test.

The potential benefits of real reservoir application of NAST are listed below:

- The PPCA adsorption rate has increased.
- Desorption of PPCA is slower and more controlled.
- There is a fast reachability to equilibrium which could lead to shorter shut in time and less inhibitor injected.
- NAST is a one-time application, so after the first application. This is back to a regular commercial application.

8.3. Recommendations for Future Work

- (i) Static compatibility tests have to be designed in order to assess NAST coupled with other minerals. This work should be stretched to include compatibility static adsorption tests for PPCA adsorption on COOH-MWCNTs retained onto silica, it can then be extended to carbonate minerals with COOH-MWCNTs. It will be a significant advance if the PPCA adsorption are following trends of an isotherm with various rock

chemistries. Dynamic tests also have to be assessed with various rock chemistries, to reinforce the theory that NAST can be applied on various type of oilfields.

- (ii) Optimisation of transport and retention of nanoparticles through porous media. The CNTs do not need to reach saturation in core in order to be effective at retaining PPCA. A lower concentration would lead to a better CNT dispersed solution, thus leading to less log jamming, entrapment and permeability impairment.
- (iii) Desorption of the scale inhibitor has to be optimised. Mass balance calculation show that there is still some inhibitor present in the porous media by end of the postflush. A modification in the injected brine chemistry during the post flush could enhance the desorption of the extra inhibitor.
- (iv) Further characterisation of the interaction between PPCA and CNTs has to be carried out.
- (v) To explore the potential of combining NAST with other known squeeze life enhancers, such as additives or precipitation squeeze for instance.
- (vi) The design and operational experiences acquired from traditional squeeze treatment should be exploited in development efforts to enable NAST to be applied in practical pilot and oilfield applications in the near future.
- (vii) In order to make NAST a widely used methodology, there is a need to develop cost-effective and environmentally-acceptable nanoparticles.
- (viii) Reaching a fundamental understanding of NAST adsorption and desorption requires performing accurate calculation and to create comprehensive models. This remains a challenge though there is

progress with the PPCA adsorption isotherm fitting Freundlich adsorption isotherm.

References

1. LLC NPP. Scale Image 2011. Available from: <http://www.plumbingpluslc.com/home/repipe>.
2. Kelland. Effect of Various Cations on the Formation of Calcium Carbonate and Barium Sulfate Scale with and without Scale Inhibitors. *industrial and engineering chemistry research* 2011;50(5582-5861).
3. Kelland. Scale Control. *Production Chemicals for the Oil and Gas Industry*: CRC Press; 2009.
4. Ponce da Motta E, Plavnik B, Schechter RS. *Optimizing Sandstone Acidization*. Society of Petroleum Engineers. 1992.
5. Mike Crabtree DE, Ashley Johnson, George King. *Fighting Scale-Removal and prevention*. Society of Petroleum Engineers. 1999.
6. Ghorbani N. *Nanotechnology Enhanced Squeeze Treatments for Efficient Oilfield Scale Management [PhD]*: University of Leeds; 2012.
7. Sorbie KS. *A Simple Model of Precipitation Squeeze Treatments*. SPE: Society of Petroleum Engineers.
8. Ziauddin FWWa. In: Richardson, editor. *Formation Removal and inhibition of inorganic scale in the oilfield environment*: Society of petroleum Engineers; 2008. p. 230.
9. Eseosa A, Atubokiki AJ. *Prediction and Monitoring of Oilfield Carbonate Scales Using Scale Check*. 2011/1/1/. SPE: Society of Petroleum Engineers.
10. Söhnel O, Mullin JW. A method for the determination of precipitation induction periods. *Journal of Crystal Growth*. 1978;44(4):377-82.
11. Hopkirk RJ, Gilby DJ. 20 - On Nuclide Transport, Precipitation, Dissolution and Shared Solubility Limits. In: Tsang C-F, editor. *Coupled Processes Associated with Nuclear Waste Repositories*: Academic Press; 1987. p. 259-73.
12. Eroini V. *Kinetic study of calcium carbonate formation and inhibition by using an in-situ flow cell*: Leeds; 2011.
13. Pytkowicz RM. Rates of Inorganic Calcium Carbonate Nucleation. *The Journal of Geology*. 1965;73(1):196-9.
14. Eroini V, Kapur N, Neville A, Euvrard M. *Preventing Scale Formation Using Modified Surfaces*. 2011/1/1/. NACE: NACE International.
15. Mullen J. *Crystallisation*. Elsevier, editor 2001.
16. Mullin JW. 6 - Crystal growth. In: Mullin JW, editor. *Crystallization (Fourth Edition)*. Oxford: Butterworth-Heinemann; 2001. p. 216-88.

17. Walton AG. Nucleation in liquids and solutions in Nucleation. 1969.
18. Otsuka M, Matsuda Y, Suwa Y, Fox JL, Higuchi WI. Effect of particle size of metastable calcium phosphates on mechanical strength of a novel self-setting bioactive calcium phosphate cement. *Journal of Biomedical Materials Research*. 1995;29(1):25-32.
19. Neville A, Wang C. Inhibitor Performance on Corrosion and Erosion/Corrosion Under Turbulent Flow With Sand and CO₂—An AC Impedance Study.
20. Brečević L, Nielsen AE. Solubility of amorphous calcium carbonate. *Journal of Crystal Growth*. 1989;98(3):504-10.
21. Amjad Z. *The Science and Technology of Industrial Water Treatment*. PRESS C, editor: CRC PRESS; 2010.
22. Yu J, Lei M, Cheng B, Zhao X. Facile preparation of calcium carbonate particles with unusual morphologies by precipitation reaction. *Journal of Crystal Growth*. 2004;261(4):566-70.
23. Ketrane R, Saidani B, Gil O, Leleyter L, Baraud F. Efficiency of five scale inhibitors on calcium carbonate precipitation from hard water: Effect of temperature and concentration. *Desalination*. 2009;249(3):1397-404.
24. Chen J, Xiang L. Controllable synthesis of calcium carbonate polymorphs at different temperatures. *Powder Technology*. 2009;189(1):64-9.
25. Gómez-Morales J, Torrent-Burgués J, Rodríguez-Clemente R. Nucleation of calcium carbonate at different initial pH conditions. *Journal of Crystal Growth*. 1996;169(2):331-8.
26. Mackay EJ. Modeling In-Situ Scale Deposition: The Impact of Reservoir and Well Geometries and Kinetic Reaction Rates.
27. Andritsos N, Karabelas AJ. The Influence of Particulates on CaCO₃ Scale Formation. *Journal of Heat Transfer*. 1999;121(1):225-7.
28. Ho K, Chen T, Chen P, Hagen T, Montgomerie H, Benvie R, et al. Development of Test Methods and Inhibitors for Halite Deposition in Oilfield Water Treatment. *CORROSION 2013*; 2013/3/17/; Orlando, Florida. NACE: NACE International; 2013.
29. Farooqui NM. A detailed study of the scale inhibitor phase envelope of PPCA in the context of precipitation squeeze. Edinburgh: Heriot-Watt University; 2015.
30. Zhang P. Synthesis and application of phosphonate scale inhibitor nanomaterials for oilfield control 2010.
31. Jianjun Xiao ATK, Mason B. Tomson. The fate of scale inhibitors in oil and gas productions.
32. Chen T, Neville A, Yuan M. Influence of on formation—bulk precipitation and surface deposition. *Chemical Engineering Science*. 2006;61(16):5318-27.

33. Quraishi F, Saini. Natural components as corrosion inhibitors. 1999.
34. Tantayakom V, Sreethawong T, Fogler HS, de Moraes FF, Chavadej S. Scale inhibition study by turbidity measurement. *Journal of Colloid and Interface Science*. 2005;284(1):57-65.
35. Graham GM, McMahon CP. The Effect of Scale Inhibitor Performance Against Bulk (Homogeneous) and Surface (Heterogeneous) Scale Nucleation and Growth by the Addition of Film Forming Corrosion Inhibitors. 2002/1/1/. NACE: NACE International.
36. Jones F, Stanley A, Oliveira A, Rohl A, Reyhani M, Parkinson G, et al. The role of phosphonate speciation on the inhibition of barium sulfate precipitation. *Journal of Crystal Growth*. 2003;249(3):584-93.
37. Schwamborn M. Chemical synthesis of polyaspartates: a biodegradable alternative to currently used polycarboxylate homo- and copolymers. *Polymer Degradation and Stability*. 1998;59(1-3):39-45.
38. Vazquez O, Mackay EJ, Al Shuaili KH, Sorbie KS, Jordan MM. Modelling a Surfactant Preflush with Non-Aqueous and Aqueous Scale Inhibitor Squeeze Treatments. 2008/1/1/. SPE: Society of Petroleum Engineers.
39. Yuan MD, Sorbie KS, Todd AC, Atkinson LM, Riley H, Gurden S. The Modelling of Adsorption and Precipitation Scale Inhibitor Squeeze Treatments in North Sea Fields. 1993/1/1/. SPE: Society of Petroleum Engineers.
40. Fleming N, Ramstad K, Mathisen AM, Selle OM, Tjomsland T, Fadnes FH. Squeeze Related Well Productivity Impairment Mechanisms & Preventative/Remedial Measures Utilised. 2010/1/1/. SPE: Society of Petroleum Engineers.
41. Engineering. Scale Basics 2009. Available from: http://gekengineering.com/Downloads/Free_Downloads/Scale_Basics.pdf.
42. Jimenez PD. Improving squeeze scale inhibitor adsorption and flow back characteristics with surfactants 2014.
43. Kelland. Production Chemicals for the oil and Gas Industry 2009.
44. Gdanski RD, Funkhouser GP. Mineralogy Driven Scale Inhibitor Squeeze Designs. 2005/1/1/. SPE: Society of Petroleum Engineers.
45. Wat R, Montgomerie H, Hagen T, Børeng R, Kotlar HK, Vikane O. Development of an Oil-Soluble Scale Inhibitor for a Subsea Satellite Field. SPE International Symposium on Oilfield Chemistry; 1999/1/1/; Houston, Texas. SPE: Society of Petroleum Engineers; 1999.
46. Montgomerie H. Novel inhibitor chemistry for oilfield scale application: University of Huddersfield 2014.
47. Vazquez O, Mackay EJ, Sorbie KS. Modelling the Placement of Scale Squeeze Treatments in Heterogeneous Formations with Pressurised Layers. 8th European Formation Damage Conference; 2009/1/1/; Scheveningen, The Netherlands. SPE: Society of Petroleum Engineers; 2009.

48. Vazquez O, Mackay EJ, Sorbie KS. Development of a Non-Aqueous Scale Inhibitor Squeeze Simulator. SPE International Oilfield Scale Symposium; Aberdeen, UK. SPE: Society of Petroleum Engineers; 2006.
49. Ibrahim JMBM. Establishing Scale Inhibitor Retention Mechanisms in Pure Adsorption and Coupled Adsorption/Precipitation Treatments. Edinburgh, Scotland, UK: Heriot-Watt University; 2011.
50. Vetter OJ. The Chemical Squeeze Process Some New Information on Some Old Misconceptions. SPE-3544-PA. 1973.
51. Durham D, editor Equations for Prediction of Scale Inhibitor Return After Squeeze Treatment. SPE California Regional Meeting; 1983: Society of Petroleum Engineers.
52. Payne GE. A History Of Downhole Scale Inhibition By Squeeze Treatments On The Murchison Platform. 1987/1/1/. SPE: Society of Petroleum Engineers.
53. Breen PJ, Diel BN, Downs HH. Correlation of Scale Inhibitor Structure With Adsorption Thermodynamics and Performance in Inhibition of Barium Sulfate in Low-pH Environments. 1990/1/1/. SPE: Society of Petroleum Engineers.
54. King GE, Warden SL. Introductory Work in Scale Inhibitor Squeeze Performance: Core Tests and Field Results. 1989/1/1/. SPE: Society of Petroleum Engineers.
55. Vetter OJ, Kandarpa V, Schalge AL, Stratton M, Veith E. Test and Evaluation Methodology for Scale Inhibitor Evaluations. 1987/1/1/. SPE: Society of Petroleum Engineers.
56. Przybylinski JL. Adsorption and Desorption Characteristics of Mineral Scale Inhibitors as Related to the Design of Squeeze Treatments. 1989/1/1/. SPE: Society of Petroleum Engineers.
57. Kan A, Yan L, Bedient PB, Oddo JE, Tomson MB. Sorption and Fate of Phosphonate Scale Inhibitors in the Sandstone Reservoir: Studied by Laboratory Apparatus With Core Material. 1991/1/1/. SPE: Society of Petroleum Engineers.
58. Sutherland L, Jordan M, Champion N. Enhancing Scale Inhibitor Squeeze Retention in Carbonate Reservoirs. SPE International Oilfield Scale Conference and Exhibition; 2018/6/20/; Aberdeen, Scotland, UK. SPE: Society of Petroleum Engineers; 2018.
59. Farooqui N. Non equilibrium sand pack study of PPCA: Dynamic precipitation flood. 2013-2016.
60. Ayatollahi S, Zerafat MM. Nanotechnology-Assisted EOR Techniques: New Solutions to Old Challenges. 2012/1/1/. SPE: Society of Petroleum Engineers.
61. Cheng Q. Dispersion of Single-Walled Carbon Nanotubes in Organic Solvents. Dublin: Dublin Institute of Technology.

62. Yang J, Bitter J, A. Smith B, Howard Fairbrother D, Ball W. Transport of Oxidized Multi-Walled Carbon Nanotubes through Silica Based Porous Media: Influences of Aquatic Chemistry, Surface Chemistry, and Natural Organic Matter 2013.
63. Iijima S. Helical microtubules of graphitic carbon. *Nature*. 1991;354:56.
64. Gallagher MJ, Chen D, Jacobsen BP, Sarid D, Lamb LD, Tinker FA, et al. Characterization of carbon nanotubes by scanning probe microscopy. *Surface Science Letters*. 1993;281(3):335-40.
65. Cheng H-M, Yang Q-H, Liu C. Hydrogen storage in carbon nanotubes. *Carbon*. 2001;39(10):1447-54.
66. Makoto I, Masamichi Y, Kazuyuki U. Simultaneous Measurement of Topography and Contact Current by Contact Mode Atomic Force Microscopy with Carbon Nanotube Probe. *Japanese Journal of Applied Physics*. 2002;41(7S):4908.
67. Masamichi Y, Sadaharu J, Kazuyuki U. Fabrication of Carbon Nanostructure onto the Apex of Scanning Tunneling Microscopy Probe by Chemical Vapor Deposition. *Japanese Journal of Applied Physics*. 2003;42(7S):4841.
68. Stevens RM. New carbon nanotube AFM probe technology. *Materials Today*. 2009;12(10):42-5.
69. Mohammed L, Ansari MNM, Pua G, Jawaid M, Islam MS. A Review on Natural Fiber Reinforced Polymer Composite and Its Applications. *International Journal of Polymer Science*. 2015;2015:15.
70. Maleki Dizaj S, Mennati A, Jafari S, Khezri K, Adibkia K. Antimicrobial Activity of Carbon-Based Nanoparticles. *Advanced Pharmaceutical Bulletin*. 2015;5(1):19-23.
71. Yang J. Adsorption and transport properties of oxidized multi-walled carbon nanotubes: Johns Hopkins University; 2014.
72. Sudan P, Züttel A, Mauron P, Emmenegger C, Wenger P, Schlapbach L. Physisorption of hydrogen in single-walled carbon nanotubes. *Carbon*. 2003;41(12):2377-83.
73. Thiraphattaraphun L. Structure/Property Relationships in Polypropylene Nanocomposites 2013.
74. Gao CH. Factors affecting particle retention in porous media. *Emirates Journal for Engineering Research*. 2007;12(3):1-7.
75. Kang J-K, Yi I-G, Park J-A, Kim S-B, Kim H, Han Y, et al. Transport of carboxyl-functionalized carbon black nanoparticles in saturated porous media: Column experiments and model analyses. *Journal of Contaminant Hydrology*. 2015;177(Supplement C):194-205.
76. Yi P, Chen KL. Release Kinetics of Multiwalled Carbon Nanotubes Deposited on Silica Surfaces: Quartz Crystal Microbalance with Dissipation

(QCM-D) Measurements and Modeling. *Environmental Science & Technology*. 2014;48(8):4406-13.

77. Yuan B, Wang W, Moghanloo RG, Su Y, Wang K, Jiang M. Permeability Reduction of Berea Cores Owing to Nanoparticle Adsorption onto the Pore Surface: Mechanistic Modeling and Experimental Work. *Energy & Fuels*. 2017;31(1):795-804.

78. Hendraningrat L, Li S, Torsater O. A Coreflood Investigation of Nanofluid Enhanced Oil Recovery in Low-Medium Permeability Berea Sandstone. *SPE International Symposium on Oilfield Chemistry*; 2013/4/8; The Woodlands, Texas, USA. SPE: Society of Petroleum Engineers; 2013. p. 14.

79. Han B, Liu W, Zhao X, Cai Z, Zhao D. Transport of multi-walled carbon nanotubes stabilized by carboxymethyl cellulose and starch in saturated porous media: Influences of electrolyte, clay and humic acid. *Science of The Total Environment*. 2017;599-600:188-97.

80. Rouhi S. Molecular dynamics simulation of the adsorption of polymer chains on CNTs, BNNTs and GaNNTs. *Fibers and Polymers*. 2016;17(3):333-42.

81. Lu C, Chiu H, Liu C. Removal of Zinc(II) from Aqueous Solution by Purified Carbon Nanotubes: Kinetics and Equilibrium Studies. *Industrial & Engineering Chemistry Research*. 2006;45(8):2850-5.

82. Cho H-H, Wepasnick K, Smith BA, Bangash FK, Fairbrother DH, Ball WP. Sorption of Aqueous Zn[II] and Cd[II] by Multiwall Carbon Nanotubes: The Relative Roles of Oxygen-Containing Functional Groups and Graphenic Carbon. *Langmuir*. 2010;26(2):967-81.

83. Li Q-L, Yuan D-X, Lin Q-M. Evaluation of multi-walled carbon nanotubes as an adsorbent for trapping volatile organic compounds from environmental samples. *Journal of Chromatography A*. 2004;1026(1):283-8.

84. Wang H. Dispersing carbon nanotubes using surfactants. *Current Opinion in Colloid & Interface Science*. 2009;14(5):364-71.

85. Fernandes RMF, Abreu B, Claro B, Buzaglo M, Regev O, Furó I, et al. Dispersing Carbon Nanotubes with Ionic Surfactants under Controlled Conditions: Comparisons and Insight. *Langmuir*. 2015;31(40):10955-65.

86. Kato H, Mizuno K, Shimada M, Nakamura A, Takahashi K, Hata K, et al. Observations of bound Tween80 surfactant molecules on single-walled carbon nanotubes in an aqueous solution. *Carbon*. 2009;47(15):3434-40.

87. Kato H, Nakamura A, Horie M. Behavior of surfactants in aqueous dispersions of single-walled carbon nanotubes. *RSC Advances*. 2014;4(5):2129-36.

88. Pramanik C, Gissinger JR, Kumar S, Heinz H. Carbon Nanotube Dispersion in Solvents and Polymer Solutions: Mechanisms, Assembly, and Preferences. *ACS Nano*. 2017;11(12):12805-16.

89. Metwalli E, Haines D, Becker O, Conzone S, Pantano CG. Surface characterizations of mono-, di-, and tri-aminosilane treated glass substrates. *Journal of Colloid and Interface Science*. 2006;298(2):825-31.
90. Lee J-H, Rhee KY, Park SJ. Silane modification of carbon nanotubes and its effects on the material properties of carbon/CNT/epoxy three-phase composites. *Composites Part A: Applied Science and Manufacturing*. 2011;42(5):478-83.
91. Ma PC, Kim J-K, Tang BZ. Effects of silane functionalization on the properties of carbon nanotube/epoxy nanocomposites. *Composites Science and Technology*. 2007;67(14):2965-72.
92. Ma PC, Kim J-K, Tang BZ. Functionalization of carbon nanotubes using a silane coupling agent. *Carbon*. 2006;44(15):3232-8.
93. James C. A petrographic investigation into the durability of common replacement sandstones to the crystallisation of de-icing salts: University Of Glasgow; 2016.
94. Marshalls. Sandstone.
95. Prieto C, Calvo L. Performance of the Biocompatible Surfactant Tween 80, for the Formation of Microemulsions Suitable for New Pharmaceutical Processing. *Journal of Applied Chemistry*. 2013;2013:10.
96. Kahrwad M, Sorbie KS, Boak LS. Coupled Adsorption/Precipitation Of Scale Inhibitors: Experimental Results And Modelling. 2008/1/1/. SPE: Society of Petroleum Engineers.
97. Li M, Zhao Y. Chapter 9 - Hydrocarbon Reservoir Logging Evaluation Methods and Technologies. In: Zhao ML, editor. *Geophysical Exploration Technology*. Oxford: Elsevier; 2014. p. 239-303.
98. Magritek. NMR for porous media application 2015. Available from: <http://www.magritek.com/>.
99. Yang H, Kang W, Wu H, Yu Y, Zhu Z, Wang P, et al. Stability, rheological property and oil-displacement mechanism of a dispersed low-elastic microsphere system for enhanced oil recovery. *RSC Advances*. 2017;7(14):8118-30.
100. Sartor M. Dynamic light scattering. University of California, San Diego. 2003:2-21.
101. Aleandri S, Vaccaro A, Armenta R, Völker A, Kuentz M. Dynamic Light Scattering of Biopharmaceuticals—Can Analytical Performance Be Enhanced by Laser Power? *Pharmaceutics*. 2018;10(3):94.
102. Rabaioli MR, Lockhart TP. Solubility and phase behavior of polyacrylate scale inhibitors. *Journal of Petroleum Science and Engineering*. 1996;15(2):115-26.
103. Yang J, Bitter JL, Smith BA, Fairbrother DH, Ball WP. Transport of Oxidized Multi-Walled Carbon Nanotubes through Silica Based Porous Media:

Influences of Aquatic Chemistry, Surface Chemistry, and Natural Organic Matter. *Environmental Science & Technology*. 2013;47(24):14034-43.

104. Sang Y, Fu A, Li H, Zhang J, Li Z, Li H, et al. Experimental and theoretical studies on the effect of functional groups on carbon nanotubes to its oxygen reduction reaction activity. *Colloids and Surfaces A: Physicochemical and Engineering Aspects*. 2016;506:476-84.

105. Atieh MA, Bakather OY, Al-Tawbini B, Bukhari AA, Abuilaiwi FA, Fettouhi MB. Effect of Carboxylic Functional Group Functionalized on Carbon Nanotubes Surface on the Removal of Lead from Water. *Bioinorganic Chemistry and Applications*. 2010;2010:9.

106. Perez-Aguilar NV, Muñoz-Sandoval E, Diaz-Flores PE, Rangel-Mendez JR. Adsorption of cadmium and lead onto oxidized nitrogen-doped multiwall carbon nanotubes in aqueous solution: equilibrium and kinetics. *Journal of Nanoparticle Research*. 2010;12(2):467-80.

107. direct S. Point of Zero Charge. 2019.

108. Sorbie KS, Yuan MD, Chen P, Todd AC, Wat RMS. The Effect of pH on the Adsorption and Transport of Phosphonate Scale Inhibitor Through Porous Media. *SPE International Symposium on Oilfield Chemistry*; 1993/1/1/; New Orleans, Louisiana. SPE: Society of Petroleum Engineers; 1993.

109. Pan B, Xing B. Adsorption Mechanisms of Organic Chemicals on Carbon Nanotubes. *Environmental Science & Technology*. 2008;42(24):9005-13.

110. Abou El Fadl F. Radiation grafting of ionically crosslinked alginate/chitosan beads with acrylic acid for lead sorption. *Journal of Radioanalytical and Nuclear Chemistry*. 2014;301(2):529-35.

111. Li Y, Wang Y, Pennell KD, Abriola LM. Investigation of the Transport and Deposition of Fullerene (C60) Nanoparticles in Quartz Sands under Varying Flow Conditions. *Environmental Science & Technology*. 2008;42(19):7174-80.

112. Johnson PR, Elimelech M. Dynamics of Colloid Deposition in Porous Media: Blocking Based on Random Sequential Adsorption. *Langmuir*. 1995;11(3):801-12.

113. Liu X, O'Carroll DM, Petersen EJ, Huang Q, Anderson CL. Mobility of Multiwalled Carbon Nanotubes in Porous Media. *Environmental Science & Technology*. 2009;43(21):8153-8.

114. Rastogi R, Kaushal R, Tripathi SK, Sharma A, Kaur I, Bharadwaj L. Comparative study of carbon nanotube dispersion using surfactants 2008. 421-8 p.

115. Cheng M, Zeng G, Huang D, Yang C, Lai C, Zhang C, et al. Advantages and challenges of Tween 80 surfactant-enhanced technologies for the remediation of soils contaminated with hydrophobic organic compounds. *Chemical Engineering Journal*. 2017;314:98-113.

116. Datsyuk V, Kalyva M, Papagelis K, Parthenios J, Tasis D, Siokou A, et al. Chemical oxidation of multiwalled carbon nanotubes. *Carbon*. 2008;46(6):833-40.
117. Gosens I, Post JA, de la Fonteyne LJJ, Jansen EHJM, Geus JW, Cassee FR, et al. Impact of agglomeration state of nano- and submicron sized gold particles on pulmonary inflammation. *Particle and Fibre Toxicology*. 2010;7(1):37.
118. Zhang P, Shen D, Kan AT, Tomson MB. Synthesis and laboratory testing of a novel calcium-phosphonate reverse micelle nanofluid for oilfield mineral scale control. *RSC Advances*. 2016;6(46):39883-95.
119. Ruan G, Kan AT, Yan F, Zhang F, Bhandari N, Alsaiani HA, et al. Citrate Assisted Metal Phosphonate Colloidal Scale Inhibitors For Long-Term Squeeze Treatments. 2016/5/11/. SPE: Society of Petroleum Engineers.
120. Du J, Wang S, You H, Zhao X. Understanding the toxicity of carbon nanotubes in the environment is crucial to the control of nanomaterials in producing and processing and the assessment of health risk for human: A review. *Environmental Toxicology and Pharmacology*. 2013;36(2):451-62.
121. Ghorbani N, Wilson M, Kapur N, Fleming N, Neville A. Using Nanoscale Dispersed Particles to Assist in the Retention of Polyphosphinocarboxylic Acid (PPCA) Scale Inhibitor on Rock. SPE International Oilfield Nanotechnology Conference and Exhibition; 2012/1/1/; Noordwijk, The Netherlands. SPE: Society of Petroleum Engineers; 2012.
122. Meyers KO, Skillman HL, Herring GD. Control of Formation Damage at Prudhoe Bay, Alaska, by Inhibitor Squeeze Treatment.
123. Bennion DB, Thomas FB, Bennion DW, Bietz RF. Mechanisms of Formation Damage and Permeability Impairment Associated With the Drilling, Completion and Production of Low API Gravity Oil Reservoirs. SPE International Heavy Oil Symposium; 1995/1/1/; Calgary, Alberta, Canada. SPE: Society of Petroleum Engineers; 1995.
124. Kerver JK, Heilhecker JK. Scale Inhibition by the Squeeze Technique. 1969.
125. Zhang P, Ruan G, Kan AT, Tomson MB. Functional scale inhibitor nanoparticle capsule delivery vehicles for oilfield mineral scale control. *RSC Advances*. 2016;6(49):43016-27.
126. Yan C, Tomson R, Yan F, Tomson MB, Zhu H, Wang L, et al. Boehmite Based Sulphonated Polymer Nanoparticles with Improved Squeeze Performance for Deepwater Scale Control. Offshore Technology Conference; 2013/5/6/; Houston, Texas, USA. OTC: Offshore Technology Conference; 2013. p. 12.
127. Vazquez O, Mackay EJ, Sorbie KS. Modelling of Non-Aqueous and Aqueous Scale Inhibitor Squeeze Treatments. International Symposium on Oilfield Chemistry; 2007/1/1/; Houston, Texas, U.S.A. SPE: Society of Petroleum Engineers; 2007.

128. Jordan MM, Sorbie KS, Yuan MD, Taylor K, Hourston KE, Ramstad K, et al. Static and Dynamic Adsorption of Phosphonate and Polymeric Scale Inhibitors Onto Reservoir Core From Laboratory Tests to Field Application. 1995/1/1/. SPE: Society of Petroleum Engineers.
129. Sutherland L, Jordan M. Enhancing Scale Inhibitor Squeeze Retention With Additives. SPE International Oilfield Scale Conference and Exhibition; 2016/5/11/; Aberdeen, Scotland, UK. SPE: Society of Petroleum Engineers; 2016.
130. Jordan M, Sutherl L. Enhancing Phosphonate Scale Inhibitor Squeeze Retention in Carbonate Reservoirs. SEG/AAPG/EAGE/SPE Research and Development Petroleum Conference and Exhibition; 2018/7/11/; Abu Dhabi, UAE. SEG: Society of Exploration Geophysicists; 2018.
131. Zhang P, Shen D, Kan AT, Tomson MB. Phosphino-polycarboxylic acid modified inhibitor nanomaterial for oilfield scale control: transport and inhibitor return in formation media. RSC Advances. 2016;6(64):59195-205.
132. Zhang P, Ruan G, Shen D, Kan AT, Tomson MB. Transport and return of an oilfield scale inhibitor reverse micelle nanofluid: impact of preflush and overflush. RSC Advances. 2016;6(71):66672-81.
133. Zhang P, Kan AT, Fan C, Work S, Lu H, Yu J, et al. Silica-Templated Synthesis Of Novel Zinc-DTPMP Nanoparticles, Their Transport In Carbonate And Sandstone Porous Media And Scale Inhibition. SPE International Conference on Oilfield Scale; 2010/1/1/; Aberdeen, UK. SPE: Society of Petroleum Engineers; 2010.
134. Yu F, Ma J, Han S. Adsorption of tetracycline from aqueous solutions onto multi-walled carbon nanotubes with different oxygen contents 2014. 5326 p.
135. Cho HH, Smith BA, Wnuk JD, Fairbrother DH, Ball WP. Influence of surface oxides on the adsorption of naphthalene onto multiwalled carbon nanotubes. Environ Sci Technol. 2008;42:2899.
136. Gurevitch I, Srebnik S. Conformational behavior of polymers adsorbed on nanotubes. J Chem Phys. 2008;128:1.
137. Wang XL, Lu JL, Xing BS. Sorption of organic contaminants by carbon nanotubes: Influence of adsorbed organic matter. Environ Sci Technol. 2008;42:3207.
138. Zeino A, Abulkibash A, Khaled M, Atieh M. Bromate Removal from Water Using Doped Iron Nanoparticles on Multiwalled Carbon Nanotubes (CNTS). Journal of Nanomaterials. 2014;2014:1-9.
139. Lin K, Pan J, Chen Y, Cheng R, Xu X. Study the adsorption of phenol from aqueous solution on hydroxyapatite nanopowders. Journal of Hazardous Materials. 2009;161(1):231-40.
140. Xiao D, Sun W, Dai H, Zhang Y, Qin X, Li L, et al. Influence of Charge States on the π - π Interactions of Aromatic Side Chains with Surface of

Graphene Sheet and Single-Walled Carbon Nanotubes in Bioelectrodes. *The Journal of Physical Chemistry C*. 2014;118(35):20694-701.

141. Lin D, Xing B. Adsorption of Phenolic Compounds by Carbon Nanotubes: Role of Aromaticity and Substitution of Hydroxyl Groups. *Environmental Science & Technology*. 2008;42(19):7254-9.

142. Ma J, Yu F, Zhou L, Jin L, Yang M, Luan J, et al. Enhanced Adsorptive Removal of Methyl Orange and Methylene Blue from Aqueous Solution by Alkali-Activated Multiwalled Carbon Nanotubes. *ACS Applied Materials & Interfaces*. 2012;4(11):5749-60.

143. Xiaofei Sun YZ, Guangpeng Chen and Zhiyong Gai. Application of Nanoparticles in Enhanced Oil Recovery: A Critical Review of Recent Progress. 2017.

144. Engeset B. The potential of hydrophilic silica : Nanoparticles for EOR purposes: NTNU-Trondheim; 2012.

145. Raychoudhury T, Tufenkji N, Ghoshal S. Straining of polyelectrolyte-stabilized nanoscale zero valent iron particles during transport through granular porous media. *Water Research*. 2014;50:80-9.

146. Ahfir N-D, Hammadi A, Alem A, Wang H, Le Bras G, Ouahbi T. Porous media grain size distribution and hydrodynamic forces effects on transport and deposition of suspended particles. *Journal of Environmental Sciences*. 2017;53:161-72.

147. Gardner KH, Arias MS. Clay Swelling and Formation Permeability Reductions Induced by a Nonionic Surfactant. *Environmental Science & Technology*. 2000;34(1):160-6.

148. Vaughan PJ. 39 - Analysis of Permeability Reduction During Flow of Heated, Aqueous Fluid Through Westerly Granite. In: Tsang C-F, editor. *Coupled Processes Associated with Nuclear Waste Repositories*: Academic Press; 1987. p. 529-39.

149. Kan AT, Fu G, Al-Saiari HA, Tomson MB, Shen D. Enhanced Scale-Inhibitor Treatments With the Addition of Zinc.

150. Berlin JM, Yu J, Lu W, Walsh EE, Zhang L, Zhang P, et al. Engineered nanoparticles for hydrocarbon detection in oil-field rocks. *Energy & Environmental Science*. 2011;4(2):505-9.

Appendix A Design of Pressure Cell

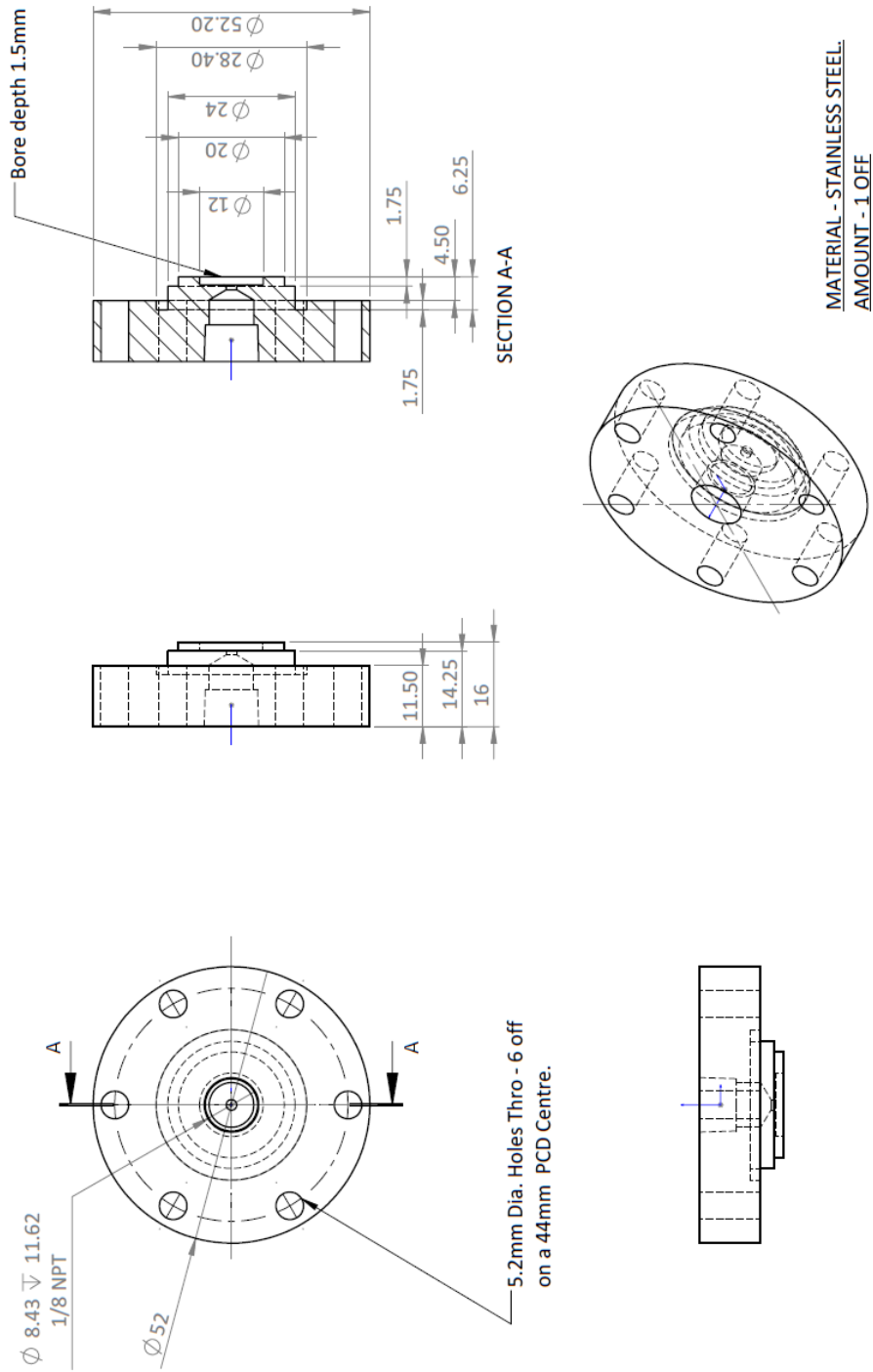


Figure 0-1 Design details of pressure cell lid used for pressure profiling tests

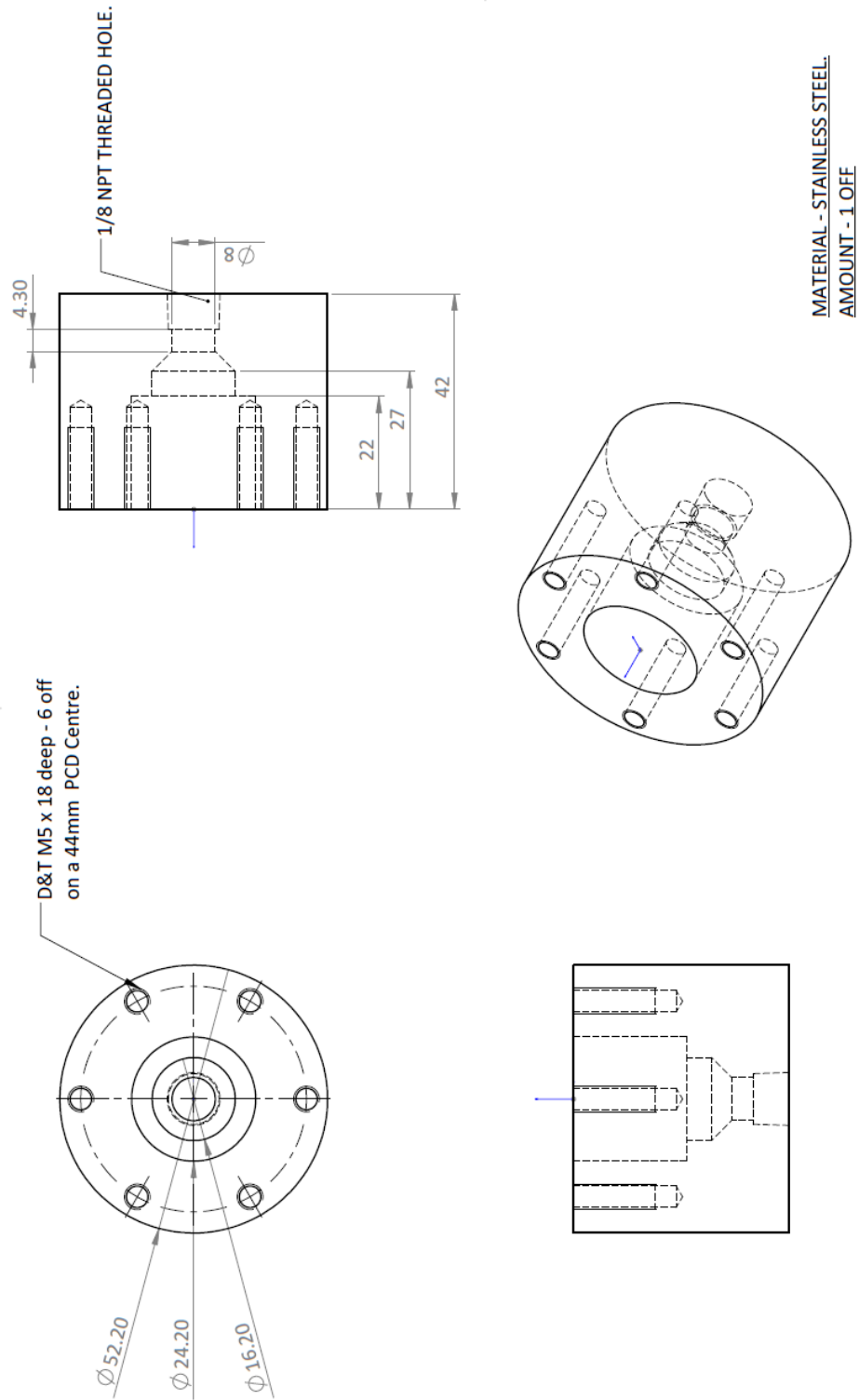


Figure 0-2 Design details of pressure cell body used for pressure profiling tests

Appendix B Detection of CNTs on in Postflush effluents

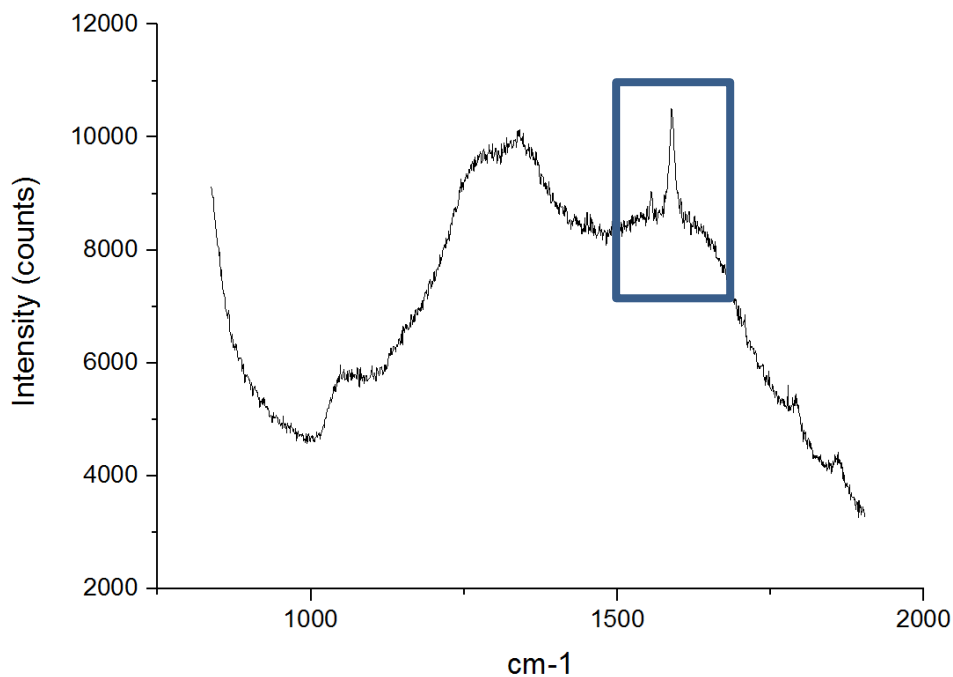


Figure 0-1 At 15 PV, during PPCA post flush period of the sand pack experiment done at 50°C. Result shows little desorption of CNTs in a sample by the presence of a G peak. It was not detectable in other PVs inspected.

Appendix C Hyamine method procedure

The steps required to determine the concentration of PPCA with the C18 Sep pak/hyamine method are described below:

1. Dilute the inhibitor stock solution down to make 50mL standards at active concentrations of 0 - 10ppm in the appropriate brine diluent solution.
2. Adjust 50 mL of each standard solution to pH 1.5 - 2.0 by dropwise addition of hydrochloric acid 10% v/v.
3. Attach a 5 mL syringe of methanol to end of a Sep-Pak C18 cartridge. Pass the methanol through the cartridge dropwise and discard the expelled solution.
4. Using a syringe, pass 10 mL of distilled water slowly through the cartridge and discard the expelled solution.
5. Using a 50 mL syringe and a syringe pump, pass inhibitor solution through the cartridge. Collect the fluid in a cup.
6. Wash the cartridge from the same end with 10 mL of distilled water from a syringe, again utilising a syringe pump. The combined collected fluids from steps 5 & 6 for each of the standard solutions can now be discarded, as the inhibitor should be adsorbed onto the cartridge.
7. Invert the cartridge and attach to the other end, a 10 mL syringe containing 10 mL of a 5% solution of sodium citrate in distilled water.
8. Elute the inhibitor slowly from the C18 cartridge using the 10 mL of sodium citrate solution on the syringe pumps and collect each eluent in a 50 mL volumetric flask.
9. Using the same 10 mL syringe, pass 10 mL of distilled water through the C18 cartridge, again collecting the eluent in the 50 mL volumetric flask.

10. Pipette 10 mL of aqueous solution of Hyamine 1622 (as supplied) into the flask and dilute to the mark (50 mL) with distilled water.

11. Shake the volumetric flask quickly to ensure that the solutions are mixed and leave to stand for 40 minutes.

12. After 40 minutes, measure the absorbance of each of the standard solutions at 500nm using a spectrophotometer.